



universität
wien

MASTERARBEIT / MASTER'S THESIS

Titel der Masterarbeit / Title of the Master's Thesis

„DNA Methylation Analysis of Hippocampal Tissue in
Trained *Rattus norvegicus*“

verfasst von / submitted by

Georg Clemens Pretsch, BSc

angestrebter akademischer Grad / in partial fulfilment of the requirements for the degree of
Master of Science (MSc)

Wien, 2019 / Vienna 2019

Studienkennzahl lt. Studienblatt /
degree programme code as it appears on
the student record sheet:

A 066 863

Studienrichtung lt. Studienblatt /
degree programme as it appears on
the student record sheet:

Masterstudium Biologische Chemie

Betreut von / Supervisor:

Univ.-Prof. Mag. Dr. Margit Cichna-Markl

Acknowledgment

I want to thank my family and friends, who supported and never stopped encouraging me during my studies and in writing this thesis.

Special thanks go to Univ.-Prof. Mag. Dr. Margit Cichna-Markl for her great supervision throughout my work. I also want to thank my colleagues in her working group, who assisted me with help and advice.

For enabling this thesis and providing the samples, I also want to thank our cooperation partner Univ.-Prof. Dr. Gert Lubec, Paracelsus Medical University, Salzburg, and his co-workers Jovana Malikovich and Roman Smidak.

Table of content

1 Introduction.....	1
1.1 Epigenetics and DNA methylation	1
1.2 Gene regulation by DNA methylation	2
1.3 Epigenetic factors	2
1.4 Hippocampus and memory	3
1.5 DNA methylation in the brain.....	4
1.6 Effect of aging on DNA methylation in the brain	6
1.7 Insulin-like growth factor 1 receptor (<i>IGF1R</i>).....	6
1.8 Fragile X mental retardation (<i>FMR1</i>).....	7
1.9 Doublecortin X (<i>DCX</i>)	8
1.10 Glutamate metabotropic receptor 5 (<i>GRM5</i>).....	8
2 Aims.....	10
3 Theoretical background.....	11
3.1 RNA and DNA	11
3.2 DNA and RNA extraction	13
3.3 Photometric determination of RNA & DNA yield	14
3.4 Polymerase chain reaction (PCR).....	14
3.4.1 Reverse transcription.....	16
3.4.2 Real-time PCR.....	16
3.4.3 Melting analysis	17
3.5 Agarose gel electrophoresis	18
3.6 Bisulfite conversion	19
3.7 Pyrosequencing (PSQ).....	20
4 Results & discussion	22
4.1 <i>IGF1R</i>	22
4.1.1 <i>IGF1R</i> DNA methylation analysis.....	22
4.1.2 <i>IGF1R</i> gene expression analysis	25
4.1.3 <i>IGF1R</i> results and discussion.....	27
4.2 <i>FMR1</i>	28
4.2.1 <i>FMR1</i> DNA methylation analysis.....	28
4.2.2 <i>FMR1</i> gene expression analysis	31
4.2.3 <i>FMR1</i> results and discussion.....	33
4.3 <i>DCX</i>	34
4.3.1 <i>DCX</i> DNA methylation analysis	34
4.3.2 <i>DCX</i> gene expression analysis	38

4.3.3 <i>DCX</i> results and discussion.....	39
4.4 <i>GRM5</i>	43
4.4.1 <i>GRM5</i> DNA methylation analysis	43
4.4.2 <i>GRM5</i> gene expression analysis.....	47
4.4.3 <i>GRM5</i> results and discussion	48
4.5 Glyceraldehyde 3-phosphate dehydrogenase (<i>GAPDH</i>)	50
4.5.1 <i>GAPDH</i> gene expression analysis	50
5 Conclusion	52
6 Experimental section.....	53
6.1 Assay and primer design.....	53
6.2 Animal training and sample preparation.....	53
6.3 Extraction.....	54
6.3.1 RNA extraction	54
6.3.2 DNA extraction.....	55
6.4 Reverse transcription of extracted RNA	55
6.5 Real-time PCR	56
6.6 Bisulfite conversion of DNA.....	57
6.7 PCR for subsequent pyrosequencing.....	58
6.8 Agarose gel electrophoresis	60
6.9 Pyrosequencing	60
6.10 Data evaluation and statistics	61
6.11 Materials and software.....	63
7 Attachment.....	66
7.1 Abstract.....	66
7.2 Zusammenfassung	66
7.3 List of abbreviations	67
7.4 Raw data	68
7.4.1 Obtained RNA and DNA concentration of the extracts	68
7.4.2 Data from gene expression analysis	70
7.4.3 Determined methylation degree by pyrosequencing.....	72
7.5 Index of Figures.....	78
7.6 Index of Tables.....	79
7.7 References	80

1 Introduction

This thesis aimed to investigate the association of DNA methylation and gene expression levels of certain genes with aging and memory formation. For this purpose, hippocampal subregions of aged and trained *Rattus norvegicus* were studied. The hippocampus is the main region of the brain, where memory formation takes place. Target genes were *IGF1R*, *FMR1*, *DCX* and *GRM5*, which have previously been linked to this process.

1.1 Epigenetics and DNA methylation

Epigenetics is a field of study that investigates gene alteration, in which not the DNA sequence is changed, but its molecular structure is modified. The modifications are known for their reversibility in response to multiple internal and external factors. They can be subdivided into two major groups.

The first one is the modification of histone proteins. Four histone isoforms form an octamer complex consisting of two proteins of each isoform. DNA is organized on these histone complexes by wrapping around them, forming a nucleosome. Its structure is often referred to as beads on a string or 10 nm fibre [1]. Histones contain many basic amino acids, like arginine and lysine, that interact with the negative charged phosphate backbone of DNA. The strength of this interaction is influenced by several posttranslational modifications of the histones, such as acetylation and phosphorylation, which alter the charge of single amino acids. Hence, the density of DNA packaging is variable, making the genetic information easier or harder to access by transcription factors and influencing the initiation of transcription [2].

Second, DNA itself may be modified by methylation of single nucleotides. While N(4)-methyl-cytosine and N(6)-methyl-adenine are often found in prokaryotes [3], the most dominant modification in eukaryotes is the methylation of C5 in cytosine. Prerequisite is that it must be part of a dinucleotide consisting of cytosine and guanine (CpG) [4]. In mammals, the methylation is mediated by a group of enzymes named DNA methyltransferases (DNMTs). They catalyse the transfer of a methyl group from S-adenosyl-L-methionine (SAM), a common biological methyl donor, to the target cytosine [5].

Three DNMTs with DNA methylation activity are known so far. DNMT3a and DNMT3b are important for DNA *de novo* methylation. This process becomes especially important during embryonal development, as it was shown in mice by Okano *et al.* in 1999. The fertilized egg undergoes global DNA demethylation to remove most of parental methylation patterns. Afterwards, intensive reprogramming occurs and new patterns are established. A lack of one or both DNMT3 enzymes causes early embryonic lethality, demonstrating their importance during development [6–8].

In adult and differentiated cells, the methylation pattern is already established and needs to be conserved during cell division and genome replication. By its nature, one strand of the newly generated double-stranded DNA is from the predecessor and displays a distinct

methylation pattern. In order to keep this information, the pattern is transferred to the new unmethylated strand by DNMT1 [9]. The conservative function of this enzyme demonstrates that DNA methylation is a stable and self-perpetuating process of information storage.

1.2 Gene regulation by DNA methylation

Multiple ways are known how DNA methylation can influence gene expression. One is methylation in the promoter region. About 60 % of human genes are associated with CpG islands in their 5'-end, including house-keeping genes. CpG islands are characterized by a relative high density of CpGs, being one dinucleotide every 10 bases on average over a sequence of 1000 bases. This is ten times the ratio that can be found in the rest of the genome. It is estimated that CpG islands comprise about 1 % of the human genome [10–12].

Methylation of CpGs in promoter regions is mostly linked to gene silencing. This is due to a decrease in binding capability of transcription factors during the initial step of transcription [13,14]. The added methyl group reaches into the major groove of the double helix (see 3.1) and has a thereby narrowing effect on the minor groove that hinders shape readout by transcription factors. Without correct binding of transcription factors, polymerase cannot be recruited [15].

Another way how DNA methylation inhibits transcription is the recruitment of repression complexes like the methyl-CpG binding protein (MeCP2) and similar proteins. The molecule contains a methyl-CpG binding domain (MBD), which binds to methylated CpGs, and a SIN3-histone deacetylase complex. By binding of this protein to methylated DNA in a nucleosome, histones are deacetylated which causes an increase in DNA packing density and a subsequent decrease in gene expression [16].

Despite the CpG dense promoter regions, DNA methylation was also found in the gene body, which is defined as the sequence after the first exon (see 3.1 RNA and DNA). Methylation in the gene body is positively correlated with gene expression. This was shown in multiple tissues and cell types, like B-lymphocyte, placenta, peripheral white blood cells and fibroblasts. In case of hypomethylation of these sites, gene inactivation was found, with the exception of slowly dividing and non-proliferative tissues (e.g. brain tissue) [17,18].

Statistically, CpGs in intragenic regions are more frequently in exons than in introns. It was reported that the methylation in intragenic sites had high influence on alternative splicing as well. Inhibition of DNA methylation led to dysfunction in splicing and exon skipping in human cells, while methylation increased expression of an exon. MeCP2 and histone deacetylase played a major role in this process, since exon skipping was also seen after their knock-out [19]. A study by Li *et al.* confirmed these observations across several human tissues [20].

1.3 Epigenetic factors

In contrast to conventional genetic changes, epigenetic modifications are subjected to alteration throughout an organism's lifespan. Even monozygotic twins develop a different epigenetic pattern of modifications due to environmental factors [21].

Aging has a well-known epigenetic impact, since many studies reported increased methylation levels in promoter regions of aged individuals. Additionally, the remaining genome is often found in a hypomethylated state. Altered methylation due to aging frequently leads to silencing of tumor suppressor genes, increasing the risk of cancer development [22,23]. An example is the methylation of *RASSF1A*, a tumor suppressor gene that is involved in cell cycle control. Its silencing is one of the main causes for renal cancer [24]. The correlation between cancer risk and age-related DNA methylation was found to be tissue-independent [25].

Beside aging, multiple environmental factors were found to influence DNA methylation. One example is the constant uptake of heavy metals and their accumulation in the body. Arsenic can be found in soil and drinking water, as well as airborne particles. Exposure to this heavy metal has already been linked to a variety of cancer types. This may partly be due to epigenetic silencing of p53 and p16, two main tumor suppressor genes. Concerning these genes, a study by Chanda *et al.* observed altered promoter methylation, depending on the arsenic concentration in drinking water [26].

Another example is the discussed influence of air quality. Many people live in cities where air pollution has become an influence on health. De Prins *et al.* studied alteration in DNA methylation that occurred due to everyday exposure to particulate matter, as well as O₃ and N₂ values, that were below European limit thresholds. They reported a correlation between global hypomethylation in white blood cells of healthy adults and the exposure to increased values of pollutants [27].

1.4 Hippocampus and memory

The bilateral brain region of the hippocampus is named after the Greek word for sea horse, which shows similarities in terms of shape. It is subdivided into several subregions: dentate gyrus (DG), *cornu ammonis* 1/2/3 (CA1/CA2/CA3), subiculum, parasubiculum and the entorhinal cortex. The main function of this part of the brain is the episodic memory, which stores personal experiences. It was famously reported by Scoville and Milner, that people with damaged hippocampus are unable to acquire new long-term memory but were able to live an otherwise normal life at the same time [28].

Synaptic plasticity describes a process how memories are generated and stored. It follows a theory that was originally postulated by Donald Hebb in 1949 [29]. He claimed that if a neuron fires persistently and repeatedly over a long period of time to excite a second neuron, metabolic and growth changes will occur to strengthen the link and the transmission between them. This mechanism, today known as long-term potentiation (LTP), was proven to occur in CA1, CA3 and DG, as well as in other parts of the brain [30]. LTP depends strongly on glutamatergic signaling, a process of signal transduction between neurons where glutamate is used as transmitter [31]. The process can be influenced artificially by electric high or low frequency stimulation, which helped to elucidate the mechanism [32]. Synaptic plasticity is assumed to be a key factor for memory encoding and its stabilisation. The

reverse effect was also observed, named long term depression, which weakens a neuronal link [33].

Another process of memory formation, beside synaptic plasticity, is the generation of new neurons from precursor cells. The DG and striatum are the only regions of the brain where the process of neurogenesis takes place in adults [34]. In case of DG in human and mouse, neural progenitor cells proliferate into dentate granule cells and migrate into the inner layer of the dentate gyrus. There they become polarized by developing dendrites and axons. In the following, the cells project into the CA3 and connect with neuronal network [35]. This mechanism is thought to be a major contribution to learning and pattern recognition [36].

The hippocampus is also linked to spatial recognition and orientation. First discovered in rats, several cells (place cells) were found to fire when the animal is at a distinct location. The cells are gathered in place fields, which are each associated with a space that is already familiar to the animal. These place cells were extensively studied in rats but were also found in other mammals. Remarkably, they do not only fire when the animal is at specific location, but also independently from external conditions (e.g. light) and regardless of the direction the animal approaches. Additional information like odour cues or landmarks that are related to a spatial position, is also stored in the hippocampus [37–39]. The pioneer work on this field was awarded with a Nobel prize in physiology or medicine to John O'Keefe, May-Britt Moser and Edvard I. Moser in 2014 [40].

1.5 DNA methylation in the brain

The importance of DNA methylation for brain development was recognized after knock-out of DNMTs. Since a genomic knock-out led to prenatal death, the gene was specifically inactivated in postnatal post-mitotic neurons in mice. Feng *et al.* found that single conditional knock-out of only DNMT1 or DNMT3a did not impact DNA methylation, proposing a redundant role. But the double knock-out of both resulted in smaller cell sizes and impaired mental abilities, mainly reducing spatial memory performance and memory consolidation [41].

The process of memory formation, a major process of the brain, depends on the correct expression of various genes after an input and corresponding development of neurons. DNA methylation enables a control of expression in a fast and dynamical manner, although the processes are yet not fully understood. It was assumed that any disturbance could lead to severe mental or psychological diseases [42–44].

One exemplary gene that is important for memory consolidation in mammals, is brain-derived neurotrophic factor (*BDNF*). The gene has several exons with respective promoters, which are differently expressed during the steps of the process. Different expression patterns that depend on the region were also found. Lubin *et al.* suggested that the dynamic regulation of different exons is managed via DNA methylation. During memory consolidation phase, after contextual fear conditioning in rodents, the promoter of *BDNF* exon IV became demethylated in the hippocampus, which increased expression of exon IV

containing transcripts. Administration of DNMT inhibitor also led to increased expression in exon I, IV and VI and a corresponding increased transcription of these exons. Their aberrant expression is assumed to be linked to cognitive dysfunction in psychiatric disorders [42,45].

Protein phosphatase 1 (PP1), which functions as a memory suppressor, is methylated upon neuronal excitation. Gene expression decreases in the following, which allows the formation and consolidation of new memories. By administration of DNMT inhibitor 6 h after exposure, methylation and subsequent repression of this gene were disabled. This caused a significantly weakened effect of contextual fear conditioning. In the same study, which was carried out by Miller and Sweatt, the expression of *REELIN* was increased after neuronal excitation. This observation corresponded with demethylation in the promoter region. The gene is known for its critical role in synaptic plasticity and LTP. Up-regulation caused an increased learning effect that could be improved by inhibiting DNMT. Demethylation below the promoter's natural degree could also further improve the effect. Expression levels of both genes returned to baseline after 24 h [46].

In contrast to the quick change in gene regulation described above, DNA methylation is also responsible for persistent effects, that may even appear a long time after the initial trigger. For instance, prenatal stress and exterior factors during early childhood showed an influence on the adult animal's behaviour [47–49]. One example for long lasting effects is the glucocorticoid receptor and its encoding gene *NR3C1*. Weaver *et al.* reported that the promoter exon 1₇ is differently methylated in mice, depending on maternal care in the first week after birth. If a dam showed increased pup-licking and arched-back nursing, exon 1₇ was lower methylated in the offspring. As result the glucocorticoid receptor was expressed in higher amounts. The opposite could also be observed where the methylation degree was higher after decreased maternal care, resulting in negative gene regulation. Experiments with cross-fostering, where the offspring received the interchanged treatment, revealed reversibility between the two observations. The established effect on gene regulation was found to be persistent into adulthood, where a decreased expression of the receptor protein causes the animal to be more susceptible to stress-induced depression [50,51].

The results are comparable to human. The genes between both species are similar and a homolog to mouse exon 1₇ exists, named exon 1_F. McGowan *et al.* investigated methylation in this region by studying the genome of suicide victims that experienced child abuse. The results are the same as it was observed in rodents. Individuals that experienced less care during their childhood, had an increased methylation in exon 1_F and thus a down-regulation of glucocorticoid receptor. The results were compared to individuals with normal childhood experiences [52].

1.6 Effect of aging on DNA methylation in the brain

Aging is the most fundamental process of life. Statistics prove that the life expectancy of an average human is now longer than it was ever before [53]. But albeit the advances, a longer life is accompanied by an increased risk of disease. Especially memory impairment is not uncommon in elderly people. Most prominent, dementia and Alzheimer's disease are often diagnosed to be the cause for the decline of mental capabilities [54].

Many studies investigated the mechanisms and processes in brain that contribute to aging. But since it is known that DNA methylation plays a major role in the complex process of memory formation, (see above in 1.5) this mechanism deserves further attention.

Recent studies reported significant changes in gene expression in the hippocampus and the medial prefrontal cortex in aged rats [55]. Those genes are often important for synaptic plasticity, memory consolidation and retrieval, like *ARC* and *EGR1* [56,57]. In addition, Oliveira *et al.* discovered a decreased *DNMT3a* expression in the hippocampus of aged mice, which led to memory impairment as well. The latter process was found to be reversible, since a rescue experiment restored the cognitive functions by inducing increased expression of the enzyme [58].

Probably due to the decreased expression of *DNMT3a*, the genome appears in a generally hypomethylated state in aged people [59]. This concerns also non-coding regions like LINE-1 and interspersed Alu elements [60]. In contrast, promoter CpG islands were mostly found hypermethylated. This aberrant methylation paves the way for a variety of diseases like cancer, memory impairment and auto-immune diseases [61]. But beside the genome-wide or promoter-wide methylation degree, Haberman *et al.* assumed that the methylation state of single CpGs plays a more important role in gene expression [62].

1.7 Insulin-like growth factor 1 receptor (*IGF1R*)

This gene encodes for a protein of the same name. Spanning the cell membrane, the main binding partner of this receptor protein is the insulin-like growth factor 1 (IGF1). In addition, IGF2 and insulin are also bound with lower affinity. Upon binding of IGF1 the intercellular subunits of the receptor are autophosphorylated. This recruits several signaling molecules that activate the IGF signaling pathway, leading to cell growth and proliferation [63].

The tetrameric receptor shares a high sequence homology with the insulin receptor. This fact allows them to mix their subunits and form still functional hybrids, which was mainly observed in tumor cells, where they exhibited an increased mitogenic effect compared to the single type receptors alone [64,65].

The activity of IGF1R was originally related to its role in liver and skeletal tissue. But recently research started to focus on its role in neuronal development and expression in the brain. For instance, studies found induction of neuronal proliferation in adult rat hippocampus after peripheral administration of IGF1 and thus an increased signaling via the IGF1 pathway [66].

Several studies showed an increased risk for diabetes patients to develop Alzheimer's disease. Further studies had proven that those patients also display reduced *IGF1R* expression, establishing a direct link between these two observations [67,68].

Logan *et al.* performed a knock-down of *IGF1R* in mice astrocytes, which are brain cells that are important for brain maintenance and support. During their research they discovered a significantly decreased working memory performance in rodents that were trained in a Morris-water maze. Primary cell cultures made from extracted tissue had a significantly decreased IGF1 signaling and glucose metabolism. Oxygen metabolism was impaired as well, in parallel with decreased mitochondrial performance [69].

Mice with low serum levels of IGF1 and thus decreased IGF signaling capability, showed impaired LTP in the hippocampus and poor performance in orientation tasks [70]. This finding is supported by the observation that IGF1 signaling is influencing reconstruction of the essential myelin coat in nerve cells after its removal [71].

In addition to observations that establish a link between learning and IGF1 signaling, multiple studies also agree that *IGF1R* expression decreases during aging [68,72]. All together, these findings corroborate a connection between the availability of IGF1R and memory formation, in addition to its already known function in cell growth.

1.8 Fragile X mental retardation (*FMR1*)

FMR1 encodes for the fragile X mental retardation protein (FMRP). It acts as a translational repressor in multiple processes of brain cells and is an important factor for memory formation. About 4 % of neuronal transcripts are possible targets for FMRP [73,74]. In the 5' untranslated region of *FMR1*, a variable number of CGG trinucleotides can be found that varies individually and is the key factor for abnormal expression. An average phenotype without symptoms possesses up to 50 repeats. Individuals with 50 to 200 repeats are considered premutation carriers, while patients with more than 200 repeats often develop fragile X syndrome [75]. The number of repeats is susceptible to mutation and is passed on to the next generation. Typical symptoms involve learning disability, prevalence of concurrent autism spectrum disorder and various other psychological and neurological occurrences [76]. Another diagnosed disease that can also affect premutation carriers, is fragile X associated tremor/ataxia syndrome (FXTAS), which causes impaired movement and is also linked to cognitive disorders [77,78].

As mentioned, the main criteria for clinical diagnosis is the extent of the trinucleotide repeat [75]. Each repeat contains a CpG dinucleotide that is a possible site for DNA methylation [79]. An increased methylation in the region leads to silencing of the gene and, in the following, abnormal development of neurons [80–82]. It was shown in mice, that a lack of FMRP causes overexpression of cytoskeletal proteins (e.g. ARC) and increasing amounts of GRM1 and GRM5 as well as a decrease in AMPA receptors. These effects impaired synaptic plasticity and therefore brain function [83]. Studying *FMR1* knock-out mice also revealed that symptoms get more severe with increasing age [84].

1.9 Doublecortin X (*DCX*)

Since *DCX* is known for its critical role in neurogenesis, its expression is often used as a marker for brain development and learning [85–87]. The protein is an important factor for neuronal migration during and after brain development, participating in formation of microtubules [85,88]. Therefore, doublecortin is classified as microtubule associated protein (MAP). It acts stabilising on this filament, preventing its shortening [89]. This enables the protrusion of neurons and formation of new links, as it is done during learning and brain development. Hence, a disturbed expression is fatal for mental capabilities [90].

Succeeding its first discovery, the gene was linked with brain malformations, mainly lissencephaly and subcortical band heterotopia [91]. Lissencephaly is characterised by completely or partially absent brain convolutions (agyria and pachygyria). Genes with decreased expression, which are closely related to this condition are *DCX*, *LIS1* and *TUBA1A*, which are important for neuronal migration in embryonic development. The condition of subcortical band heterotopia is caused by disturbed migration as well and the subsequent formation of abnormal cortical layers beneath the grey matter. Both diseases, lissencephaly and subcortical band heterotopia, cause mental retardation. Often intellectual disabilities are diagnosed at the same time [92–95].

1.10 Glutamate metabotropic receptor 5 (*GRM5*)

The gene *GRM5* codes for the glutamate metabotropic receptor 5, which has homologs in many mammals. The protein is a G-protein-coupled-receptor that is spanning across the cell membrane. It is nearly ubiquitously expressed in every brain region and participates in post-synaptic signal transmission [96]. Activation of the receptor is achieved by binding of the neurotransmitter L-glutamate on its extracellular domain, resulting in activation of intracellular phospholipase C. A subsequent cleavage of messenger molecule phosphatidyl inositol occurs and through continuation of the cascade, calcium ion channels are opened and depolarisation of the neuron for further signal transmission is initiated [97,98].

By performing spatial training with mice, a correlation between the increased expression of *GRM5* in the hippocampus and enhanced LTP is already established [99,100]. For instance, experiments found elevated *GRM5* mRNA levels right after induction of LTP, indicating its involvement in this process [101]. By administration of *GRM5* antagonists in different intervals before and after spatial training, a certain time dependency was revealed. By inhibiting the receptor closely before and after the training, the learning effect was nullified. But there was nearly no effect by administration in larger intervals after training which suggests a major role in the initial induction of LTP [99].

The importance of *GRM5* in the memory consolidation phase of rats was studied by Riedel *et al.* [102]. In the first day after training the expression increased 3-fold in the hippocampal subregion CA3, correlating with induction of memory formation. Within ten days after training the mRNA expression decreased in CA3 while an increase was found in the subregion CA1 and DG. These observations revealed a time dependent expression pattern of

GRM5 during learning and suggests an important role in CA1 and DG during memory consolidation.

Together these findings indicate a strong role of *GRM5* in the learning process and LTP in short- and long-term memory.

2 Aims

As it is shown in numerous publications, aging has a significant influence on memory performance. But how memory is formed and maintained on the molecular level, is still not fully understood and is the objective in various studies. One known mechanism of regulation is DNA methylation, which may have a significant impact on gene expression. Because of its role in episodic and spatial memory, the hippocampus is thereby of special importance.

Investigated genes are linked to mental and cognitive impairment: insulin-like growth factor 1 receptor (*IGF1R*), fragile X mental retardation 1 (*FMR1*), doublecortin X (*DCX*) and the glutamate metabotropic receptor 5 (*GRM5*). Tissues of interest were hippocampal subregions CA1, CA3 and DG from aged *Rattus norvegicus* that were trained in a radial arm maze.

The aim of this thesis was to investigate gene expression and DNA methylation in hippocampal tissue. For this purpose, RNA and DNA were extracted using a trizol protocol. To determine gene expression levels, RNA was reverse transcribed into cDNA, which enabled a quantitative analysis via real-time PCR. After method development, DNA methylation in the respective promoter region was investigated. The development comprised PCR and pyrosequencing, which was performed after bisulfite conversion of the extracted DNA.

The results should give insight, if gene expression and DNA methylation are associated with the age of the animals and their learning performance. Additionally, the expression rates and methylation degrees in the different hippocampal subregions should be analysed. *DCX* and *GRM5* were of special interest, since they are already linked to neuronal activity.

3 Theoretical background

Various RNA and DNA based methods were used in this thesis. Starting with the extraction from samples ranging to the analysis via real-time PCR (polymerase chain reaction) and pyrosequencing (PSQ). The following section covers the theory and principals behind these experiments.

3.1 RNA and DNA

DNA is the fundamental component that is the base of every life form on our planet. Its main parts are the four DNA bases adenine (A) and guanine (G), derivatives of purine, and thymine (T) and cytosine (C), which are derivatives of pyrimidine. They are bound to a molecule of 2-deoxy- β -D-ribofuranose (deoxyribose) via a N-glycosidic bond. Phosphate is bound to the 5'-OH group of the sugar component, building a nucleotide, the basic monomer of DNA. By forming a phosphodiester bond (see Figure 1) at 3'-OH, multiple nucleotides build a polymeric DNA strand, with interchangeable monomers that differ only in the DNA base. In this way, information is encoded by a sequence comprising the four DNA bases. The strand of alternating deoxyribose and phosphate is the backbone of DNA, where phosphate provides a negative charge. Strands are read from 5'- to 3'-end *in vivo*, which is also the direction of its general depiction.

DNA bases form hydrogen bonds between each other, but only two specific combinations are possible. The pairs, first described by Watson and Crick, are adenine/thymine and guanine/cytosine. The recognition is performed by the number of hydrogen bonds a base can form. Adenine/thymine are capable of forming two, while guanine/cytosine are connected by three hydrogen bonds (Figure 1). This results in two DNA strands interacting with each other, stabilised by hydrogen bonds and additional non-covalent forces. One strand is complementary to the other in terms of DNA base pairs. The two complementary strands form the widely known DNA double helix. It exposes the backbone on the outside, while the DNA bases are turned inwards. The gap between the two strands is named minor, while the one between double strands is the major groove [103]. The strands can be separated from each other, by a process called melting, in which the temperature is increased above the melting point of the sequence. At this sequence-specific temperature the hydrogen bonds break up, but the single strands remain intact. Since guanine and cytosine form an additional hydrogen bond compared to adenine and thymine, higher GC-content increases the melting point.

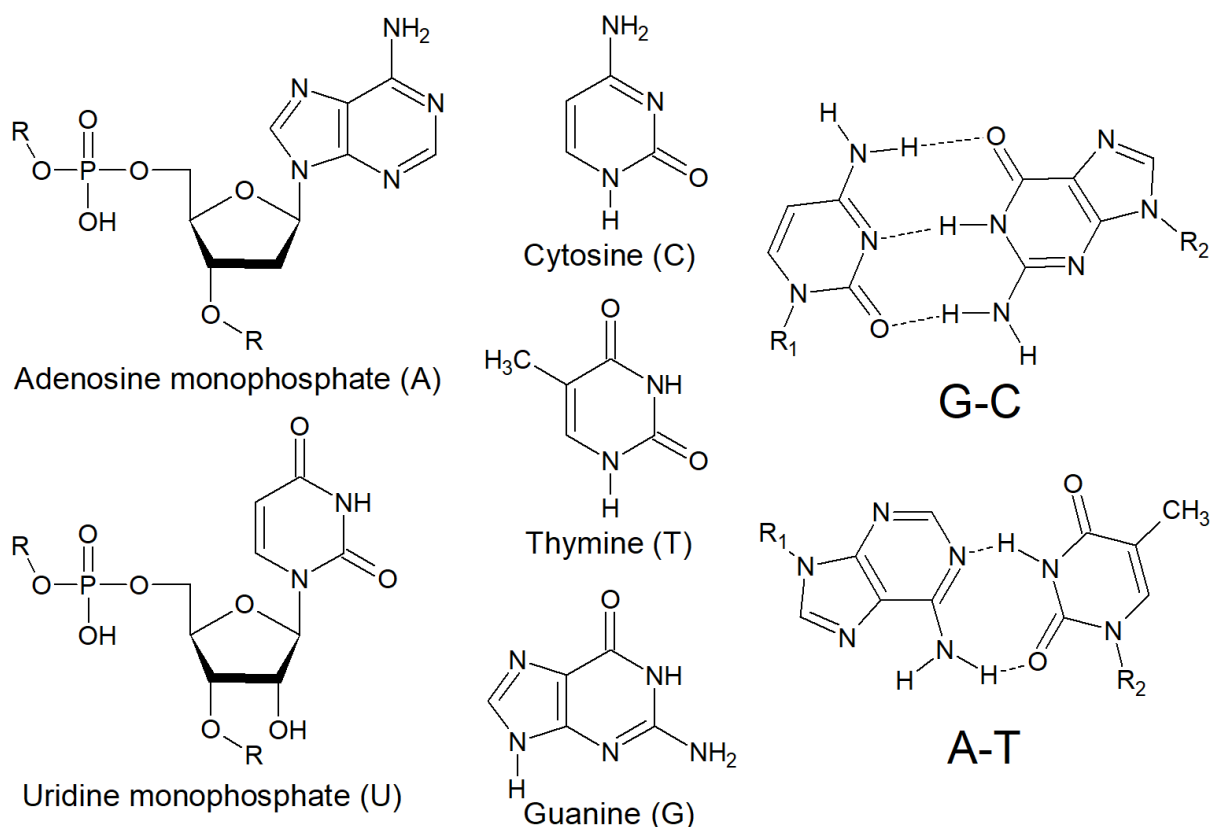


Figure 1: Molecular structure of DNA/RNA (R = continuous DNA chain) and the hydrogen bonds between them (R_1+R_2 = individual DNA chains).

The complementarity is the key for DNA replication *in vivo*. The double strand is separated into single strands, and to each single strand, a complementary strand is generated. DNA read-out works in a similar way, except DNA is transcribed into mRNA. This oligonucleotide functions as a messenger between DNA information and the encoded protein sequence. The structure of RNA is similar to DNA but has two major differences. The RNA base uracil (U) is incorporated into the strand instead of thymine in DNA. Secondly, the carbohydrate backbone, which is deoxyribose in DNA, contains ribose with an additional 2'-OH group in comparison. This weakens the structure of RNA and makes it more susceptible to degradation and other chemical reactions [104].

A gene is structured into several parts. A promoter region marks the starting point for transcription, while a terminator sequence flags the end. In between of these regions lies the gene body. Most of the genes comprise several coding regions (exons) and non-coding regions (introns). To connect all coding regions in order to form a functional sequence, splicing of pre-mRNA, the first transcript, is performed. Introns are cut out and exons are connected to a single sequence (see Figure 2). This mRNA sequence, containing all information required, is translated into protein. Alternative splicing was shown to effect gene expression in a tissue- or species-specific manner, by transcribing only certain exons or by splicing pre-mRNA differently. In this way multiple related mRNA sequences, and thus proteins, are formed, although they originate from the same DNA sequence [105–107].

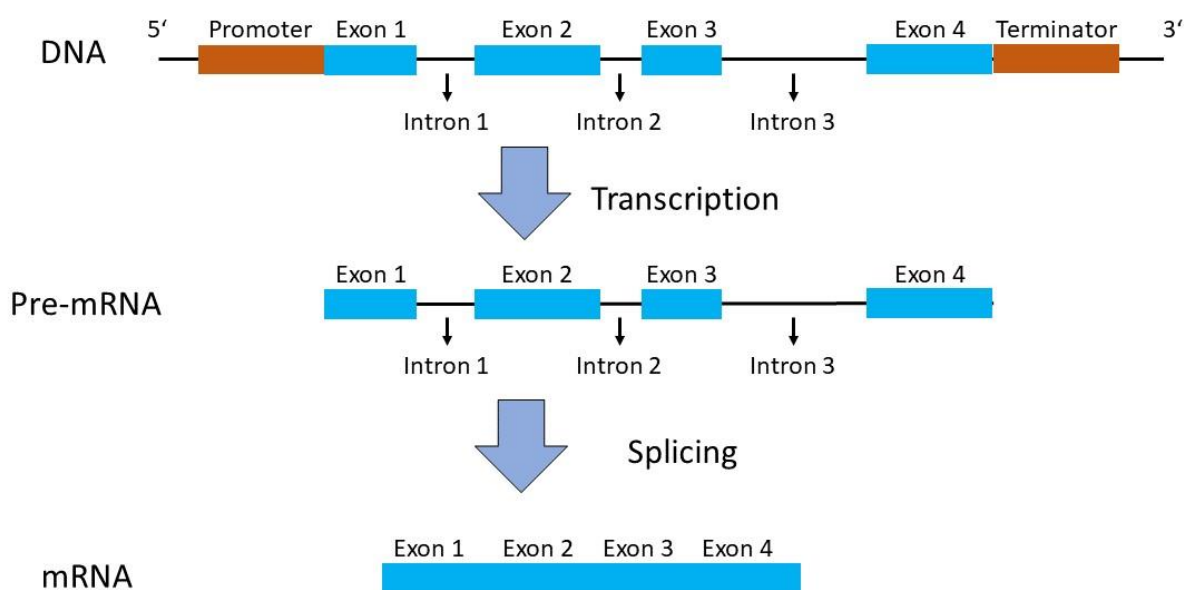


Figure 2: Simplified depiction of transcription and splicing.

3.2 DNA and RNA extraction

Due to their molecular similarity, it is difficult to separate RNA and DNA. In this thesis, a trizol extraction protocol, provided by Thermo Fisher [108], was applied. This reagent is a monophasic solution of guanidinium isothiocyanate and phenol that allows sequential isolation of RNA, DNA and proteins without addition of further enzymes. Guanidinium isothiocyanate is a chaotropic agent, which denatures proteins and thus inactivates nucleases to prevent RNA/DNA degradation. Additional advantages of extraction with trizol are thorough precipitation and more soluble protein pellets compared to other methods [109,110].

The method resembles phenol-chloroform extraction, as it takes advantage of the same reagents to separate and precipitate nucleic acids. In the applied method, addition of chloroform to a trizol sample induces phase separation between organic and aqueous solvent. Under neutral pH nucleic acids have a negative net charge due to their backbone (see 3.1) and can be found in the aqueous phase. In contrast proteins possess multiple hydrophilic and hydrophobic domains and aggregate preferably in the organic- or interphase.

DNA has a lower pKa compared to RNA and is therefore more likely to be protonated. This results in a neutral net charge of DNA if the pH is decreased, as it is the case in trizol. DNA subsequently migrates into the interphase while RNA remains in the aqueous phase. After isolation of the RNA containing phase, precipitation is performed by addition of isopropanol, which lowers the polarity of the solvent and therefore the solubility of the oligonucleotides. Afterwards the precipitate is washed with 70 % ethanol to remove co-precipitated salts.

After withdrawal of the aqueous phase that contains RNA, DNA and proteins are found in the phenolic phase. The nucleic acids are precipitated by addition of 100 % ethanol. This creates a more hydrophilic environment, in which DNA is insoluble under acidic conditions and therefore precipitates. The protein remains in the supernatant and is withdrawn.

Additional washing steps with 70 % ethanol are performed to eliminate co-precipitated salts in the DNA pellet. While the increased polarity of this solvent is sufficient to remove contaminants, DNA is also susceptible to solubilisation. This can be avoided by using only cold reagents and quick processing of the samples [111–113].

Glycogen was added to the RNA and DNA extracts prior to their precipitation. The huge polymeric structure of glycogen is insoluble and entangles with the nucleic acids. In this way their molecular weight is increased, allowing an easier and thorough precipitation by centrifugation. It also slightly increases the size and visibility of generated pellets, facilitating its recognition in the washing steps. Hence, it increases the yield in extractions, if low amounts of nucleic acids are to be expected [114].

3.3 Photometric determination of RNA & DNA yield

The concentration of RNA and DNA can easily be assessed by photometric methods. Because of their aromatic structure, nucleic acids absorb light at 260 nm. By applying the law of Lambert-Beer, which states that absorbance is proportional to the concentration of the analyte, the concentration can thus be quantified. The absorbance at 280 nm is also determined. Light at this wavelength is absorbed by aromatic amino acids, phenol and other contaminants. By calculating the absorbance ratio 260 nm/280 nm the purity of the DNA sample is estimated. The optimal ratio for pure DNA extracts is 1.8, while it is 2.0 for RNA extracts. Lower ratios indicate impurities in the solution. Other contaminants are indicated by a high absorbance at 230 nm, for example the phenolate ion, which is a main contaminant in this case due to the extraction method [115,116].

3.4 Polymerase chain reaction (PCR)

The discovery of PCR was a milestone in biochemistry and was awarded with a Nobel prize for Kary Mullis in 1993 [117]. He utilized polymerase, the enzyme responsible for DNA replication, and created a method that allows copying of any DNA sequence in high amounts. In theory one single template strand is sufficient to carry out the experiment. The method works accurately and is widely used, not only in research but also in other fields like forensics and paternity tests, where small variations in base sequences are investigated.

Three successive steps can be distinguished when conducting PCR experiments: Melting, primer annealing and elongation. These steps form a cycle that starts again after completion. After each cycle the amount of amplicon, copies of the target sequence, is theoretically doubled (Figure 3).

The experiment is initiated with template DNA that is melted by increasing the temperature until only single stranded DNA (ssDNA) is present (Figure 3, 1). In practise the temperature is

mostly set to 94-95 °C, which is sufficient to melt any double stranded DNA (dsDNA), without risking the denaturation of the molecule itself.

Small DNA sequences (primers) are complementary to the sites next to the target sequence that needs to be amplified. A forward and a reverse primer are designed, since both complementary DNA strands need to be amplified. After melting of the initial DNA sample, the template, primers anneal at a lower temperature to both of the strands (Figure 3, 2). Most important for a correct temperature setting is the melting temperature of the primer, which increases with length and a higher GC base pair content. A higher annealing temperature is favourable, since it increases the probability of correct primer binding. Otherwise they may bind in an unspecific manner to sequences that are only partially complementary. If the temperature is too high, primers could be prevented from annealing completely, which reduces the amplification efficiency.

Upon successful annealing of the primers, DNA polymerase elongates them from their 3'-end, creating a complementary strand to the template. This results in the generation of two dsDNA sequences per ssDNA template (Figure 3, 3). For this step, the temperature is set to the optimum for polymerase activity.

Once this phase is finished a new cycle is started by melting the generated double strands. In theory the number of amplicons doubles each cycle, which leads to large amounts that can be analysed [118,119].

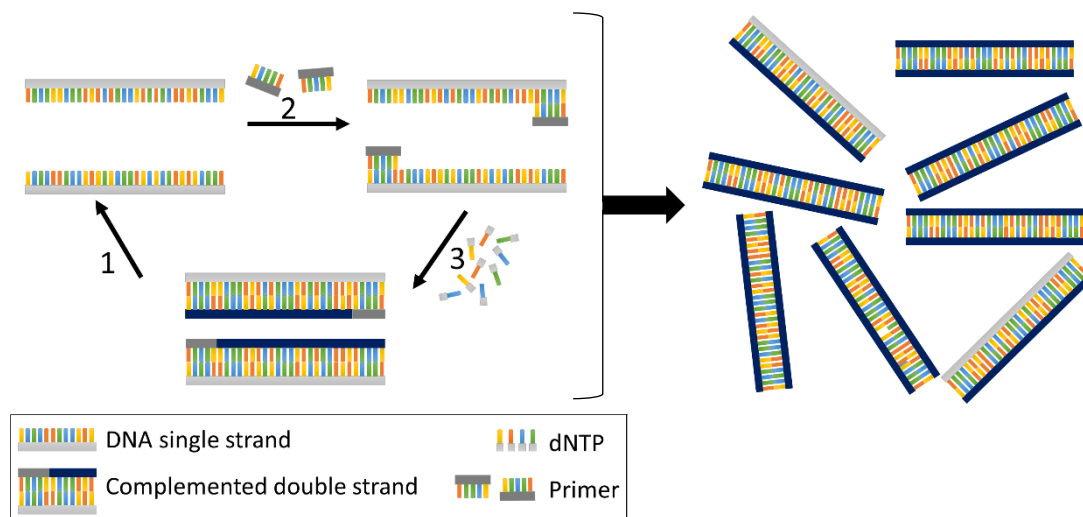


Figure 3: Depiction of the single steps during PCR (1= Melting, 2= Primer annealing, 3= Elongation).

To maintain the activity of polymerase, a buffer keeps pH and salt concentration constant at optimal conditions. Especially the concentration of polymerase co-factor Mg^{2+} is of great importance and can be varied to increase the amplicon yield. Deoxyribose nucleoside triphosphates (dNTPs) are part of the reaction mix, to provide DNA monomers for the newly generated strands [119].

The discovery of Taq-polymerase from the extremophile *Thermus aquaticus* improved the PCR fundamentally [120]. Its heat-resistance removed the necessary step of adding new

enzyme after each cycle, since the first used DNA polymerase from *E. coli* degraded during the melting step. This also reduces the risk of contamination with external DNA, because there is no need to open the reaction vessel during the PCR. The enzyme is commonly bound to an antibody that inhibits polymerase activity and only after an extended phase of heating the antibody is cleaved and PCR can start. By using this hot-start polymerase, an early start of PCR is prevented as well as the formation of incomplete side products [121].

3.4.1 Reverse transcription

The structure of RNA resembles DNA, with the difference that the base thymine is replaced with uracil. The additional hydroxyl group in the ribose phosphate backbone makes it more susceptible to degradation compared to DNA. To eliminate these risks and facilitate the analysis, it is common to reverse-transcribe RNA into complementary DNA (cDNA), a process adapted from viruses. The reaction, which is similar to PCR, is enabled by RNA-dependent DNA polymerase (reverse transcriptase). Small random primers are used in the process, which bind to any RNA sequence and deliver an entire transcription of the available RNA. Another method includes the use of primers that bind to the poly-A tail of eukaryotic mRNA.

Once cDNA is generated, conventional PCR is used for further amplification. Since remaining genomic DNA (gDNA) is also amplified in this step, it must be eliminated prior to reverse transcription to avoid contamination. For this purpose, the applied kit uses gDNA degrading buffer, which probably contains DNase. As additional measure to inhibit the amplification of genomic DNA, the chosen amplicon mostly covers two exons. In this way only the already spliced mRNA is amplified [122].

The experiment enables the subsequent determination of initial mRNA amounts and comparing them by gene expression analysis like described in 3.4.2.

3.4.2 Real-time PCR

Real-time PCR (also known as qPCR) is an adaptation of conventional PCR, used for relative quantification of RNA and DNA, as well as identification of PCR products. The setup is similar to conventional PCR, with the difference that the amplification can be traced in real-time. Two approaches are common for this purpose. The first is the use of fluorescently labelled oligonucleotide probes that are specific for the PCR target. For the second approach a dsDNA intercalating fluorescent dye is used to detect PCR products in a more unspecific way. This was also the method of choice in the present thesis.

The dye is colourless in an unbound state and does not disturb the PCR. It intercalates selectively into dsDNA, which changes conformation of the dye and emits fluorescence after excitation. The fluorescence is measured in the end of each amplification cycle after the elongation step. The obtained signal is proportional to the amount of double stranded DNA in the reaction vessel, which theoretically doubles each cycle. However, this is only true for the first cycles, as the amplification efficiency decreases with time. Four phases are

observable during amplification: baseline, exponential, linear and plateau (compare to Figure 4).

The most reliable quantitative results are obtained during exponential phase, because the amplification efficiency is already decreased in the following linear phase, and the dsDNA does not double every cycle. The cycle in which the signal rises above the background noise is determined and named threshold cycle (Ct). Higher initial amounts of DNA result in lower Ct-values, since it needs less amplification cycles for signal increase [123].

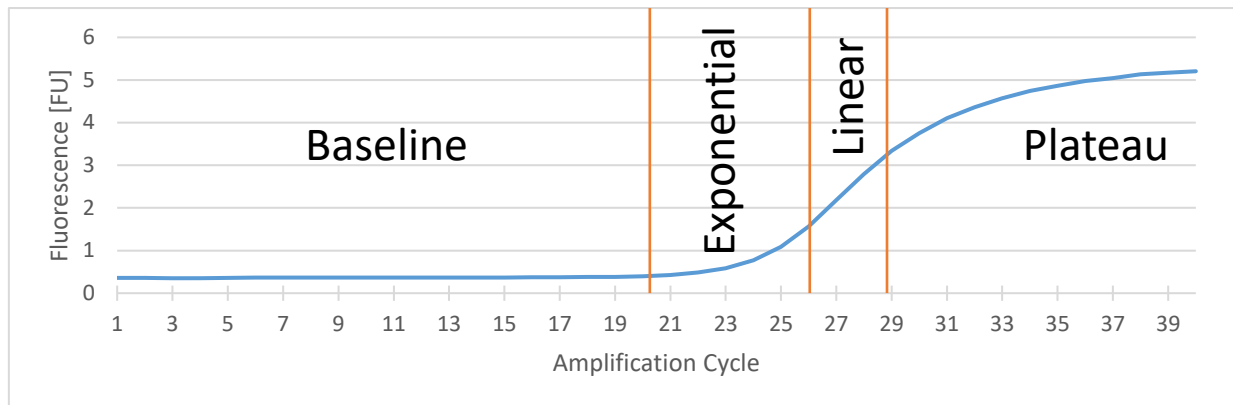


Figure 4: Depiction of the four phases in real-time PCR: baseline, exponential, linear, plateau.

Although absolute quantification of gene expression is possible using real-time PCR, a standard curve had to be generated for this purpose. But since the target of this thesis is to compare changes of gene expression between samples, relative quantification is more suitable.

Many variables influence the experiment, including small variations during extraction and in sample quality. To eliminate these variations and normalize the results, the expression of a house-keeping gene is analysed additionally. This kind of gene were found to be expressed in a constant manner in cells of the same tissue. Examples for commonly used house-keeping genes are glyceraldehyde 3-phosphate dehydrogenase (*GAPDH*), which is crucial for glycolysis and ATP-generation, or α -tubulin (*TUBA*) and β -actin (*ACTB*), that are both necessary parts of the cytoskeleton. In this thesis *GAPDH* was applied as reference gene, since it is most commonly used [124–126].

3.4.3 Melting analysis

An additional advantage of the nonspecific signals from intercalating dyes (see 3.4.3) is the possibility of melting analysis after the PCR is finished. It can be used as a control of the correct amplification based on the known amplicon sequence. The temperature of the sample is increased by small increments while the fluorescence is measured after each step. Depending on the amplicon properties, especially GC-content and length, dsDNA is separated into two ssDNAs at a certain melting temperature. Therefore, the fluorescence of the dsDNA intercalating dye is terminated once a threshold is reached [127–129].

The result is a graph that displays the obtained fluorescence as function of applied temperature. If more than one amplicon or a false one was generated, it can be seen by additional or shifted curves. For more comprehensible results the first negative derivative is applied to display melting peaks of amplicons, which are more informative than the inflection points in the originally recorded curve (compare to Figure 5) [130].

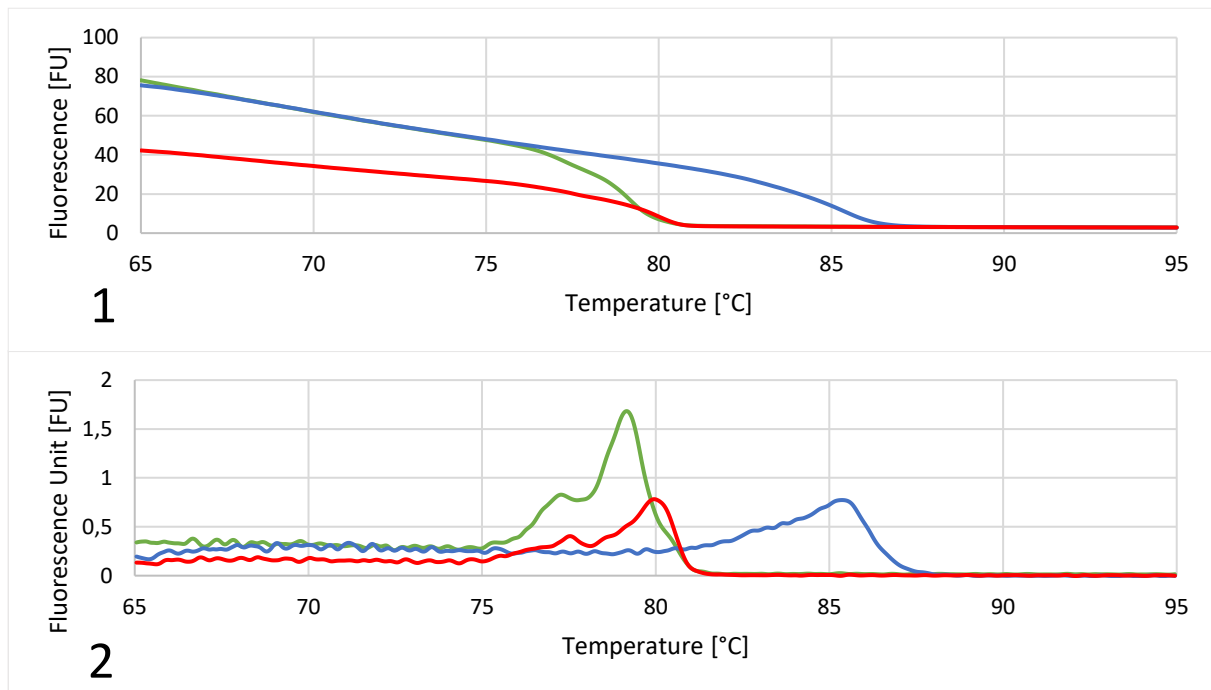


Figure 5: Comparison between melting curve (1) and derivative (2).

3.5 Agarose gel electrophoresis

Gel electrophoresis is a method that allows qualitative verification of nucleic acids and proteins. The method relies on separation of macromolecules by size or charge. A charged analyte is loaded into pockets of a gel and the application of an electric current induces the migration through the dense gel meshwork. The density can easily be adjusted by changing the ratio of the reagents during the preparation of the gel, depending on the size of the analyte of interest. The main components are monomers that polymerize to a meshwork. In agarose gel electrophoresis, for the separation of DNA, the applied concentration of agarose determines the density of the meshwork. When preparing polyacrylamide gels, which is mainly used for protein analysis, additional reagents change the density. For example, the amount of the polymerisation starter ammonium persulfate and the cross-linking agent bisacrylamide have a strong influence.

During gel electrophoresis the gel is covered by a buffer that keeps pH constant and is crucial for the flow of the electric current. While small fragments can migrate faster through the meshwork of the gel, bigger ones are retained. Therefore, molecules of different sizes are separated effectively over time.

Regarding DNA analysis, the negatively charged phosphate backbone causes the migration in an electric field towards the anode. A ladder, containing oligonucleotides of various known

lengths, is applied in parallel to the samples. Additionally, a loading buffer must be added to the ladder and the samples prior to loading. It contains a dye that has nearly no hindrance in the gel and allows the determination of the distance the samples have migrated. Loading buffer also contains glycerol, which has the purpose of increasing the sample mass. In this way, DNA does not dissolve into the surrounding buffer, but sinks down into the gel loading pocket. After completion of the electrophoresis, DNA is visualized by an intercalating dye that emits fluorescence under UV-light. Usual methods include incubation of the gel with ethidium bromide. Alternatively, non-toxic dyes like SYBR-green and gel-red are added to the sample during sample preparation [131,132].

3.6 Bisulfite conversion

Methylated and unmethylated cytosine cannot be discriminated by DNA polymerase. To differentiate between them in CpG sites, bisulfite conversion is performed, which converts unmethylated cytosine into uracil (Figure 6). By incubation with bisulfite the base is sulphonated (2) and subsequent hydrolytical deamination converts cytosine into uracil (3). The base is then desulphonated (4). The last step is the most important since uracil sulphonate residues may inhibit DNA polymerase in subsequent reactions. Methylated DNA cannot undergo the initial sulphonation, because the additional group blocks the position (5) [133,134].

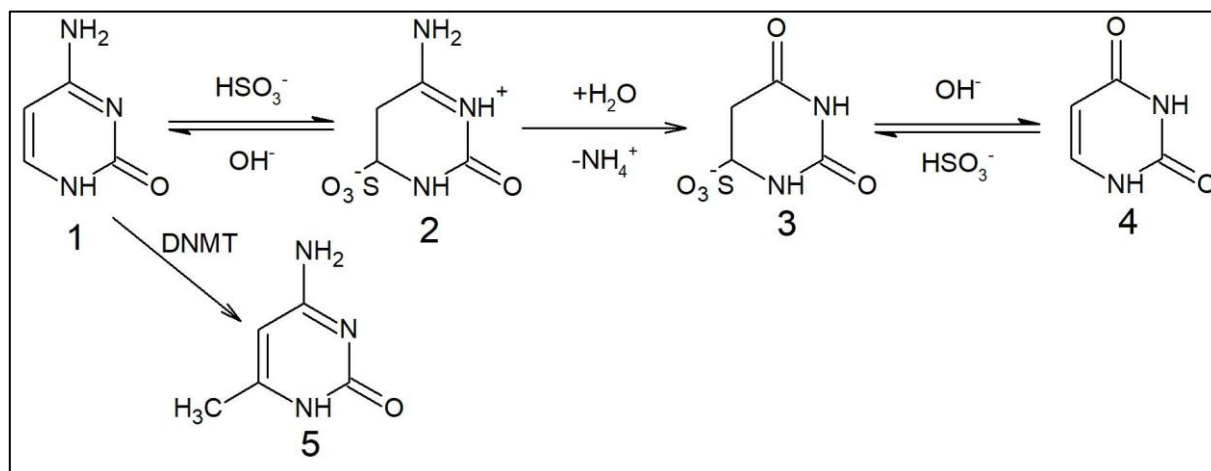


Figure 6: Reaction mechanism of bisulfite conversion (Source: Shapiro et al. [134], 1= Unmethylated cytosine, 2= Cytosine sulphonate, 3= Uracil sulphonate, 4= Uracil, 5= 5-Methylcytosine, DNMT= DNA-methyl-transferase).

Depending on the methylation status, the cytosine in a CpG dinucleotide is present as cytosine or uracil after the conversion. Because DNA polymerase can incorporate thymine but not uracil, the latter one is replaced in a subsequent PCR. This creates an altered sequence at unmethylated CpG positions [135].

DNA degradation is a major risk when using this technique, due to the salt concentrations that must be applied. It was found that depurination is the main cause of strand break during this procedure [136]. The reagents used in this reaction also shift the light absorption properties, which complicates measuring the DNA concentration (see section 3.3). For these reasons purification of converted DNA is an additional necessary step.

3.7 Pyrosequencing (PSQ)

Pyrosequencing relies on sequencing by synthesis and is capable of detecting changes in single nucleotides. Similar to PCR, a polymerase-mediated incorporation of nucleotides takes place to complement the analysed template strand. One of the major differences is the sequential addition of only one kind of nucleotide to the complement strand. The incorporation of nucleotide is recorded by measurement of light emission and gives insight into the analysed sequence.

Prior to the sequencing reaction, the target sequence must be amplified by PCR. Subsequent denaturation of the double stranded amplicon enables annealing of a sequencing primer. The primer is complementary to the sequence of interest within the amplicon and determines the starting site for sequencing. For the key reaction, polymerase, which lacks proofreading function (3' to 5' exonuclease activity), is added together with a mixture of enzymes and substrates that are necessary for signal detection. They comprise of the enzymes luciferase, sulfurylase, apyrase and the substrate adenosine phosphosulfate (APS) [137,138].

Although *de novo* sequencing is possible using this technique, it is uncommon, because only relatively short sequences can be analysed compared to other methods. If the sequence that follows the sequencing primer is known, dNTPs, which are corresponding to the expected sequence, are dispensed sequentially. This is the case in methylation analysis or investigation of single nucleotide polymorphisms (SNPs). Dispensation of the correct nucleotide leads to incorporation by the polymerase, which releases adenosine monophosphate (AMP) and pyrophosphate (PPi). Under the consumption of APS, PPi is converted into adenosine triphosphate (ATP). This energy-rich molecule is consumed by luciferase, which causes light emission (see Figure 7) [138]. To avoid the reaction of sulfurylase with dispensed ATP for incorporation, deoxyadenosine alphathio triphosphate (dATP α S), a derivative that cannot be used as substrate by the enzyme, is applied for sequencing. The obtained signal intensity is proportional to the number of same nucleotides that are incorporated subsequently. Excessive nucleotide is degraded by apyrase after the reaction to prepare for the next incorporation [137].

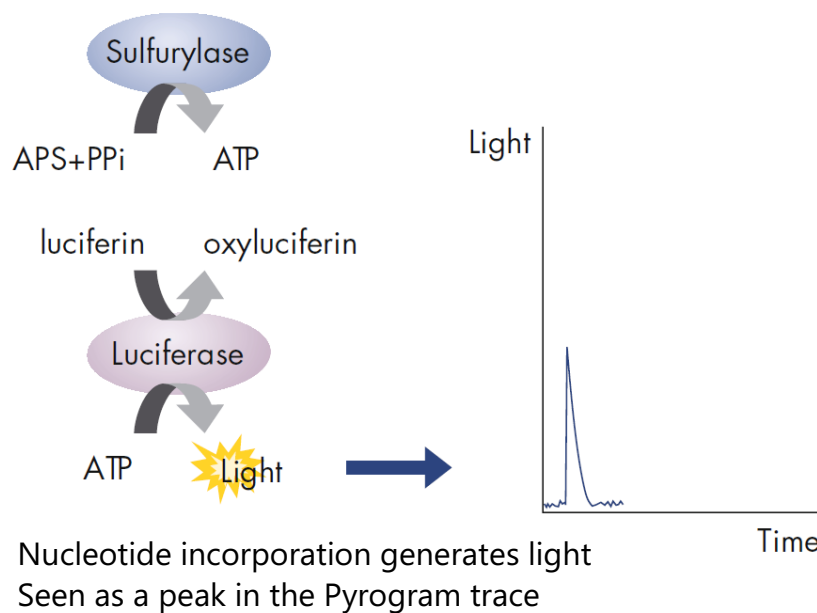


Figure 7: Depiction of the processes during pyrosequencing and the generation of signals (modified from Kreutz et al. [138]).

In the case of methylation studies, the DNA is bisulfite converted, which creates variable positions of either cytosine or thymine in CpGs. For discrimination purposes, the two bases are added one by one to investigate which of them is incorporated. Thymine thereby indicates an unmethylated cytosine in the original DNA. The methylation degree is determined by the signal ratio between incorporated thymine and cytosine at the same position.

A bisulfite control at the position of a non-CpG cytosine is also implemented in the assay. If cytosine is falsely incorporated at this position instead of thymine, it is an indicator that bisulfite conversion was not complete and the results in variable positions are unreliable. Due to the correlation between signal intensity and the number of subsequently incorporated nucleotides, a pyrogram is obtained. It is compared with a histogram that displays the theoretical pattern based on the ratio of nucleotides that should be incorporated subsequently in the known sequence. If the peak heights vary strongly from each other, despite incorporating the same number of nucleotides, the results are not reliable. The same is the case when the obtained signal pattern generally deviates from the histogram. However, a trend of slowly declining baseline is normally observed, due to dilution of the reaction mix during the experiment [138,139].

4 Results & discussion

The aim of this thesis was to investigate if learning and aging is associated with changes in gene expression and DNA methylation of certain genes in *Rattus norvegicus*. The four target genes *IGF1R*, *FMR1*, *DCX* and *GRM5* were previously linked to memory formation. Twenty animals were raised for 22 months and trained in a radial arm maze. They were grouped by their learning performance. Hippocampal subregions CA1, CA3 and DG were then taken for analysis and samples from 6 animals with the best/worst performance were further analysed. Additional samples from a group of six control animals that were 17 weeks old and received no training were also analysed (section 6.2). Biological components RNA, DNA and proteins were extracted from the samples via trizol extraction (section 6.3). RNA was immediately reverse transcribed into cDNA and the relative amount of target mRNA determined by real-time PCR (section 6.4 and 6.5). DNA methylation in promoter regions was analysed by performing bisulfite conversion, conventional PCR and pyrosequencing (section 6.6, 6.7 and 6.9). The protein fraction was given to our cooperation partners for analysis.

PCR and pyrosequencing methods for investigation of the methylation status were developed in this thesis. Primer sequences for gene expression analysis were taken from literature.

4.1 *IGF1R*

4.1.1 *IGF1R* DNA methylation analysis

Design of *IGF1R* primer was performed based on the sequence in NCBI database entry M37807.1. In Figure 8 the position of the primers and the amplicon within the sequence are shown prior to bisulfite conversion. The amplicon is located in the gene's promoter region and allows the determination of the methylation degrees in nine CpGs. The properties of the designed primers and the amplicon are summarised in Table 1.

Primer design was performed in silico, applying all criteria that are explained in section 6.1. They showed no tendency of secondary structure formation. The average melting temperature of forward and reverse primer was 60.4 °C. In addition, the primer pair showed a low probability for homo- or hetero dimer formation.

The resulting amplicons were analysed by using agarose gel electrophoresis, which showed the effects of different annealing temperatures (Figure 9). For both, methylated and unmethylated standard, a specific PCR product was obtained, independent of the annealing temperature. Band intensities did not vary, indicating equal amplification for methylated and unmethylated DNA. Since an annealing temperature of 61 °C resulted in bands with lower intensity (Figure 9, lanes 3/6/9), an annealing temperature of 60°C was used in all further experiments.

Table 2: Loading scheme for the agarose gel in Figure 9 for IGF1R PCR method optimization using a primer concentration of 0.4 μ M (NTC= No-template control).

ID	Methylation Degree [%]	Annealing Temperature [°C]
M	25 bp ladder	
1	0	59.0
2	0	60.1
3	0	61.0
4	50	59.0
5	50	60.1
6	50	61.0
7	100	59.0
8	100	60.1
9	100	61.0
10	NTC	59.0
11	NTC	60.1
12	NTC	61.0

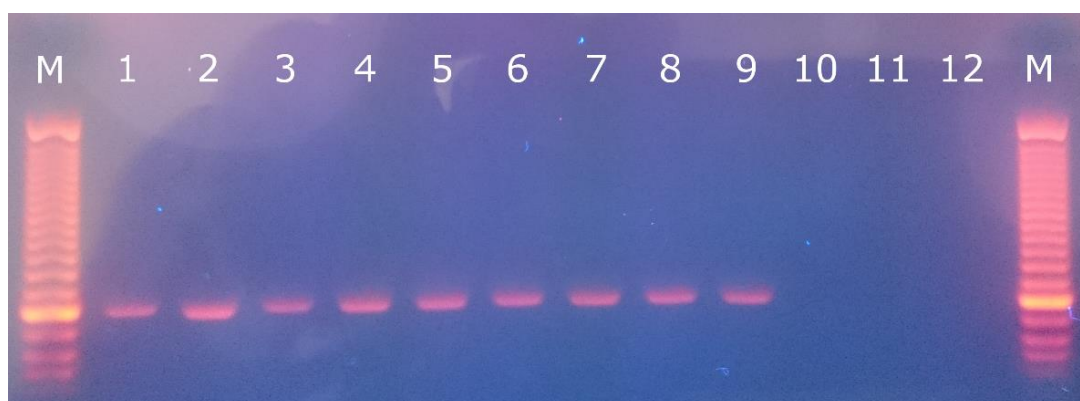


Figure 9: Results of agarose gel electrophoresis for investigating the optimal annealing temperature of IGF1R PCR, using different methylation standards and 0.4 μ M primer concentration. See Table 2 for sample IDs.

Accuracy of the pyrosequencing method was assessed with amplified standards of known methylation degrees (0 %, 50 % and 100 %). The results for the 50 % methylated standard are shown in Figure 10. The histogram, which is the expected peak pattern calculated by the assay design software, is compared to the obtained pyrogram. The pyrogram showed acceptable intensities of single (approximately 300) and multiple peaks. The obtained pattern matched the histogram. The methylation degree of the nine CpGs ranged from 38 to 43 %. These differing results can be traced to the 100 % methylation standard, which was used to generate the 50 % standard. Methylation degrees in the 100 % standard ranged from 87 to 96 % for individual CpGs (see 7.4.3), suggesting that either the standard was not 100 % methylated or the method underestimates the degree.

The developed method supports the methylation analysis of nine CpGs in the promoter region of *IGF1R*.

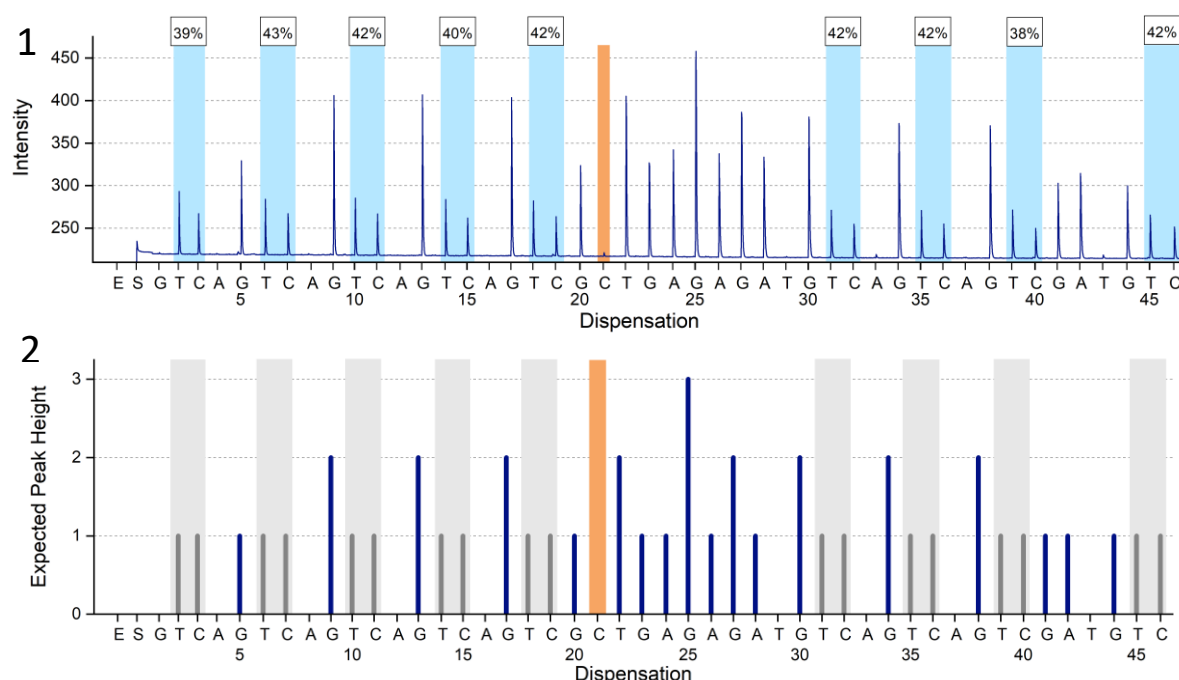


Figure 10: 1= PSQ results for a 50 % methylation standard obtained by the developed method for IGF1R. 2= Histogram showing the expected peak pattern.

4.1.2 IGF1R gene expression analysis

Primer sequences for *IGF1R* cDNA analysis were taken from a paper of Hami *et al.* [140] (see Table 3).

Table 3: Primer and amplicon sequences for gene expression analysis of IGF1R (Green= Positions of forward- and reverse primer, Yellow= Resulting amplicon).

IGF1R Primers for real-time PCR	
CACAAC TACTGCTCCAAAGACAAAATACCCATCAGAAAGTACGCCGATGGTACCATCGATGTGGAGGA GGTGACAGAAAAATCCCAAGACAGAAGTGTGCGGTGGTGATAAAGG GCCGTGCTGTGCCTGTCCTAAAA	
CGAAGCTGAGAAGCAGGCTGAGAAAGGAGGAGGCTGAGTACCGTAAAGTCTTTGAGAATTTCCCTTCAC AACTCCATCTTTGTGCCAGACCTGAGAGGAGGCGGAGAGATGTCCTGCAGGTGGCTAACACCACCAT GTCCAGC CGAAGCAGGAACACCACGGTAGC TGACACCTACAATATCACAGACCCGGAAGAGTTCGAGA CAGAATACCCCTTCTTTGAGAGCAGAGTGGATAACAAGGAGAGGACTGTCATTTCCAACCTC	
Forward Primer:	Reverse Primer:
GCCGTGCTGTGCCTGTCCTAAAAAC	GCTACCGTGGTGTTCTGCTTCG

Gene expression was investigated by determination of the initial amount of mRNA by using real-time PCR and the shown primers. To investigate the functionality of the method, different cDNA dilutions (1:10, 1:50, 1:100) were prepared and used to apply different amounts of template to real-time PCR. Amplification was successful for each sample, regardless of the analysed subregions CA1, CA3 or DG (Figure 11). In subsequent melting curve analysis, a single melting peak (84.4 °C) was observed, indicating that no unspecific products had been formed (Figure 12). A cDNA dilution of 1:10 was chosen for future experiments because it resulted in the lowest Ct-values.

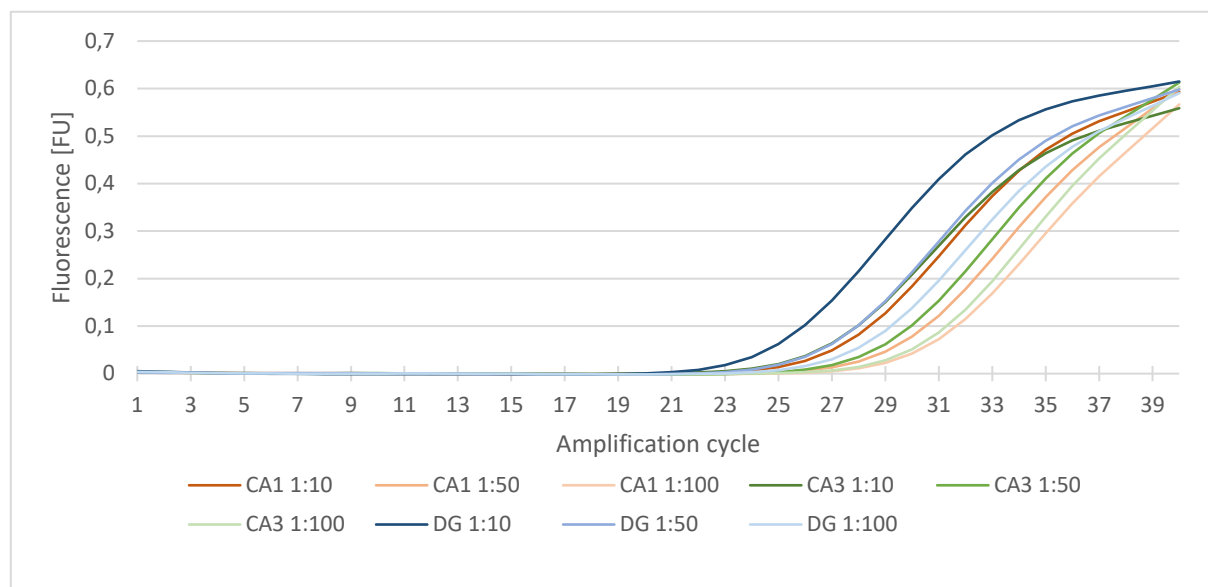


Figure 11: Amplification curves of IGF1R gene expression analysis. Different dilutions of cDNA were applied as template to investigate the optimal starting amount (CA1/3= Cornu Ammonis 1/3, DG= Dentate gyrus).

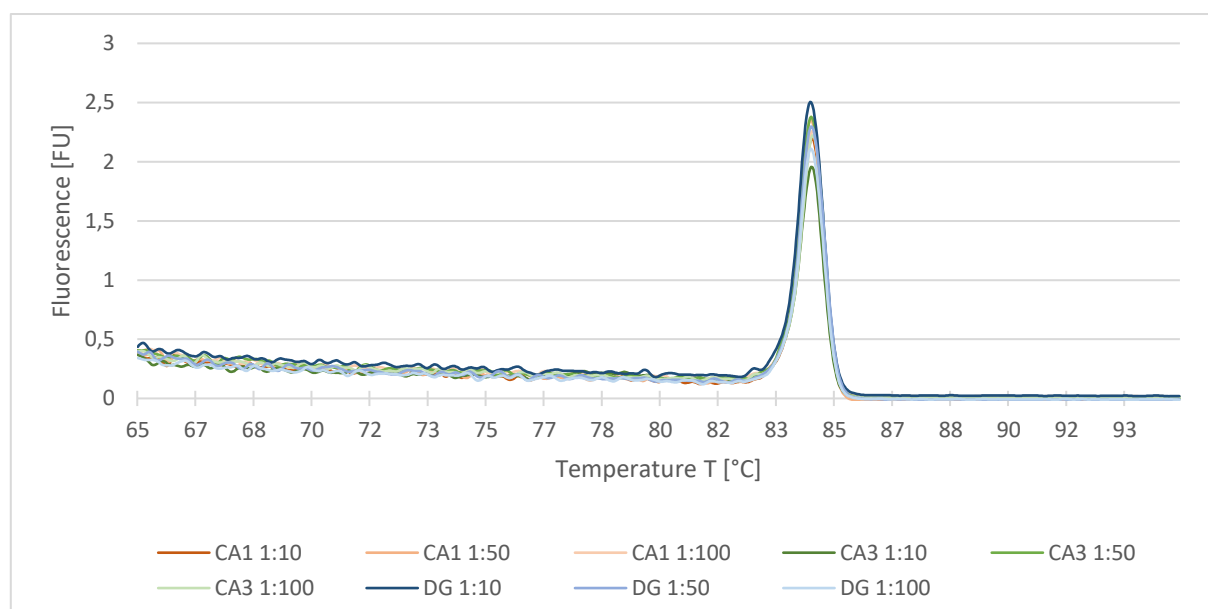


Figure 12: Melt plot obtained after gene expression analysis of IGF1R during method testing (CA1/3= Cornu Ammonis 1/3, DG= Dentate gyrus).

4.1.3 *IGF1R* results and discussion

Subjects of the investigation were tissue samples from 17 animals that showed a difference in memory performance and age. From each rodent the three hippocampal subregions CA1, CA3 and DG were investigated. While the group of aged animals with poor learning performance (OMB) and the young control group (YM) consisted of six subjects each, five animals were categorized as aged animals with good learning performance (OMG).

The developed method was able to determine the methylation degree of nine CpGs in *IGF1R* promoter region. The majority of the analysed samples showed a value that was below the respective limit of detection (LOD), which ranged from 2.0 to 5.8 % for the individual CpGs (see 6.10 and 7.4.3). Only two samples were found to have a DNA methylation degree \geq the LOD (2.0%) in CpG 9. Thus, these findings demonstrated no altered methylation degree due to learning performance or age.

Relative gene expression was examined by applying the $\Delta\Delta C_t$ method and using *GAPDH* as reference gene (see 4.5). Significance tests were performed (see 6.10) to evaluate the levels of relative gene expression between animal groups and hippocampal subregions (Figure 13).

When combining the results from all regions, a statistically significant increase ($p=0.018$) in mean expression levels was found in OMG compared to OMB. No significant differences were found in respect to age or between subregions.

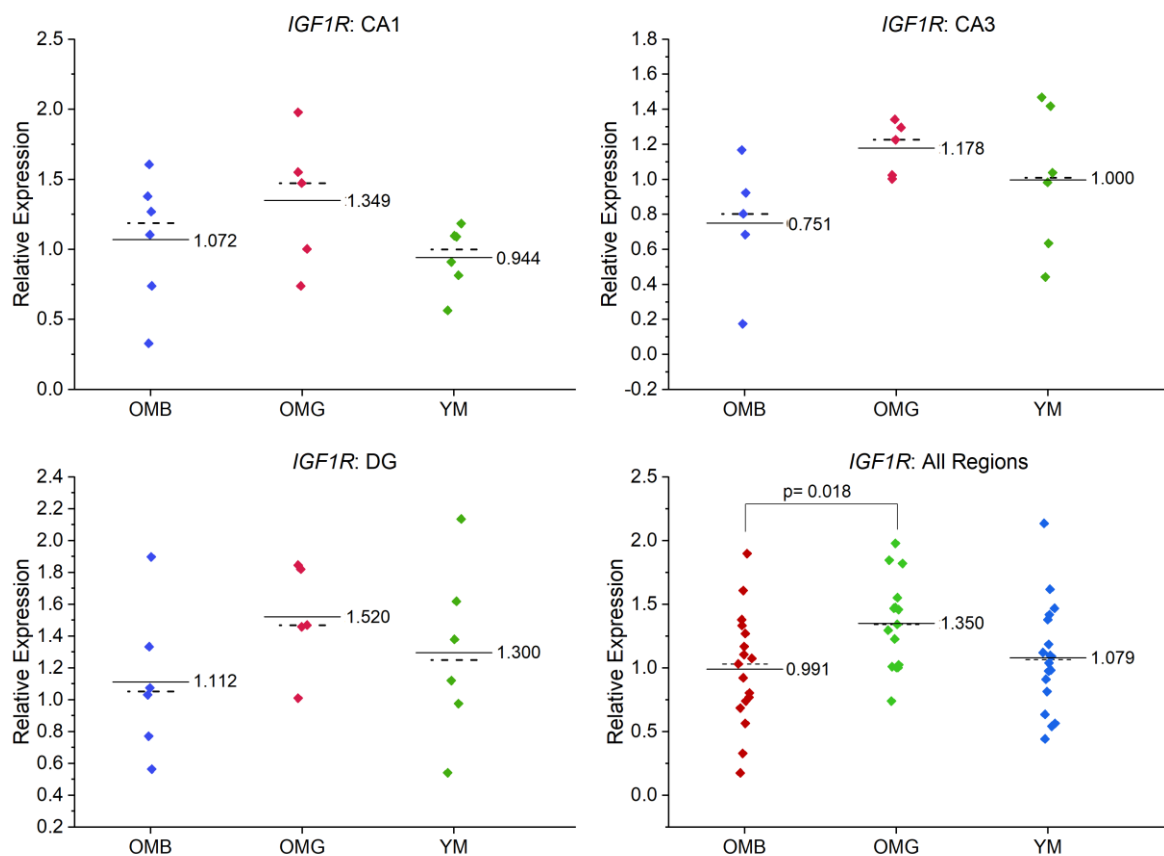


Figure 11: Dot plots of relative *IGF1R* expression sorted by animal group (Solid line= Mean value, dashed line= Median, OMB= Rats with poor learning performance (6 samples), OMG= Rats with good learning performance (5 samples), YM= Young control group (6 samples), CA1/3= Cornu Ammonis 1/3, DG= Dentate gyrus).

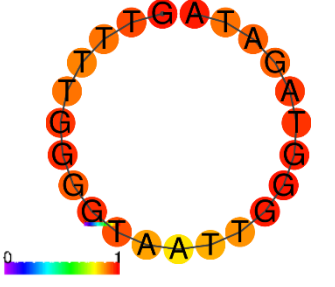
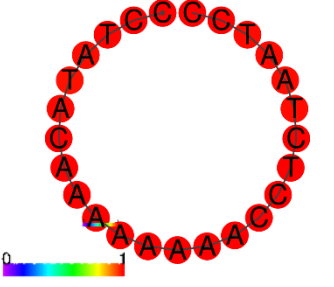

The results suggest that the extent of gene expression was not associated with the DNA methylation degree of the CpGs investigated. Nevertheless our finding that *IGFR1* expression is important for memory formation, is in accordance with results of previous studies [69,70].

4.2 *FMR1*

4.2.1 *FMR1* DNA methylation analysis

Primers were designed to target the promoter region of *FMR1* based on NCBI entry AY630337.1. The primer positions within the sequence before bisulfite treatment are shown in Figure 14, while the properties of the designed primers and amplicon are summarised in Table 4.

Table 4: Properties of the designed primers for *FMR1* PCR and PSQ analysis.

<i>FMR1</i> Primer Set	GCCTTGGGGTAAGTGGGCAGATACTTTGGCGCGCGCTGGG TGAACGCGCGGAAAGCGCAAAGGGTAGTAACAGGTCTGTGCTG CCTATGGCCAGCCGTGGGACTAGAGGCCTTTTGTACAGG		
Forward Primer (F)	Reverse Primer (R)	Sequencing Primer (S)	
Sequence: GTTTGGGGTAATTGGGTAG ATA Melting Temperature: 59.2 °C	Sequence: Biotin- CCTATACAAAAAACCTCT AATCC Melting Temperature: 59.2 °C	Sequence: GGGGTAATTGGGTAGATATT Melting Temperature: 45.3 °C	
			
Amplicon Length: 126 bp		Analysed CpGs: 9	

```

TCCCAGAAGTCAGGGTCAGTGTAGTTATAACTGTTCTTCTACATCAAAGTGTTCTCCAATCGAAGTT
ATCACTTTTAACCTCCCTCCCGCCGCGACTTCCAGTTCAATCAGGTCCCACGCCAGCGCAGTGAA
AAATGTACCCAAAGCCCCCTCCACTTCTGGTTGGGCCCCATTTTCAAAAAGTGGAGGCCTTTTCCC
ACCGTCCTCGCTTCCTCCTGTACAAAAAAGGCCTCTAGTCCCCACGGCTGGCCATAGGCAGCACGA
CCTGTTACTACCCTTTGCGCTTTCCCGCCGTTTACCCAGCGCGCGCGCCAAAGTATCTGCCAGT
TACCCCAAGGCAGGTACCCACGACGCGCGCATCGCGTGCTCAGCTGCCCAAGAGAGAGGGCGGAG
CGAAGGGGGCGGAGCCCATGGGGGAGGGGGCGCCAGGGTCACGTGGTGTCGTTTGACTGTTTACA
GGAGGCGCGGCAGAGCCCTCGGCCTCAGTCAGTCTTCGCTGGGGAGCGTTTCGGTTTCACTTCC
GGTGAGGGGGCGCGCCTGAGAGGGCGGGCAGTGAAGCCAACGACGCGAGCGCGGGCGGTGTCA
GTGACCGCGCGCGCCGCTGCCGGGGGGCGTGCGGTAACGCGGCGGCGGCGGCGAGCGGCTGGGCCTC
GAGCGCCTGCAGCCACCTCTCGGAGGCGGGCTCCCGGCGCGAGGAAGGACGAGAAGATGGAGGA
GCTGGTGGTGGAAAGTGCGGGGCTCCAATGGCGCTTTCTACAAGG

```

Figure 12: Position of FMR1 primers and the generated amplicon within the NCBI database entry AY630337.1 (Green= Forward- and reverse primer, Yellow= Amplicon, Underlined= Sequencing primer, Bold= CpG-position).

Forward and reverse primer were designed to have the same melting temperature of 59.2 °C, in order to fulfil the guidelines described in section 6.1. No tendencies towards secondary products were predicted in silico. Formation of primer homodimers was unlikely, since only four nucleotides were complementary in the middle sequence and in the 5'-ends in forward and reverse primer, respectively. The risk of the formation of heterodimers was equally low, because only five nucleotides in the A and T rich regions showed complementarity.

Rat genome methylation standards with a methylation degree of 0 %, 50 % and 100 % were used to investigate optimal conditions for amplification. Main factor was the annealing temperature, which was investigated by applying 59.2, 60.9 and 62.1 °C. In prior experiments the optimal primer concentration for PCR was determined as 0.4 µM (data not shown).

The generated amplicons were analysed by agarose gel electrophoresis to investigate the effect of annealing temperature on PCR (Figure 15). As it can be seen, no side products were obtained. The only amplicon found had the same length of approximately 126 bp, which matches the expected amplicon length. Amplification was successful at each of the annealing temperatures tested. The methylation degree of the standards did not affect the amplification efficiency. However, an annealing temperature of 62.1 °C resulted in decreased yields, compared to the lower annealing temperatures tested (Figure 15, lane 14-16). Thus, all further experiments were performed at 60.0 °C annealing temperature. Since 60.0 °C was found to be the optimum temperature for *IGFR1* PCR as well, amplification of *IGF1R* and *FMR1* could be performed in one single run.



Figure 13: Results of agarose gel electrophoresis for investigating the optimal annealing temperature of FMR1 PCR using different methylation standards and 0.4 μ M primer concentration. See Table 5 for sample IDs.

Table 5: Loading scheme for the agarose gel in Figure 15 for FMR1 PCR method optimization using a primer concentration of 0.4 μ M (NTC= No-template control).

ID	Methylation Degree [%]	Annealing Temperature [°C]
M	25 bp ladder	
1	NTC	60.9
2	NTC	59.2
3	0%	59.2
4	50%	59.2
5	100%	59.2
6	NTC	59.9
7	0%	59.9
8	50%	59.9
9	100%	59.9
10	0%	60.9
11	50%	60.9
12	100%	60.9
13	NTC	62.1
14	0%	62.1
15	50%	62.1
16	100%	62.1

Amplified genome methylation standards, which were bisulfite converted previously, were used to verify the functionality of the developed pyrosequencing method. The obtained pyrogram did not match the histogram when applying the standard protocol. Single fold peaks showed a high signal intensity of 600 and a strong signal decline over time could be observed. Therefore, the results were rendered unsuitable for any kind of interpretation (results not shown). However, the results could be improved by diluting the applied amount of amplicon 1:3 prior to the experiment (see 6.9 for further information).

By decreasing the amount of amplicon, the signal intensity was reduced, and the peak pattern matched the histogram. As it can be seen the measurement of a 50 % methylation

standard led to methylation degrees of 41-45 % in individual CpG positions (Figure 16). Reason for the difference between measurement and theoretical value may be small deviations in the standard solutions. Methylation degrees in 0 % methylation standard were determined between 2-5 % and in the 100 % methylation standard between 95-98 % (see 7.4.3), Indicating that the actual values differed only slightly from their theoretical methylation degree. This may have caused deviating degrees in the 50 % standard, which was a mix of 0 and 100 % standards.

Nevertheless, the results demonstrated that the developed method worked successfully and enabled the determination of the methylation degree of nine variable positions in the targeted sequence.

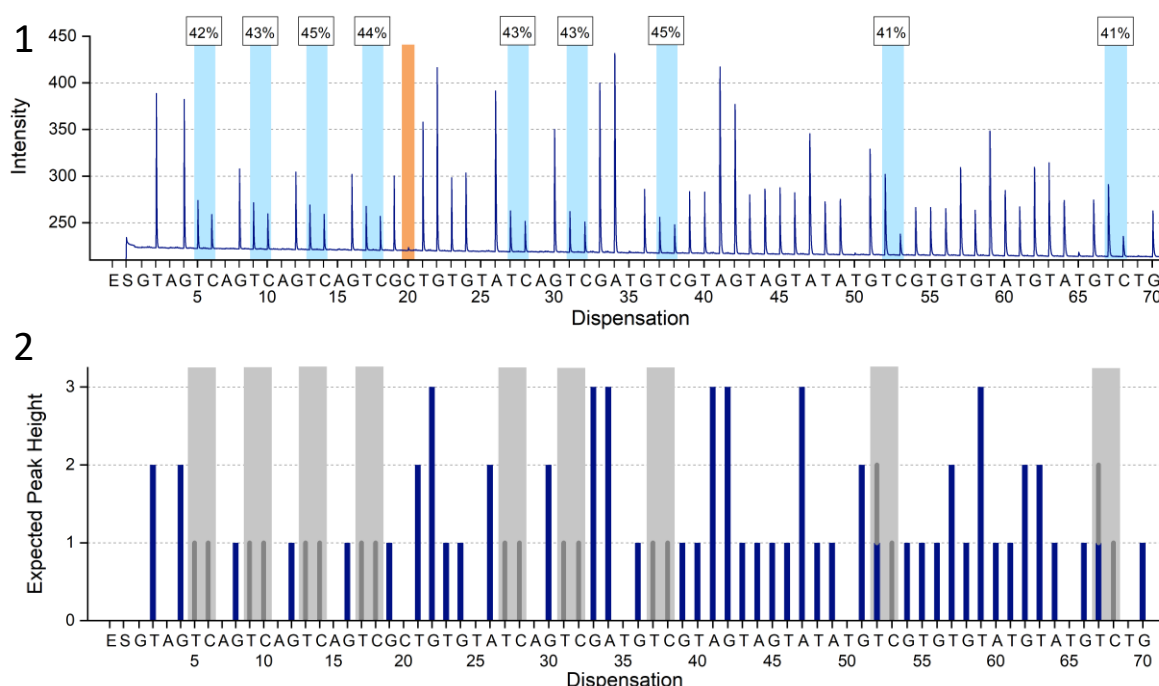


Figure 14: 1= PSQ results for a 50 % methylation standard obtained by the developed method for FMR1 using 1:3 diluted amount of amplicon. 2= Histogram showing the expected peak pattern.

4.2.2 FMR1 gene expression analysis

The primer sequences for gene expression analysis were taken from a publication of Zhang *et al.* [141]. The sequence, position and resulting amplicon are presented in Table 6.

Table 6: Primer and amplicon sequences for gene expression analysis of FMR1 cDNA (Green= Positions of forward- and reverse primer, Yellow= Resulting amplicon).

FMR1 Primers for real-time PCR	
GCGCAGAGGAGACGGACGGCGGCGTGGAGGAGGCGGAAGAGGACAAGGAGGAAGAGGAAGAGGAGGAG GTTTCAAAGGAAATGACGATCATTCCCGAACAGATAATCGTCCACGTAATCCAAGAGAGACTAAAGGA AGAACAACCTGATGGATCCCTGCAGAGCACCTCCA GTGAAGGGAGCCGGCTGCGCACCAGGAAAGATCG GAACCAGAAGAAGGAAAAGCCAGACAGCGTGGATGGGCTGCAACCACTCGTGAATGGAGTACCCTAAA CTACATAATTCTGAAGTTATATTTCTCTACTGTTTCCGTAATTCTTACTCCATTTTAGAAAACTTTA TTAGGCCAAAGACAAATAGTAGGCAAGATGGCACAGGGCATGAGGTGAA CACAAATTCTGCAAAGAAT TTTTTGGATATTGGCCATAATCAACAATCTTCCAAGTTTGACAAAAAGATCTTGAAATTTGAAGCAT AACTTTTAAGTACACTTAACACTTCAGGGCAGGATTTTACTTT	
Forward Primer: ATCCCTGCAGAGCACCTCCA	Reverse Primer: TTCACCTCATGCCCTGTGCC

Gene expression was investigated by applying the shown primers in real-time PCR and melting curve analysis. The cDNA samples were previously reverse-transcribed from extracted RNA of the hippocampal subregions CA1, CA3 and DG. The templates were applied in three different dilutions (1:10, 1:50 and 1:100) to investigate the optimal amount of template (Figure 17). The obtained amplification curves proved successful PCR in each sample. However, two melting peaks were found in melting curve analysis (Figure 18). To check for multiple melting domains in the amplicon, a melting simulation was performed by the online calculator uMelt [142]. Two peaks were predicted for the obtained amplicon, presumably because it is composed of blocks that are either rich in C/G or rich in A/T (Figure 19). They melted independently from each other, resulting in two peaks at 79.8 C° and 84.7 C. Therefore, no undesired side products were formed. Since all dilutions demonstrated equal results, 1:10 was chosen for further real-time PCR experiments in accordance with *IGF1R* expression analysis.

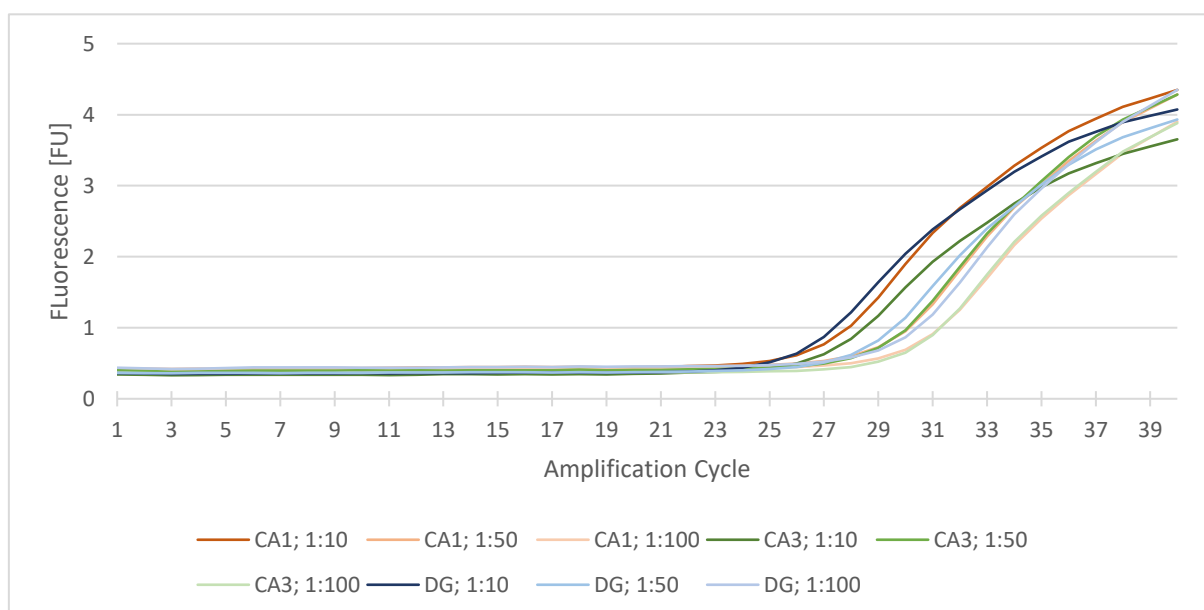


Figure 15: Amplification curves of FMR1 gene expression analysis. Different dilutions of cDNA were applied as template to investigate the optimal starting amount (CA1/3= Cornu Ammonis 1/3, DG= Dentate gyrus).

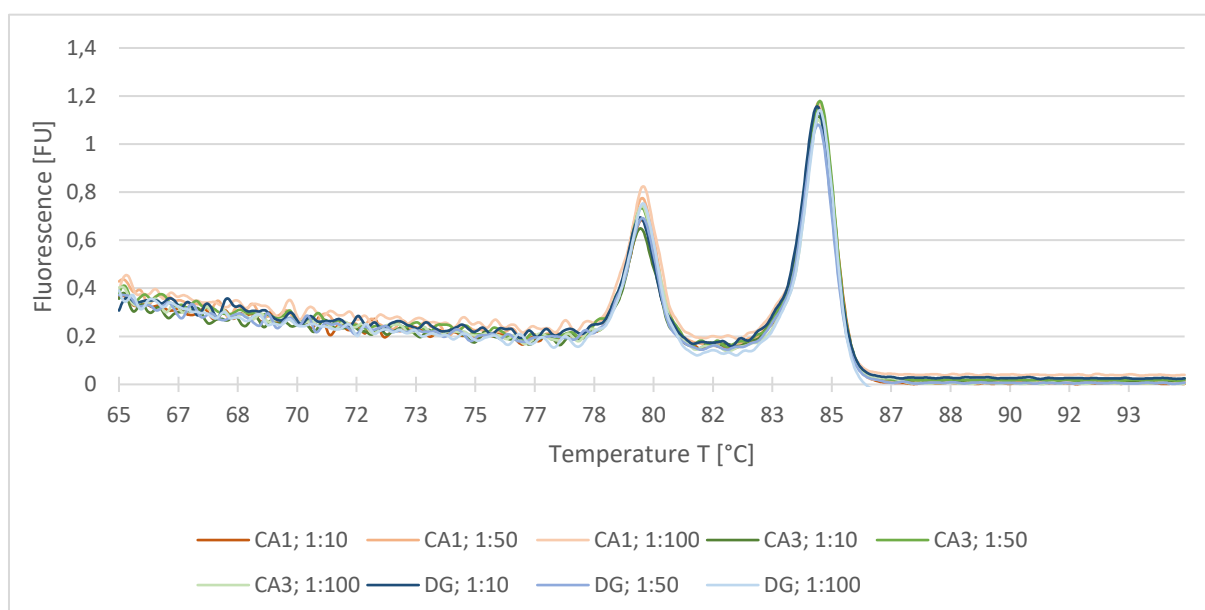


Figure 16: Melt plot obtained after gene expression analysis of FMR1 during method testing (CA1/3= Cornu Ammonis 1/3, DG= Dentate gyrus).

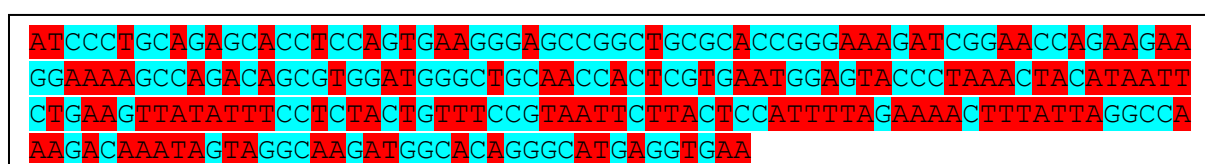


Figure 17: Depiction of FMR1 amplicon from gene expression analysis to show different melting domains (Red= A/T nucleotides, Blue= G/C nucleotides).

4.2.3 FMR1 results and discussion

The developed PCR and PSQ methods were applied to the DNA extracts from the hippocampal subregions CA1, CA3 and DG. Test subjects were five aged rats with good learning performance in the radial arm maze (OMG), 6 aged rats with poor performance (OMB) and six young animals that received no training (YM). Most of the obtained methylation results were below the calculated LOD, which was between 2.0 – 7.2 % for the individual nine CpGs analysed (see 7.4.3) Hence, no statistical difference due to learning or age could be observed when comparing brain regions or animal groups (see 6.10).

GAPDH (see section 4.5) served as reference gene for gene expression analysis. The results (Figure 20) exhibited no significant altered gene expression ($p > 0.05$) in respect to learning performance or aging. When all animal groups were considered, mean expression levels in CA3 were significantly lower than in CA1 ($p < 0.001$) and DG ($p < 0.001$).

In summary no associations between DNA methylation and gene expression levels were observed. The methylation degrees evaluated by pyrosequencing showed no significant differences, while *FMR1* expression was significantly higher in the hippocampal subregions CA1 and DG compared to CA3. These findings may suggest a certain *FMR1* expression pattern in the hippocampus.

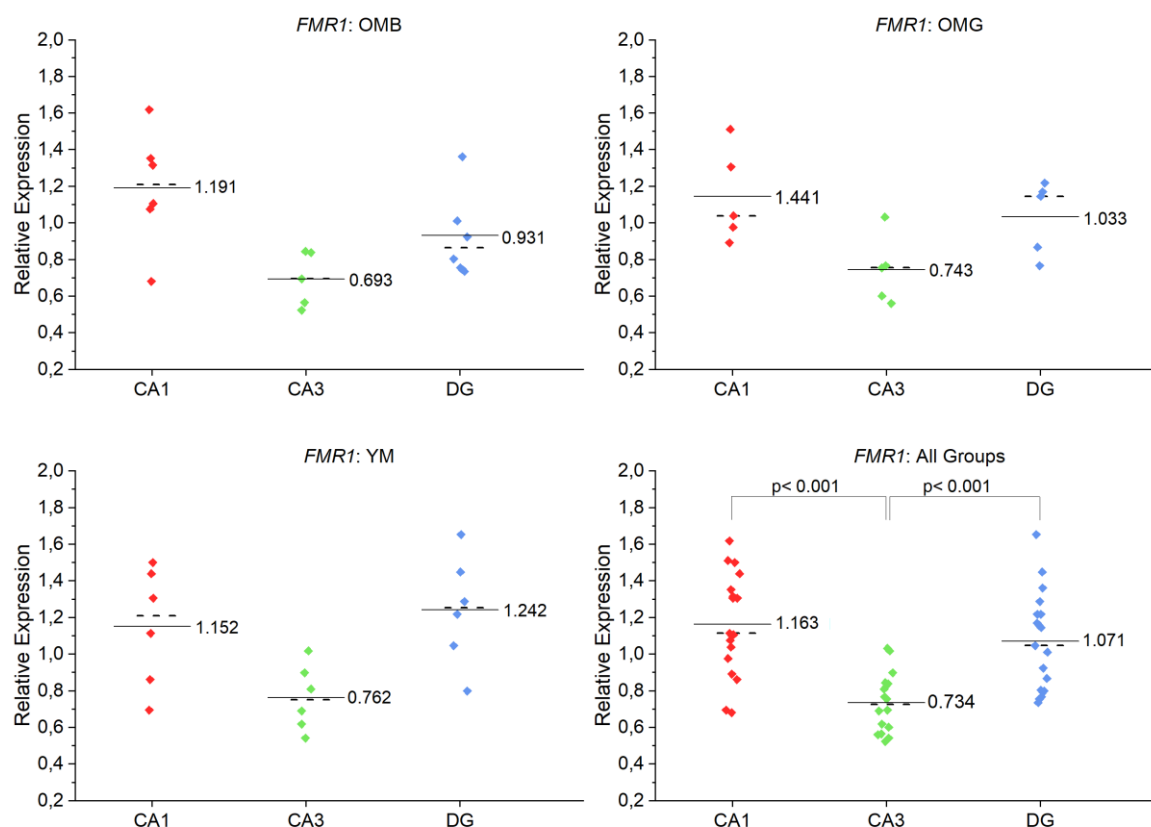


Figure 18: Dot plots of relative *FMR1* expression sorted by animal group (Solid line= Mean value, dashed line= Median, OMB= Rats with poor learning performance (6 samples), OMG= Rats with good learning performance (5 samples), YM= Young control group (6 samples), CA1/3= Cornu Ammonis 1/3, DG= Dentate gyrus).

4.3 DCX

4.3.1 DCX DNA methylation analysis

Sequence data of the DCX promoter region was obtained from entry Rnor_6.0:X:115089017:115183701:1 of ensembl.org (release 92, [143]). Figure 21 shows amplicon and primer positions within the relevant sequence prior to bisulfite conversion. The method development was performed as described in section 6.1 and the features of the final method are summarized in Table 7.

TCCTATCAAATTGTAACCT**CG**GGGCAAAATACATTAAAACTGGCATCTGCTACTTCACACATGGCC
ACATGACTAACAGTTGTAAATGAATCCATAGCCTGACAAAATCCCCTCAAAGAGAAATAGAGGGA
ACTAGCCAAGGTTAGCATCTCCAGCATAGGAAGCAGTCTTTACAACCCAGGACAATGACTAGTAT
GGGGGTGTATTAGTTTTATTTCCAGTCCCTTTTTCTGCTCTAATATGTGTATCCCCTCCCCCA
GAATAAACTAGGATTCTCTTTTAAAGGGACAGCCTCCAGGGAATACCCAGTGTCTTTGTGCTATT
CATCAAACCTCTCTCCATCAAGCTGGTGCTGCTATAC**CG**CATCCATAAGAAGTAGGCTGGGGTC
TAAAAGGGGGGAGGGATTGTCAAAAAACCAGTTATTTAGCAAGCTGTTAGCTCTGCTTTCTCTTT
GATTCCATTTGATCACAGAA**TCCTTTTTCTCCTTTTCAGGTGCTTCA**TCCCCTCCCC**CG**ACCAATGC
AGCGATATCTCTTAATGAAATAATTGG**CG**AAAGATTCCCAAATGA**GTCCCTGAATAGCATATGGG**
ACCTTTTACAAG**CG**AGGACACCTTTTCATTGTTCTGGGTTTCTCCCCTGACTGACAGAACATTTTG
TCCTCAAAGCAGGCAATTCACCTCAAACCTGTCTATTGCTTAGGTGAATTAATGGGGGCAAAAGA
AAAAGGTCATCTGTAAAGCTTGGATTTCACCCCCCTCTACCCCCCCCC**CG**AGCCCATCCCCACCA
GGAAATAAAAAAGAA**CG**CAACAATGAAAACATGCAACCAATAATATAACCAAAGCCT**CG**AC**CG**C
TTACAAAGGTAATAACTTGACATCCAAGAAACCAAACTATTAGCATTTCATCTCACAGATGGAGGA
AAAAGACTCACAAAGCAAGAGGACTCAGCTGCAATACACTGCCACATCAAGATTGCAAGGAAC**C**
GGGGAGACAGGAGATAAAAGGGGGCTGGTAGCTGGTCTATTTGCCAGGTT**CG**GTCCCCCTTTTT
CTCCAGTGTC

Figure 19: Position of DCX primers and the generated amplicon within a section of the reference sequence Rnor_6.0:X:115089017:115183701:1 (Green= Forward- and reverse primer, Yellow= Amplicon, Underlined= Sequencing primer, Bold= CpG).

Table 7: Properties of the designed primers for DCX PCR and PSQ analysis.

DCX Primer Set	TCCTTTTTCTCCTTTTCAGGTGCTTCA TCCCCTCCCC CG ACCAA TGCAG CG ATATCTCTTAATGAAATAATTGG CG AAAGATTCCC AAATGAGTCCCTGAATAGCATATGGGACCTTTAC		
Forward Primer (F)	Reverse Primer (R)	Sequencing Primer (S)	
Sequence: GTAAAGGTTTTATATGTTATT TAGGGAT Melting Temperature: 59.9 °C	Sequence: Biotin- TCCTTTTTCTCCTTTCAAATAC TTCA Melting Temperature: 60.1 °C	Sequence: TTATTTAGGGATTATTTGGG AA Melting Temperature: 53.9 °C	
Amplicon Length: 118 bp		Analysed CpGs: 3	

The calculated difference in melting temperature of forward and reverse primer was 0.2 °C, while showing a mean temperature of 60.0 °C. A performed in silico simulation revealed no secondary structures and no risk of dimer formation. Because the promoter region of *DCX* has a low density of CpG dinucleotides, the target sequence only contains three CpGs.

To optimize the conditions for PCR, an amplification of 0 %, 50 % and 100 % genome methylation standard was performed. Several annealing temperatures (57.0, 59.0, 60.3 and 61.2 °C) were assessed with two different primer concentrations (0.2 and 0.4 µM). The resulting amplicons were analysed by agarose gel electrophoresis (Figure 22).

As it can be seen, signal intensity was higher in samples obtained with a primer concentration of 0.4 µM, which indicates an increased amount of amplicon (Figure 22, lanes 13-24). Therefore, this concentration was chosen for future experiments. Only one band is visible in each lane, corresponding to a sequence of approximately 118 bp, which is the expected length of the amplicon. This indicates successful amplification of the target sequence without undesired side products. The signal intensity is equal for methylated and unmethylated standards, which suggests equal amplification independent from the methylation degree. High annealing temperatures are favourable but application of 61.2 °C annealing temperature resulted in a decreased signal intensity and thus a reduced amount of amplicon (Figure 22, lane 23-34). Therefore, the second highest assessed temperature (60.3 °C) was chosen for further experiments, which is in accordance with the amplification settings of *FMR1* and *IGF1R* (see above).

Table 8: Loading scheme for the agarose gel in Figure 22 for DCX PCR method optimization (NTC= No-template control).

ID	Primer Concentration [µM]	Methylation Degree [%]	Annealing Temperature [°C]
M	25 bp ladder		
1	0.2	NTC	57.0
2	0.2	0%	57.0
3	0.2	100%	57.0
4	0.2	NTC	59.0
5	0.2	0%	59.0
6	0.2	100%	59.0
7	0.2	NTC	60.3
8	0.2	0%	60.3
9	0.2	100%	60.3
10	0.2	NTC	61.2
11	0.2	0%	61.2
12	0.2	100%	61.2
13	0.4	NTC	57.0
14	0.4	0%	57.0
15	0.4	100%	57.0
16	0.4	NTC	59.0
17	0.4	0%	59.0
18	0.4	100%	59.0
19	0.4	NTC	60.3
20	0.4	0%	60.3
21	0.4	100%	60.3
22	0.4	NTC	61.2
23	0.4	0%	61.2
24	0.4	100%	61.2

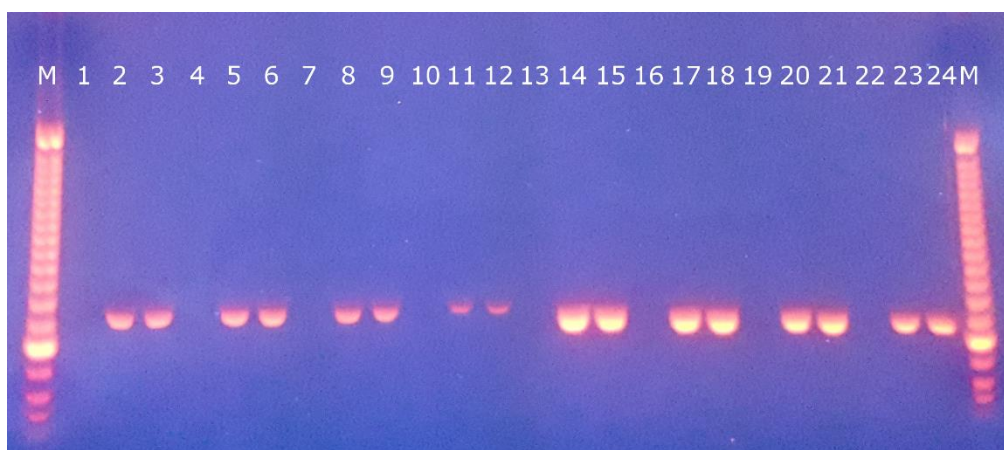


Figure 20: Results of agarose gel electrophoresis for investigating the optimal annealing temperature and primer concentration of DCX PCR using different methylation standards. See Table 8 for sample IDs.

Methylation degrees of the obtained amplicons were analysed by pyrosequencing. The developed method is able to determine the methylation degree of three CpG in the promoter region of *DCX* (Figure 23).

By analysing a 50 % methylation standard, the method determined methylation degrees of 43 % in all positions. While methylation degrees in a 0 % methylation standard were determined accurately, reliable results of a 100 % standard were 92 and 94 % for CpG2 and CpG3 (see 7.4.3). Since the 50 % methylation standard was a 1:1 mix of the two previous ones, this explains the underestimations of the shown methylation degrees.

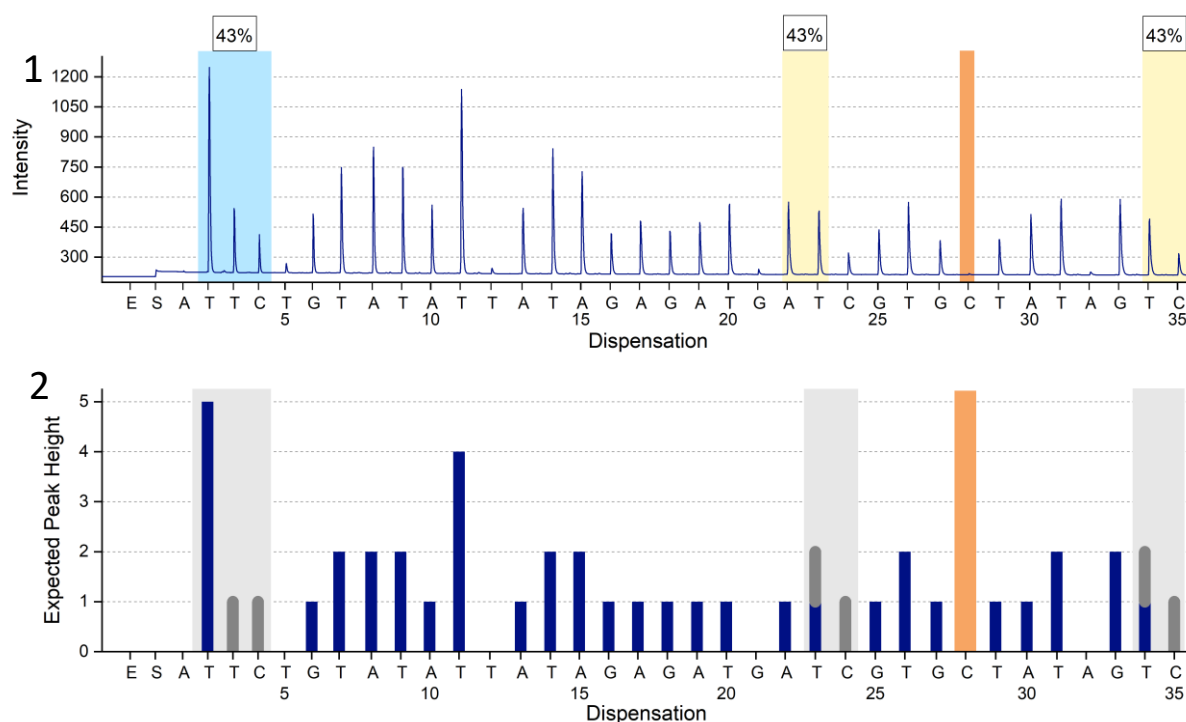


Figure 21: 1=PSQ results for a 50 % methylation standard obtained by the developed method for DCX. 2= Histogram showing the expected peak pattern.

The obtained pyrogram matched the expected histogram while having an acceptable single peak intensity of about 450. But since the first variable position is located after a T-rich region after bisulfite conversion, a 5-fold peak is measured. This poses a problem, because calculation of the methylation degree relies on the ratio between incorporated thymine and cytosine. It is not possible to distinguish between incorporated nucleotides within or outside the CpG. Without other peaks before the CpG that could be taken as reference, the calculation for methylation degree in CpG1 are unprecise and not as reliable as for the other CpGs.

4.3.2 DCX gene expression analysis

Primer sequences for determination of DCX expression were taken from Fu *et al.* [144] (Table 9).

Table 9: Primer and amplicon sequences for gene expression analysis of DCX (Green= Positions of forward- and reverse primer, Yellow= Resulting amplicon).

DCX Primers for real-time PCR	
CACTCTGTAGTATGTAGGGTTTATTTTCTTGAGTCTCTCTTCTGGGCCACTAATTCACATTTACCAA TAAGAGATAGATTGATAACCATCTTTTGAGTGACTTTTCCAGAACTGCAAAATGTGCTAGTCCATGAC CTTTCTACTGAATGCTTAGGGGCCTTTGTATTTTCCCCATTCAATTTGTGCAGAACTAGTCTTTCTT CTCTAGAAGGCTGTTTACGTACACATCGCTTAAAATGTTTATGTGTGGGGGAAAACCTTCATATGCAG ATCTAAAAGTGAAAAACCTAAGTGTCCCTTGCCTCTGTATCTTCAGAATGCTGGAGGATCTCAGGAGA GTGGCAAGTCAGATCCTTGGCCTCACTCGTTGCTCTTAATTGAGCCTCCAGTGTATTGTCTAGCATTC ATTCTGGCTGTTGAGATGGAGAAACACCAGCGACTTCCAATGTGACACCATGTGCTTAAGGCTGTGGT ATCAGACTGGCTGCAAGAGATGAGGTAGAATTTAG	
Forward Primer: ACTGAATGCTTAGGGGCCTT	Reverse Primer: CTGACTTGCCACTCTCCTGA

To investigate the functionality of the primers, real-time PCR and melting curve analysis were performed with different concentration of starting template. Three dilutions (1:10, 1:50, 1:100) of cDNA from the subregions CA1, CA3 and DG were applied (Figure 24 and Figure 25).

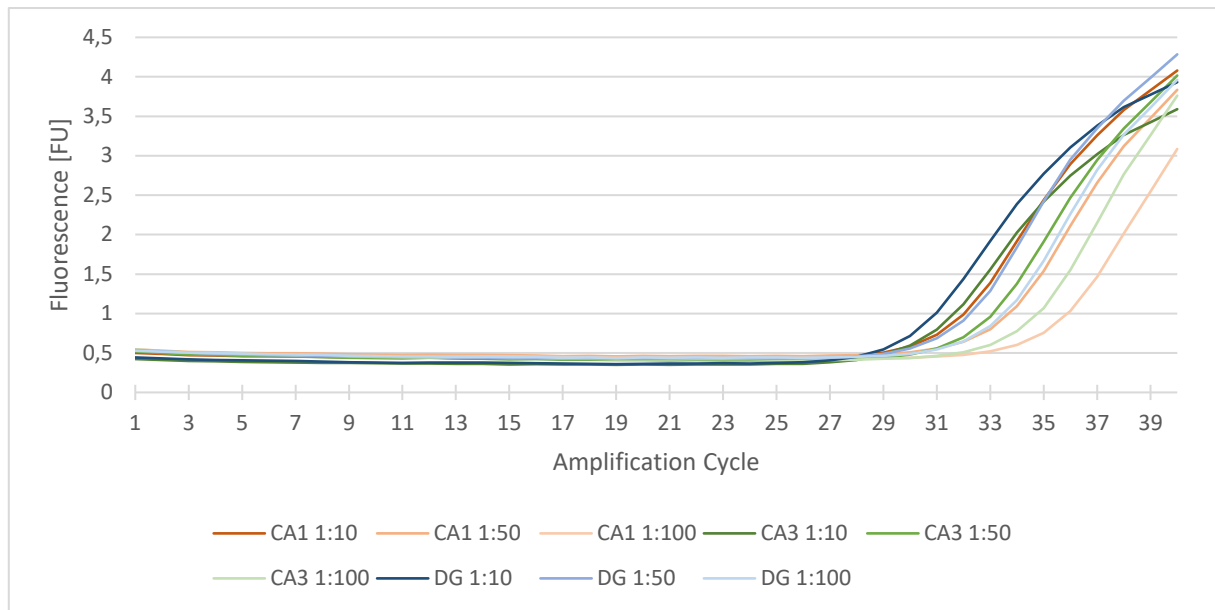


Figure 23: Amplification curves of DCX gene expression analysis. Different dilutions of cDNA were applied as template to investigate the optimal starting amount (CA1/3= Cornu Ammonis 1/3, DG= Dentate gyrus).

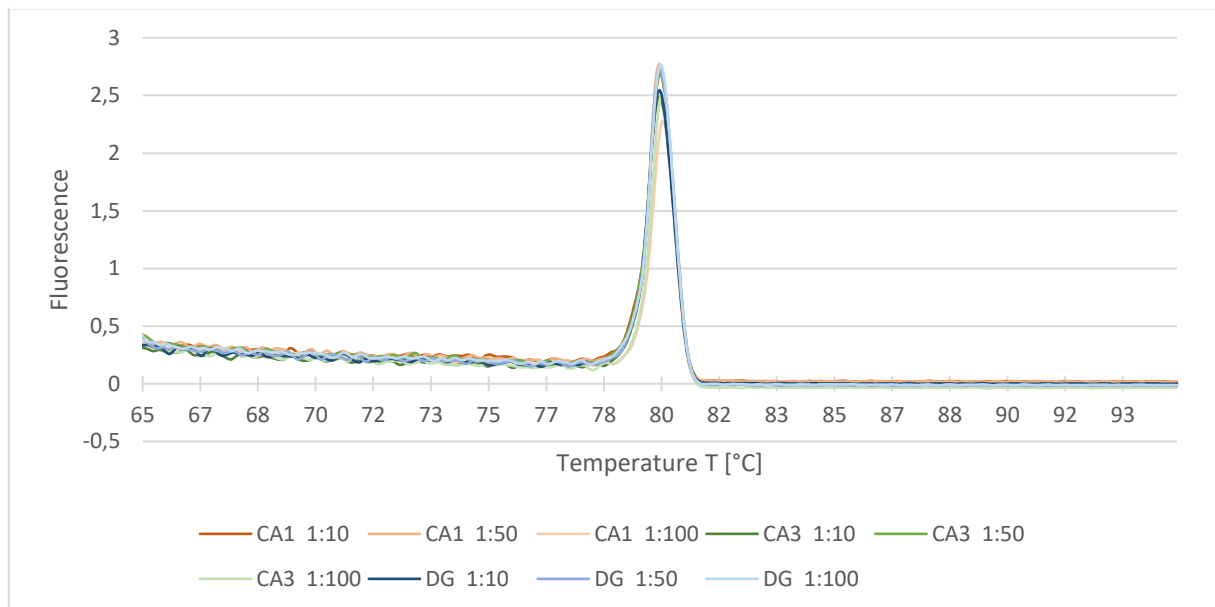


Figure 22: Melt plot obtained after gene expression analysis of DCX during method testing (CA1/3= Cornu Ammonis 1/3, DG= Dentate gyrus).

Amplification curves could be observed for every experiment. Higher Ct-values were obtained by reactions with an increased dilution factor, due to their lower amount of template. The melting diagram revealed a single peak per sample at 80 °C, indicating that no side-products had formed. To maintain continuity with the previous gene expression analysis experiments, a template dilution of 1:10 was chosen for further experiments.

4.3.3 DCX results and discussion

Samples from the hippocampal subregions CA1, CA3 and DG were obtained from 17 *Rattus norvegicus*, that were subdivided into three groups. They comprised of six grown rodents that performed poor in spatial learning (OMB) and five grown animals that showed a good

performance (OMB). The third group consisted of six young animals that received no training as control group (YM).

Each sample showed a certain CpG methylation pattern that could be observed independent from hippocampal subregion or animal group. When considering all groups, the mean methylation degree in the first CpG was 32 %, while the second and third exhibited a degree of 20 % and 17 %, respectively (Figure 27). But it must be emphasized that results for CpG1 are not as reliable as for the other CpGs. The reason for this lies in the five-fold peak as mentioned in section 4.3.1. For this reason, an additional mean value was calculated in the following analysis, which demonstrates the methylation levels without the results from CpG1. Unreliable results were generally excluded from the analysis.

No differences in methylation degrees due to learning or aging could be identified. In contrast the determined methylation showed statistical differences, depending on the hippocampal subregion (Figure 26). Analysis revealed that each single CpG was significantly lower methylated ($p < 0.001$) in DG than in CA1 and CA3. A significantly higher methylation level in CA1 compared to CA3 was only observed in CpG1 and the combined methylation levels for all CpGs.

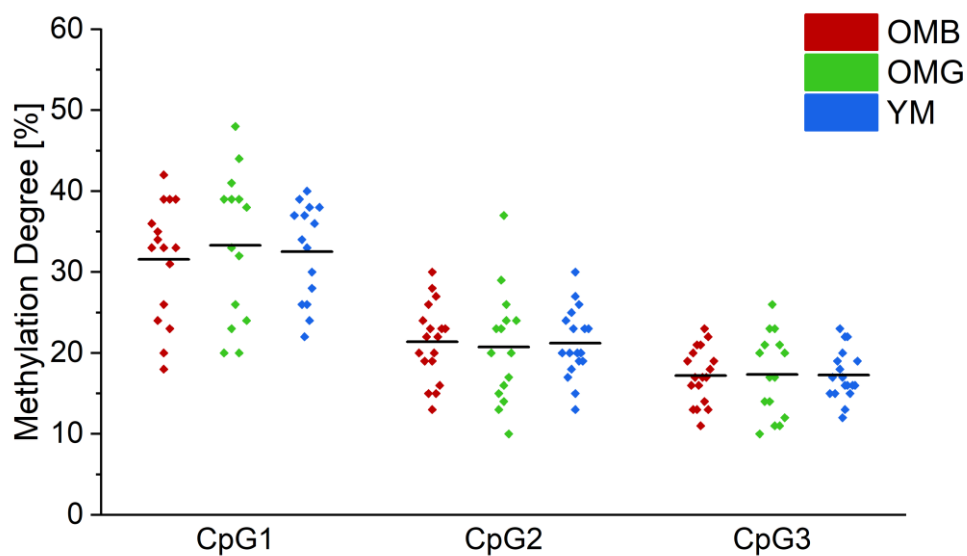


Figure 246: Methylation degree of single CpGs in the DCX promoter in rats. Unreliable results were excluded (Solid line= Mean value, OMB= Rats with poor learning performance, OMG= Rats with good learning performance, YM= Young control group).

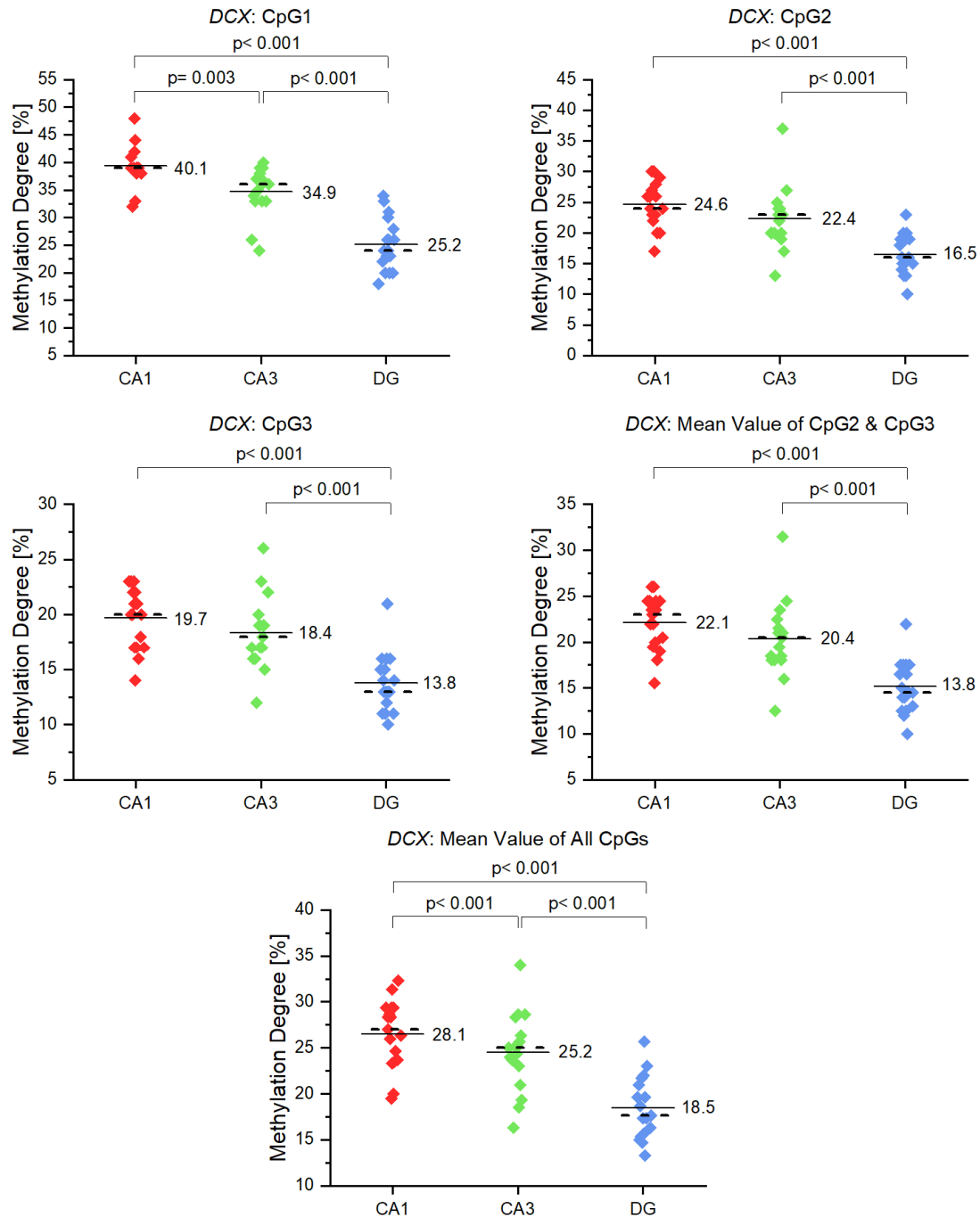


Figure 257: Dot plot of methylation degrees of analysed CpG positions in the DCX promoter region over all groups. Unreliable results were excluded (Solid line= Mean value, dashed line= Median, CA1/3= Cornu Ammonis 1/3, DG= Dentate gyrus).

The relative gene expression was evaluated by real-time PCR (Figure 28). Calculation and significance tests were performed like described in 6.10, while using *GAPDH* as reference gene (see 4.5).

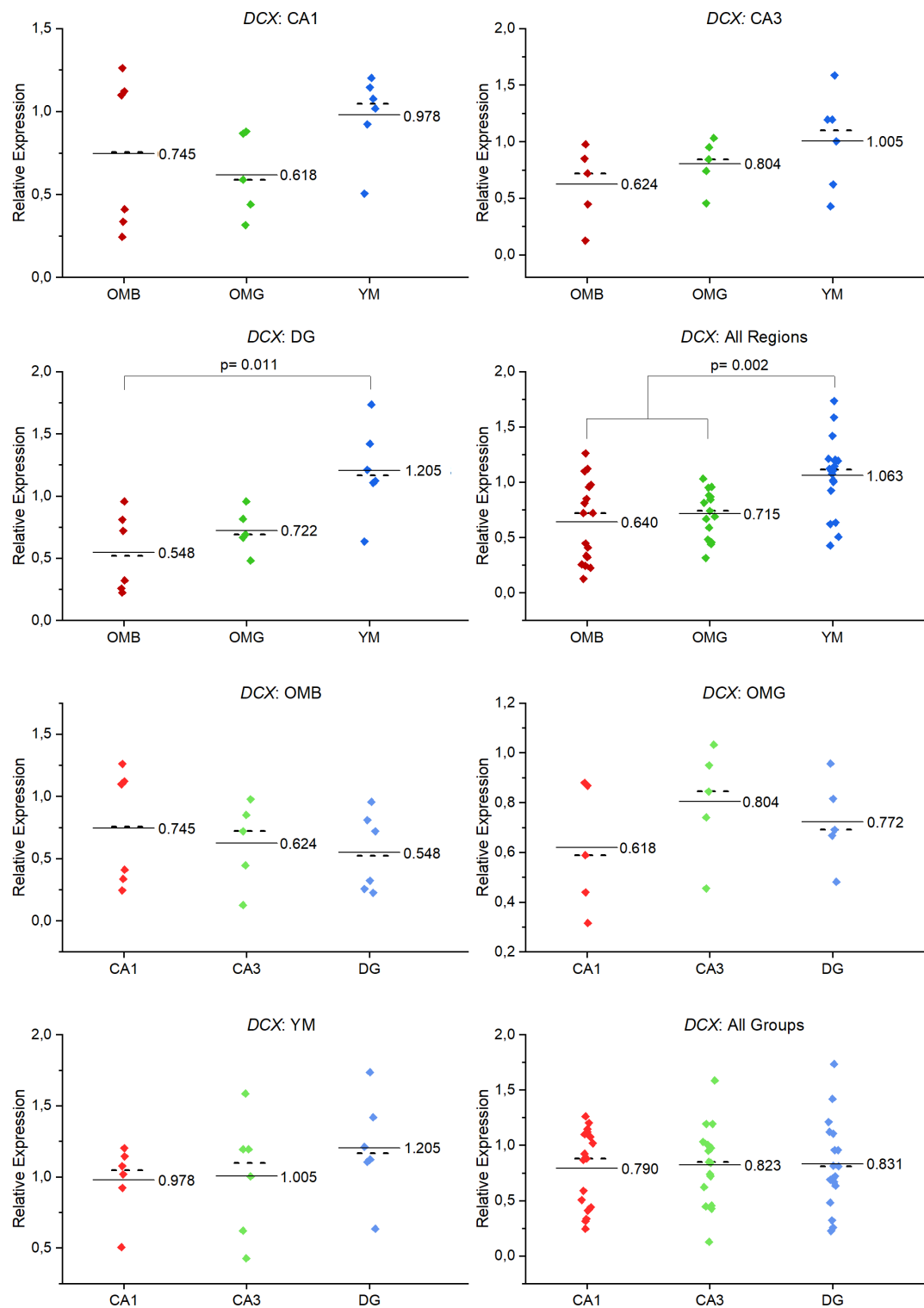


Figure 26: Dot plots of relative DCX expression sorted by animal group (Solid line= Mean value, dashed line= Median, OMB= Rats with poor learning performance (6 samples), OMG= Rats with good learning performance (5 samples), YM= Young control group (6 samples), CA1/3= Cornu Ammonis 1/3, DG= Dentate gyrus).

No significant difference in gene expression ($p < 0.05$) was observed when comparing the mean expression levels from subregions. But *DCX* expression was altered in older animals and especially in OMB. A significant decrease ($p = 0.011$) could be identified in the subregion DG when comparing the mean expression levels from OMB to the control group YM.

Likewise, when comparing the mean value over all regions, aged animals (OMB and OMG) demonstrated a significant decrease ($p=0.002$) compared to YM.

When combining the results from DNA methylation and gene expression analysis, no associations could be concluded. Although a certain methylation pattern was found, neither learning nor aging influenced the methylation degree in the studied part of the promoter sequence. In contrast gene expression was found to be significantly decreased in aged rats, especially in those with bad performance at the learning task. Since *DCX* is a marker gene for neurogenesis, this indicates that the process occurs more frequently in young individuals and during memory consolidation. Considering the examined hippocampal subregions, significant differences were found in DNA methylation. CA1 showed the highest methylation degrees, followed by CA3 and DG. Every investigated CpG showed its lowest methylation degree in DG, while CpGs in CA1 and CA3 exhibited similar results. This trend could not be seen in gene expression analysis, where no statistically significant differences between subregions can be reported.

4.4 GRM5

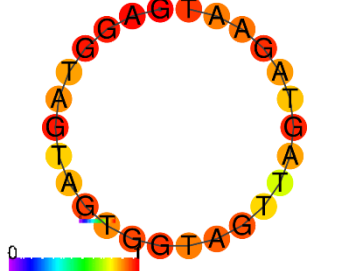
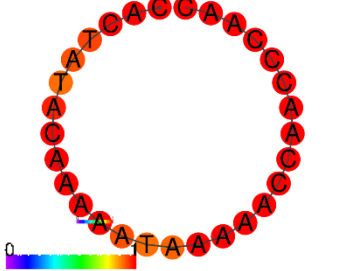
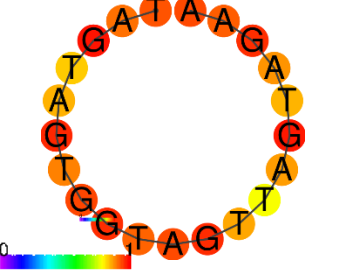
4.4.1 *GRM5* DNA methylation analysis

Primer design for methylation analysis of the *GRM5* promoter region was performed on the sequence in NCBI database entry AH007692.2. The positions of the primers and the generated amplicon are depicted in Figure 29 before bisulfite treatment. Detailed sequence and properties of the designed primers are shown in Table 10.

[illegible]

Figure 27: Position of GRM5 primers and the generated amplicon within the NCBI database entry AH007692.2 (Green= Forward- and reverse primer, Yellow= Amplicon, Underlined= Sequencing primer, Bold= CpG).

Table 10: Properties of the designed primers for GRM5 PCR and PSQ analysis.

GRM5 Primer Set	<p>GCACTGTGCAGGAGTAGGAGCCAGCCCAGCGCTGCGCTTCCA</p> <p>GCTGCGTCTTGCCCGGGCGCAGCACGTGCTCCAGGCGCTGGCG</p> <p>CGAGAGAGCGAGCGAGCGCCACCACCGCGGGCCCGCAGCGGT</p> <p>TCTGCTGGCTGCCACTACTGCCTC</p>		
Forward Primer (F)	Reverse Primer (R)	Sequencing Primer (S)	
Sequence: GAGGTAGTAGTGGTAGTTA GTAGAAT Melting Temperature: 62.9 °C	Sequence: Biotin- CACTATACAAAAATAAAAC CAACCCAAC Melting Temperature: 63.3 °C	Sequence: TAGTAGTGGTAGTTAGTAGA A Melting Temperature: 53.4 °C	
			
Amplicon Length: 149 bp		Analysed CpGs: 15	

The designed primer pair generated a relatively long amplicon of 149 bp. Due to dilution in the reaction vessel during advancement of pyrosequencing, signal intensity declines at the same rate. For this reason it is not recommended to analyse long sequences [139], but nevertheless, experiments confirmed reliable results for all 15 variable positions (see Figure 31). Forward and reverse primer differed only by 0.4 °C in their melting temperature. No secondary structures or dimer formations were predicted.

0 % and 100 % genome methylation standards were used as template to investigate equal amplification efficiency, independent from the methylation degree. To evaluate optimal PCR conditions, different primer concentrations (0.2 and 0.4 µM) and annealing temperatures (59.0, 60.1, 61.0 and 62.3 °C) were applied. The obtained amplicons were analysed by agarose gel electrophoresis (Figure 30).

A single amplicon was obtained in every experiment, and no side-products were identified. Under the same conditions, 0 % and 100 % methylation standards were equally amplified. Experiments with a primer concentration of 0.4 µM (Figure 30, lanes 13-24) had an increased amplicon yield compared to the lower concentration. Although the optimum was determined to be an annealing temperature of 59 °C, 60 °C were chosen for further experiments (Figure 30, lanes 14-15/17-18). The signal intensity was slightly lower and by choosing this annealing temperature, the amplification of all four target genes (*IGF1R*, *FMR1*, *DCX*, *GRM5*) could be performed in a single run.

Table 11: Loading scheme for the agarose gel for GRM5 PCR method optimization (see Figure 30, NTC= No-template control).

ID	Primer Concentration [μ M]	Methylation Degree [%]	Annealing Temperature [$^{\circ}$ C]
M	25 bp ladder		
1	0.2	NTC	59.0
2	0.2	0%	59.0
3	0.2	100%	59.0
4	0.2	NTC	60.1
5	0.2	0%	60.1
6	0.2	100%	60.1
7	0.2	NTC	61.0
8	0.2	0%	61.0
9	0.2	100%	61.0
10	0.2	NTC	62.3
11	0.2	0%	62.3
12	0.2	100%	62.3
13	0.4	NTC	59.0
14	0.4	0%	59.0
15	0.4	100%	59.0
16	0.4	NTC	60.1
17	0.4	0%	60.1
18	0.4	100%	60.1
19	0.4	NTC	61.0
20	0.4	0%	61.0
21	0.4	100%	61.0
22	0.4	NTC	62.3
23	0.4	0%	62.3
24	0.4	100%	62.3



Figure 28: Results of agarose gel electrophoresis for investigating the optimal primer concentration and annealing temperature of GRM5 PCR using different methylation standards. See Table 11 for sample IDs.

The developed pyrosequencing method enables the analysis of 16 CpGs in the promoter region of *GRM5*. The PCR method was used to generate amplicons from methylation standards and their methylation degree was determined by PSQ. The initial results showed, generally high peaks, not matching peak heights and missing peaks in the end of the experiment (results not shown), similar to the first results during *FMR1* method development (compare to section 4.2.1). The problem was solved in the same way by diluting the applied amount of amplicon 1:3. The signal subsequently decreased to a single peak intensity of approximately 350 and a pyrogram that matched the histogram. The exemplary results of a 10 % standard are displayed in Figure 31.

The methylation degrees were within a range of 11 % to 16 %. Since the standard was prepared by mixing 0 % and 100 % standards 1:1, the deviation could be explained by statistical errors during that process. The methylation degrees in individual CpGs of the 0 % and 100 % methylation standards were determined as 0-5 % and 85-100 %, respectively (see 7.4.3).

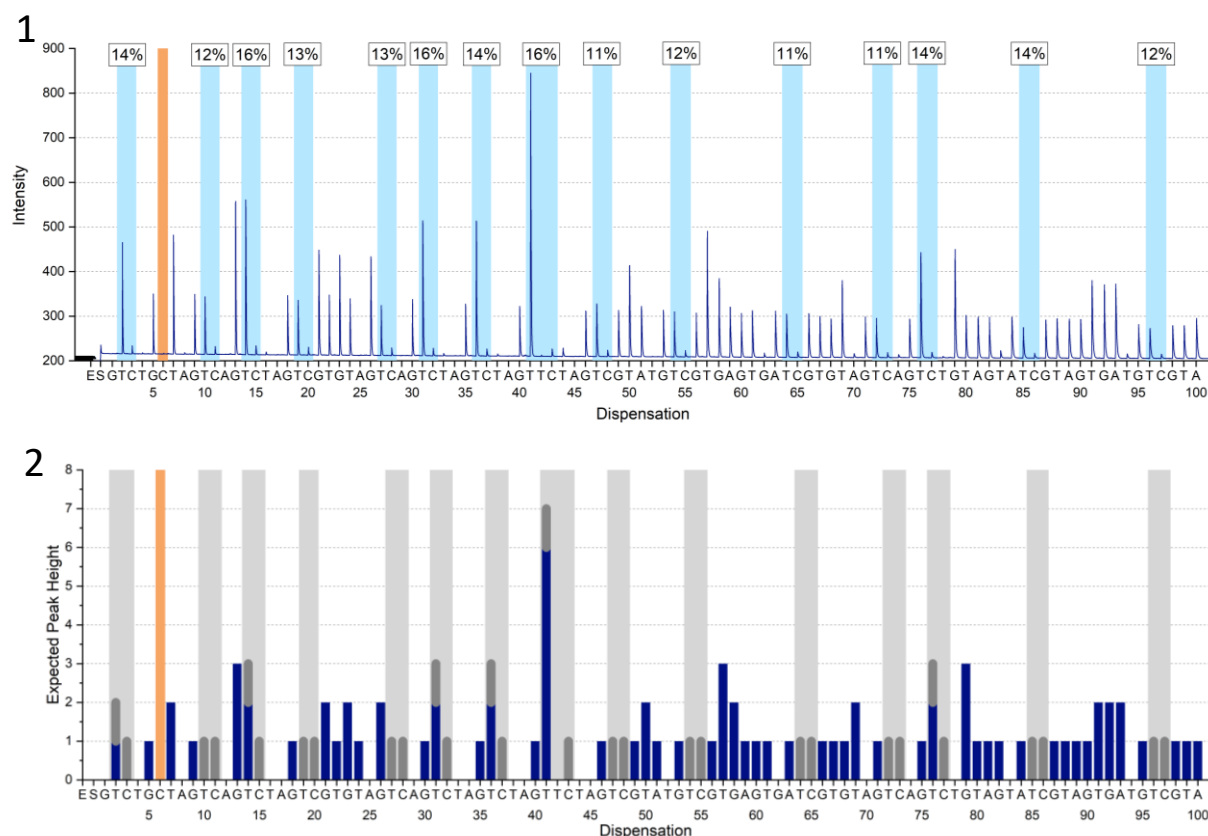


Figure 29: 1= PSQ results for a 10 % methylation standard obtained by the developed method for *GRM5* using a 1:3 diluted amount of amplicon. 2= Histogram showing the expected peak pattern.

4.4.2 GRM5 gene expression analysis

For *GRM5* expression analysis primer sequences were taken from a publication of Cai *et al.* [145]. Their position, the resulting amplicon and the sequence of the primers are shown in Table 12.

Table 12: Primer and amplicon sequences for gene expression analysis of *GRM5* (Green= Positions of forward- and reverse primer, Yellow= Resulting amplicon).

GRM5 Primers for real-time PCR	
GATTTGCATCGCCCACTCTTACAAAATTTACAGCAATGCTGGGGAACAGAGCTTTGACAAGCTGTTGAAA AAACTCAGAAGTCATTTACCTAAAGCCCGGGTGGTAGCTTGCTTCTGTGAAGGCATGACAGTTCGAGGTC TGCTCATGGCCATGAGACGCTTAGGTCTAGCAGGGGA GTTTCTACTTCTGGGCAGTGATG GCTGGGCCGA CAGGTATGACGTGACAGATGGATATCAGCGAGAAGCTGTCGGTGGAATTACAATCAAGCTTCAGTCTCCT GATGTCAAGTGTTTTGATGATTATTATCTGAAACTCCGGCC AGAAACAAACCTCAGAAACCCCTT GGTTTC AAGAATTTTGGCAGCATCGTTTTTCAGTGCCGGCTGGAAGGGTTTGCACAGGAGAACAGCAAGTACAACAA GACTTGCAACAGTTCTCTGACTCTGAGAACACATCATGTTCAAGATTCCAAAATGGGATTTGTGATAAAT	
Forward Primer: GTTTCTACTTCTGGGCAGTGATG	Reverse Primer: AAGGGTTTCTGAGGTTTGTTC

To investigate the most suitable amount of template for real-time PCR, different dilutions of cDNA (1:10, 1:50, 1:100) that originated from the hippocampal subregions CA1, CA3 and DG were applied. The template was amplified by real-time PCR (Figure 32) and analysed by melting curve analysis (Figure 33).

The amplification worked successfully for every dilution and subregion except for the 1:50 dilution of CA3 cDNA. No amplification curve was obtained from this sample, which is probably due to a preparation error, where no template was added. A single melting peak (82 °C) was achieved from each amplicon. This demonstrates that only one amplicon was generated without undesired side-products. A 1:10 dilution was used further in the following experiments, since it resulted in the lowest Ct-value.

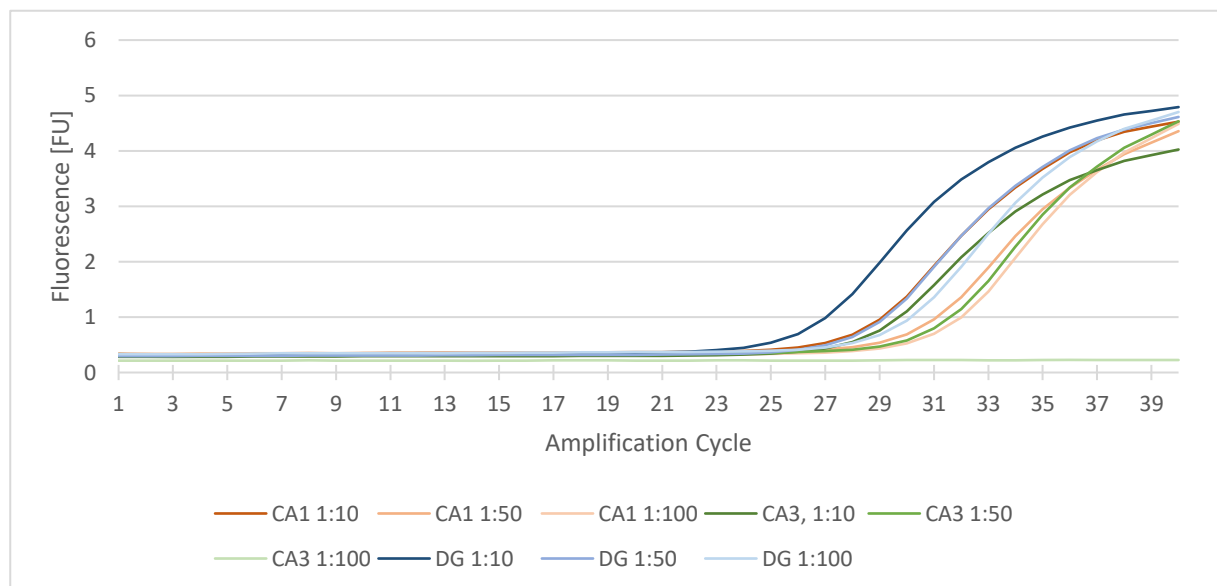


Figure 30: Amplification curves of *GRM5* gene expression analysis. Different dilutions of cDNA were applied as template to investigate the optimal starting amount (CA1/3= Cornu Ammonis 1/3, DG= Dentate gyrus).

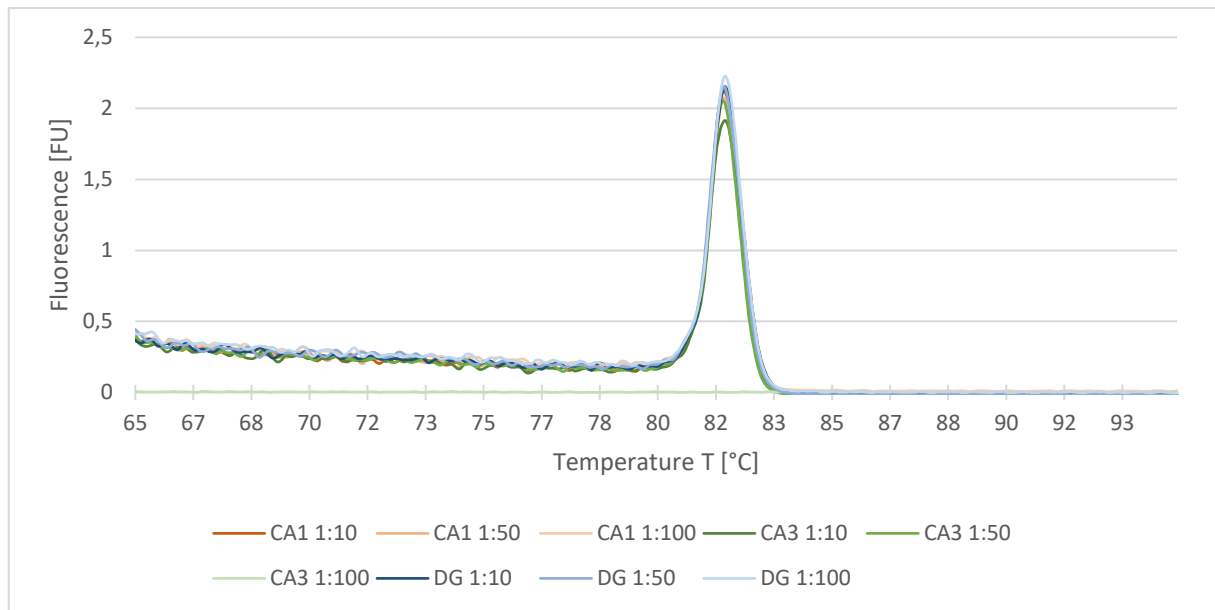


Figure 31: Melt plot obtained after gene expression analysis of *GRM5* during method testing (CA1/3= Cornu Ammonis 1/3, DG= Dentate gyrus).

4.4.3 *GRM5* results and discussion

Target of the study were the hippocampal subregions CA1, CA3 and DG from *Rattus norvegicus*. Six animals were grown to 22 months and had poor performance during spatial memory test (OMB), while five aged rodents showed a good performance (OMG). A control group that consisted of 6 young animals that received no training (YM).

The majority of the obtained methylation degrees were below the calculated LOD (see 6.10), which ranged from 1.0 to 5.0 % for individual CpGs. Only few samples showed detectable methylation degrees at CpG2/3/5/6/8/12 that were <5 %. (see 7.4.3 for raw data). No significant differences ($p < 0.05$) in methylation degrees between hippocampal subregions could be observed. Additionally, no significant change was found in respect to aging or learning performance of the animals.

Relative gene expression was calculated from the obtained Ct-values of cDNA during real-time PCR (Figure 34), using *GAPDH* as reference gene (see section 4.5). T-tests revealed a significant lower expression in OMB compared to OMG, when comparing mean gene expression levels in all hippocampal subregions ($p = 0.030$). Regarding OMG and YM, both groups expressed *GRM5* at approximately the same level. For this reason, YM showed a similar significant upregulation ($p = 0.036$) in expression compared to OMB.

Comparing the hippocampal subregions, the only significantly different expression rate was a increase in CA1 compared to CA3 when considering all animal groups ($p = 0.004$).

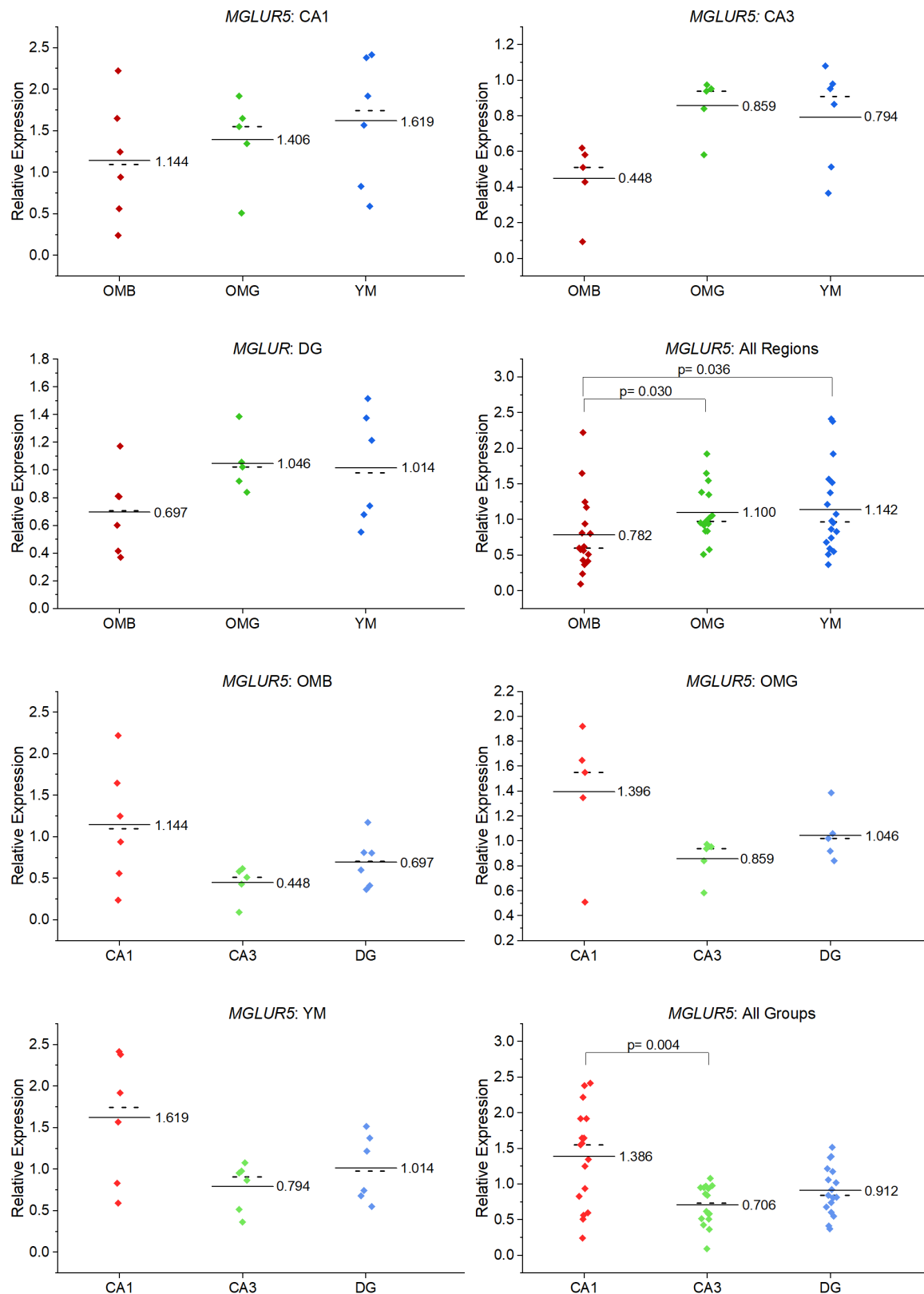


Figure 32: Dot plots of relative GRM5 expression sorted by hippocampal subregion and animal group (Solid line= Mean value, dashed line= Median, OMB= Rats with poor learning performance (6 samples), OMG= Rats with good learning performance (5 samples), YM= Young control group (6 samples), CA1/3= Cornu Ammonis 1/3, DG= Dentate gyrus).

Combining the results of both experiments, pyrosequencing and real-time PCR, no link between DNA methylation and relative gene expression could be deducted. The determined methylation degrees were below LOD, while changes in gene expression were found studying the same samples. Low gene expression rates in OMB compared to OMG and YM suggest a relation to learning performance, which is supported by the fact that the receptor is crucial for LTP [99,100]. By comparing hippocampal subregions *GRM5* was found to be expressed in elevated amounts in CA1.

4.5 Glyceraldehyde 3-phosphate dehydrogenase (*GAPDH*)

For accurate measurement of gene expression analysis, a reference was needed to make the results comparable to each other. The reference gene that was chosen is glyceraldehyde 3-phosphate dehydrogenase (*GAPDH*), since it is widely used in relative gene expression analysis [125].

4.5.1 *GAPDH* gene expression analysis

Primer sequences that were successful in previous experiments were taken for amplification (original source: Kindlundh-Högberg *et al.* [146]). Primer sequences and the generated amplicon are presented in Table 13.

Table 13: Primer and amplicon sequences for gene expression analysis of *GAPDH* (Green= Positions of forward- and reverse primer, Yellow= Resulting amplicon).

<i>GAPDH</i> Primers for real-time PCR	
GTCATCCCAGAGCTGAACGGGAAGCTCACTGGCATGGCCTTCCGTGTTTCCTACCCCCAATGTATCCGT TGTGGATCTGACATGCCGCCTGGAGAAACCTGCCAAGTATGATGACATCAAGAAGGTGGTGAAGCAGG CGGCCGAGGGCCCACTAAAGGGCATCCTGGGCTACACTGAGGACCAGGTTGTCTCCTGTGACTTCAAC AGCAACTCCCATTCTTCCACCTTTGATGCTGGGGCTGGCATTGCT	
Forward Primer: ACATGCCGCCTGGAGAAACCT	Reverse Primer: GCCCAGGATGCCCTTTAGTGG

Real-time PCR and subsequent melting curve analysis were performed, using cDNA of the three hippocampal subregions CA1, CA3 and DG to investigate the functionality of the primers. Several dilution factors of the template were applied (1:10, 1:50, 1:100). The results are shown in Figure 35 and Figure 36.

Amplification was successful in every sample, as it can be seen in the first diagram. It is noticeable that a lower Ct-value was obtained compared to the target genes *IGF1R*, *FMR1*, *DCX* and *GRM5* when the same dilution factor was applied for the template. This is probably due to the constant expression of *GAPDH* in high amounts, which is the reason why it was chosen as house-keeping gene. No side-products were created as the single peak (83.8 °C) in the melting diagram indicated.

To maintain consistency with methods for genes of interest, a 1:10 dilution was chosen for the experiments.

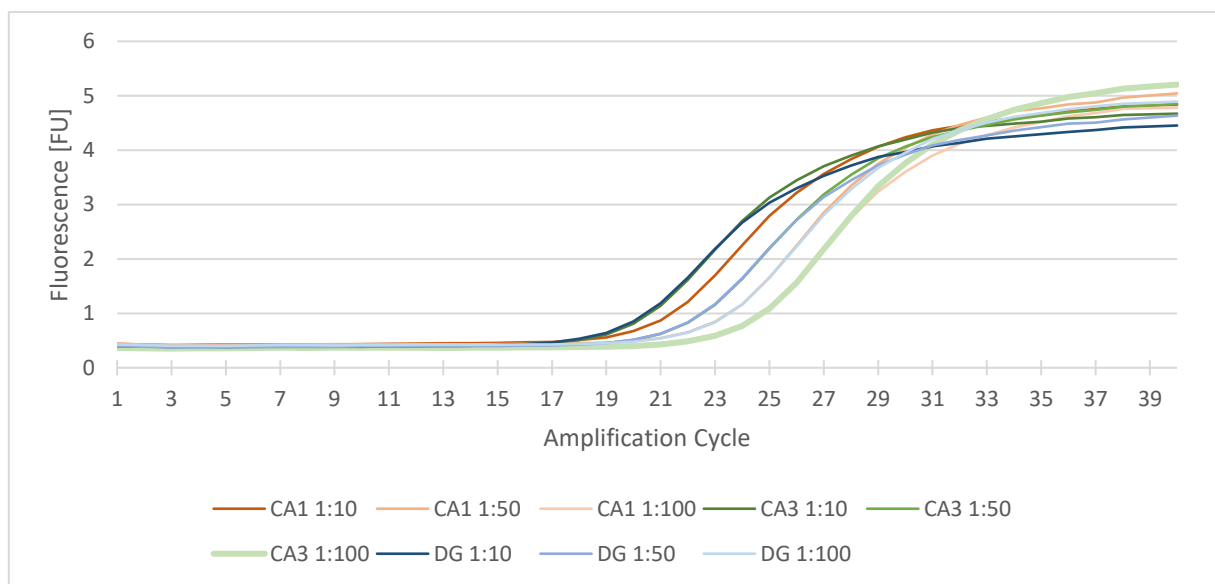


Figure 33: Amplification curves of GAPDH gene expression analysis. Different dilutions of cDNA were applied as template to investigate the optimal starting amount (CA1/3= Cornu Ammonis 1/3, DG= Dentate gyrus).

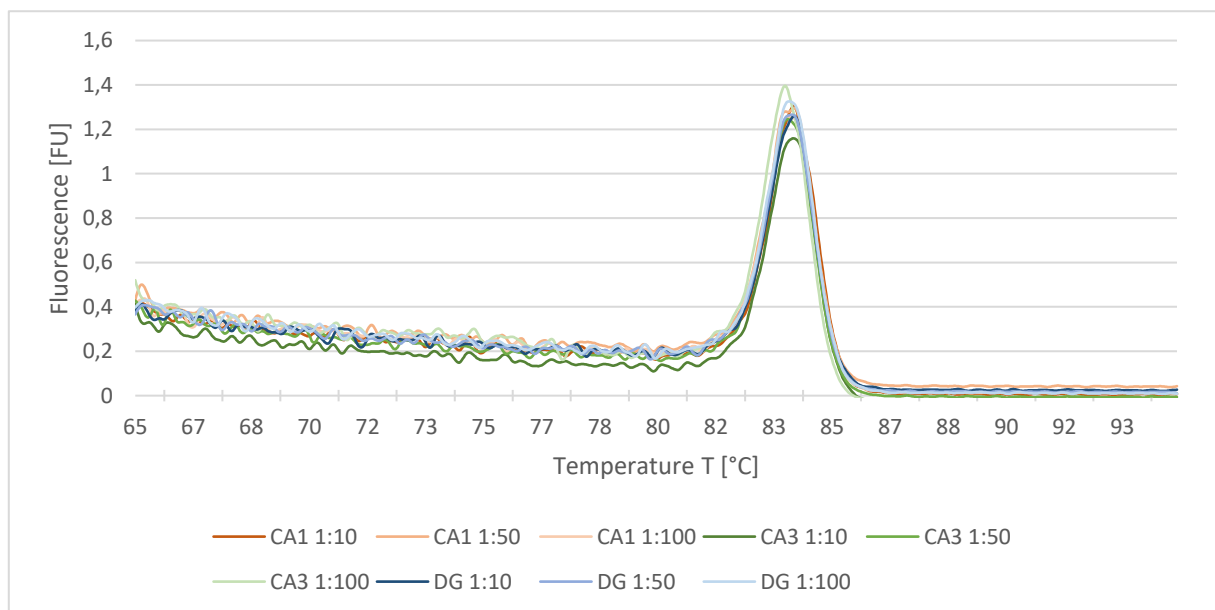


Figure 34: Melt plot obtained after gene expression analysis of GAPDH during method testing (CA1/3= Cornu Ammonis 1/3, DG= Dentate gyrus).

5 Conclusion

This thesis investigated the DNA methylation in the promoter regions of *IGF1R*, *FMR1*, *DCX* and *GRM5*. Methods for PCR and pyrosequencing of promoter regions of the target genes were successfully developed. Depending on the gene, they are suitable to amplify and determine the methylation degree of 3 to 16 CpGs. In parallel the relative gene expression was determined. The experiments were carried out on hippocampal tissue CA1, CA3 and DG of *Rattus norvegicus* that were trained in a radial arm maze (RAM) and on young untrained rodents as control group.

In none of the experiments, an association between gene expression and the DNA methylation in the studied promoter sequences could be established. However, several variations and trends that can be attributed to age or training were observed in gene expression.

IGF1R expression was found significantly decreased in rats with poor learning performance. This is in concordance with many studies that report a critical role of IGF1R in memory formation.

Analysis on *FMR1* did not show significant differences between animal groups, but between hippocampal subregions. The only significant result was an increased expression in CA3 tissue compared to the other subregions.

A certain DNA methylation pattern in the was found studied promoter sequence of *DCX*, which was not uniform in the investigated brain regions. CA1 displayed the highest methylation followed by a CA3 and DG, respectively. Neither aging nor training had a significant effect on DNA methylation in the investigated sequence. *DCX* expression was found significantly decreased in aged animals in comparison to the control group. The expression pattern could not be associated with the results of DNA methylation analysis. Since *DCX* is important for neurogenesis its expression is justified in young animals where brain development is still in progress and neurogenesis occurs more frequently.

GRM5 was significantly lower expressed in rats with poor learning performance, while animals with good training results and the young control group showed similar expression levels. This was associated with the increased LTP and learning that took place in those animals. No significant results were obtained in DNA methylation analysis.

In conclusion this thesis was able to shed some light on the expression of several genes in the hippocampus in dependence of memory formation and age. In addition, we report that DNA methylation in the investigated promoter sequences had no association with gene expression. Since we were only able to analyse the methylation degrees in short sequences of the promoter regions, it should be clarified in the future if neighbouring CpG positions influence gene expression.

6 Experimental section

Sample preparation was performed by our cooperation partners. New methods were developed for amplification of the promoter regions of *IGF1R*, *FMR1*, *DCX* and *GRM5* and the determination of their methylation degree. This involves design of new primers, as well as assays for pyrosequencing. The methods were applied on extracted DNA that was bisulfite converted. Gene expression was determined by reverse-transcription of extracted RNA and subsequent real-time PCR. The protein containing fraction of the extract was handed to our cooperation partners for analysis.

6.1 Assay and primer design

To design new primers and sequencing assays the PyroMark Assay Design 2.0 software was used. Settings were chosen to prevent the placing of a primer over variable positions. Amplicon length was set to be between 50 and 150 bp, while primer length should be in a range from 18 to 30 bp. The difference in GC base pair content between primers and amplicon had not to exceed 50 %. Additionally, it was tried to minimise the number of possible mispriming sites due to sequence similarities.

In addition to the program's checking routines, the melting temperature of the primers were determined by the online calculator OligoCalc [147]. It was calculated by taking the results of the salt adjusted melting temperature at 50 nM Na⁺. PCR-primer candidates were only taken into closer inspection, if their melting temperature was above 58 °C and the difference between forward and reverse primer did not exceed 1.5 °C.

Probability of formation of a secondary structure was simulated by RNAfold webserver [148]. Sequences with predicted hairpin structures and other intramolecular bonds were discarded from further consideration. Probability of homo- and heterodimer formation between primers was investigated by the online software Oligo Analyzer 3.1 [149]. Complementary base pairs below three were considered as optimal, while up to five were tolerated.

6.2 Animal training and sample preparation

The following part was performed by co-workers of our cooperation partner Univ.-Prof. Dr. Gert Lubec at the Core Unit of Biomedical Research, Division of Laboratory Animal Science and Genetics, Medical University of Vienna.

The animals comprised 20 male Sprague Dawley rats. They were raised to an age of 22 months, which is the last third of life expectancy of this species. Food and water were available ad libitum. Each animal was housed individually in a cage made of Makrolon and filled with autoclaved woodchips. The rodents were subjected to artificial light cycles of 12 h light and darkness each and lived under normal facility conditions (22±2 °C and 55±5 % humidity).

Training was conducted in a radial arm maze (RAM) made of black plastic. It was elevated 80 cm above the floor and numerous marks were visible distally to allow orientation. The central platform was 50 cm in diameter with 12 arms spreading radially, while the arms were each 60 cm long and 12 cm broad. As reward, food pellets were placed below the arms and 5 cm from the distal end. Start of the experiment was controlled by placing the animal under a cylinder on the central platform, which was then elevated remotely. The movement and the decisions were tracked and recorded by a camcorder.

The applied protocol was modified after Levin *et al.* [150]. Five days before the beginning of the experiment the food supply was shortened to reduce the body weight to 85 %. This should motivate the rats for foraging behaviour. In order to familiarize the animals with the experimenter, they were handled three days prior to the experiment for 15 min/day. Two days prior to the experiment the animals were habituated with the RAM. Food pellets were placed all over the maze and the rats were given 15 min for exploration and eating.

For each rat five training sessions were conducted per day. In-between the animals were brought to their cage for 30 min. The training was performed for five days. To initiate a trial, the cylinder was lifted slowly after 10 s. Three of the twelve arms were baited and the pattern stayed the same for all animals and trials. One session was given time for 4 min or until all baited arms were entered. An arm counted as entered when the entire body except the tail was in. After each trial the platform was cleaned to remove olfactory cues.

In order to compare the performances, the reference memory index (RMI) was determined for each animal. It was calculated from the total visits of baited arms (first visits and revisits) divided by the number of total visits. The time for completion of the task was also recorded.

Young animals that were 17 weeks old, were raised under same conditions. They were put into the RAM for the same amount of time but without bait and training sessions.

The hippocampi were removed and placed on a para cooler at 6 °C. Coronal slices were prepared along the longitudinal axis by a scalpel. Each slice was microdissected to separate the subregions CA1, CA3 and DG. They were transferred into cryogenic tubes with 1 ml trizol and stored at -80 °C.

6.3 Extraction

The method originates from the Trizol® reagent user guide [108] provided online by Invitrogen. In addition to small changes to the protocol, advices for small DNA concentrations were adopted from the TRI Reagent® DNA/Protein Isolation Protocol, available online by Thermo Fisher Scientific [151], as described below.

6.3.1 RNA extraction

The received samples were covered with 1 ml trizol reagent and frozen at -80 °C. Prior to homogenization and extraction it was given time to thaw up on ice for 30 min. All the following steps were carried out by cooling on ice.

Homogenization was performed by pipetting the tissue, still in trizol reagent, up and down using a micropipette and a syringe. This was first done with a 200 µl pipette tip and later with a 27G syringe needle until sufficient dissolution. The cell suspension was centrifuged (14 000 g, 5 min, 4 °C) and the supernatant transferred into a new tube. 200 µl chloroform were added and vortexed until complete intermixing of the phases. After 3 min of incubation the sample was centrifuged (12 000 g, 15 min, 4 °C) in order to achieve phase separation. The colourless and aqueous upper phase was transferred as thoroughly as possible without touching the white interphase. The lower phenolic solution was kept on ice for later DNA extraction. 10 µg glycogen were added to the isolated aqueous phase and vortexed briefly. RNA was precipitated by addition of 500 µl isopropanol and incubated for 10 min, interrupted by short vortexing. Subsequently it was centrifuged (12 000 g, 10 min, 4 °C) and the supernatant withdrawn by pipetting. Depending on the pellet's size it was washed with 200-300 µl 75 % ethanol. The washing mix was centrifuged once more (7 500 g, 5 min, 4 °C) and the supernatant removed again. The pellet was air-dried and then dissolved in 30 µl RNase-free H₂O. To ensure complete dissolving it was placed on a thermomixer (10 min, 60 °C, 350 rpm). The concentration was determined spectrophotometrically via NanoDrop. Two samples were taken per extract and analysed subsequently. If the obtained concentration was stable (difference= ±5 ng/µl), the RNA extract was reverse transcribed (see section 6.4).

6.3.2 DNA extraction

After removal of the aqueous phase during RNA extraction, 10 µg glycogen were added to the remaining phenolic phase and the white interphase. The solution was mixed by vortexing and briefly centrifuged. Then, 300 µl ethanol abs. were added. Mixing was achieved by tilting the tubes carefully several times. After 3 min incubation, DNA was precipitated by centrifugation (5 000 g, 5 min, 4 °C). The supernatant was transferred and used for later protein isolation by co-workers of our cooperation partner Univ.-Prof. Dr. Gert Lubec. It was stored at -80 °C until use. For washing purposes, 150-300 µl 70 % ethanol, depending on the pellet's size, were added. Without further mixing the sample was incubated for 10 min and centrifuged (5 000 g, 5 min, 4 °C). The supernatant was withdrawn carefully. The washing was repeated once. Afterwards the pellet was dissolved in 50 µl Buffer EB and shaken (10 h, 500 rpm, 25 °C) until completion. If the photometric signal was stable, the DNA concentration was measured, and the sample frozen at -20 °C. If this was not the case, the solution was further shaken under the same conditions, interrupted by storage at 4 °C until consistency was reached.

6.4 Reverse transcription of extracted RNA

After isolation and measurement of obtained RNA, an aliquot of 500 ng was used for reverse transcription in cDNA by using the QuantiTect Reverse Transcription Kit (Qiagen). It was applied according to the manufacturer's instruction. The samples and reagents were cooled on 4 °C except for incubation steps. A mix for gDNA wipe-out (Table 14) was prepared, while

500 ng RNA were added afterwards. Upon completion, the mix was incubated for 2 min on 42 °C. Subsequently 6 µL of a previously prepared supermix (Table 15) was added to the gDNA wipe-out mix. In the thermocycler (Bio-Rad) the samples were heated to 42 °C for 15 min, followed by 3 min at 95 °C. Afterwards they were stored at -20 °C.

Table 14: Composition of one sample for previous gDNA wipe-out during reverse transcription, using the Quantitect Reverse Transcription Kit (Qiagen).

Reagent	Volume [µl]
gDNA -Wipeout	2
RNase-free H ₂ O	Variable
RNA	Variable
Total Volume	14

Table 15: Composition of one sample during reverse transcription using the Quantitect Reverse Transcription Kit (Qiagen). A supermix was prepared according to the number of samples.

Reagent	Volume [µl]
QuantiScript RT Buffer, 5x	4
RT Primer Mix	1
QuantiScript Reverse Transcriptase	1
gDNA Wipeout sample	14
Total Volume	20

6.5 Real-time PCR

Gene expression was investigated by real-time PCR of generated cDNA using the Rotor-Gene SYBR Green Kit (Qiagen). A supermix according to Table 16 was prepared and aliquoted into strip-tubes under cooled conditions. A previously generated cDNA sample (see above) was diluted 1:10 with RNase-free H₂O before its addition to the reaction mix. PCR was performed with the temperature settings in Table 17 according to the manufacturer's instructions, using a Rotor-Gene Q Cyclor and 72-Well Rotor (Qiagen).

Table 16: Reaction mix for one real-time PCR sample, using Rotor-Gene SYBR Green Kit (Qiagen).

Reagent	Volume [µl]
2x Rotor-Gene SYBR Green PCR Master Mix	12.5
Forward primer (10 µM)	2.5
Reverse primer (10 µM)	2.5
RNase-free H ₂ O	5
cDNA template	2.5
Total Volume	25

Table 17: Cycling program and signal acquisition plan for real-time PCR of cDNA, using the Rotor-Gene SYBR Green Kit (Qiagen).

Step	Time	Temperature	Acquiring Signal
Activation	5 min	95 °C	/
Denaturation	5 s	95 °C	/
Annealing + Elongation	10 s	60 °C	Green Channel
40 cycles			
Final Elongation	10 min	72 °C	/
Final Denaturation	1 min	95 °C	/
Final Annealing	1 min	40 °C	/
Melting curve analysis	65-95 °C, 0.1 °C/sec		HRM Channel

6.6 Bisulfite conversion of DNA

To investigate the methylation degree in genes of interest, unmethylated cytosine was converted into thymine. For this purpose, the EpiTect Fast Bisulfite Conversion Kit (Qiagen) was applied. The reactions were carried out as proposed in the manufacturer's protocol. Depending on the previously determined concentration of the extracted DNA (see section 6.3.2), the highest applicable amount was converted. The mixes were prepared as shown in Table 18.

Table 18: Reaction mix of one sample for bisulfite conversion, using EpiTect Fast Bisulfite Conversion kit.

Component	(1 ng – 2 µg) Volume per reaction [µl]
DNA	Variable (max. 20 µL)
RNase-free H ₂ O	Variable (complement DNA to 20 µL)
Bisulfite Solution	85
DNA Protect Buffer	35
Total Volume	140

In order to perform the conversion, the samples were subjected to the temperature program shown in Table 19. The settings were taken from the manufacturer's protocol.

Table 19: Temperature program for bisulfite conversion.

Step	Time	Temperature
Denaturation	5 min	95 °C
Incubation	20 min	60 °C
Denaturation	5 min	95 °C
Incubation	20 min	60 °C

After the incubation, DNA was cleaned up by applying the manufacturer's instructions and using an Eppendorf centrifuge. First 310 µl Buffer BL were added to the sample, which was then vortexed. Afterwards 250 µl absolute ethanol was added and pulse vortexed for 15 s and again centrifuged. The mix was transferred onto a MinElute DNA spin column with a 2 ml collection tube and centrifuged (1 min, 14 000 rpm). Afterwards the flow-through was once again transferred onto the column and centrifuged to maximize DNA binding. The flow-through was discarded and 500 µl buffer BL was put on the column. After centrifugation (1 min, 14 000 rpm) and discarding the flow-through, 500 µl buffer BD was added to the sample and incubated for 15 min at room temperature. Upon incubation, the sample was centrifuged (1 min, 14 000 rpm) and the flow-through discarded. For washing purposes 500 µl buffer BW was added on the column and centrifuged (1 min, 14 000 rpm). The flow-through was again discarded and washing process repeated once. Afterwards 250 µl absolute ethanol was put on the column and centrifuged (1 min, 14 000 rpm). The column was then put into a new collection tube and centrifuged one more (1 min, 14 000 rpm). To remove remaining liquid thoroughly it was incubated at 60 °C for 5 min with an open lid. Finally, the column was put into a new tube and 15 µl buffer EB was added. After incubation for 1 min the DNA was eluted by centrifugation (1 min, 14 000 rpm). To maximize the DNA yield, the column was put into a new tube and again incubated with 15 µL buffer EB. It was also centrifuged under the same conditions. In the end, the concentration of obtained ssDNA was determined spectrophotometrically.

6.7 PCR for subsequent pyrosequencing

PCR for subsequent pyrosequencing was performed by using a PyroMark PCR Kit (Qiagen) by applying the instructions of the manufacturer. Exact composition of a reaction mix for a single sample can be taken from Table 20. The mixes and samples were cooled to 0 °C during preparation until the PCR was started.

Table 20: Composition of a single reaction mix for amplification of DNA for subsequent pyrosequencing, using PyroMark PCR kit (Qiagen).

Reagent	Volume per 0.2 μ M Primer Concentration [μ L]	Volume per 0.4 μ M Primer Concentration [μ L]
PyroMark PCR Mastermix, 2x	12.5	12.5
CoralLoad® Concentrate, 10x	2.5	2.5
Forward primer (10 μ M)	0.5	1
Reverse primer (10 μ M)	0.5	1
RNAse-free H ₂ O	7	6
DNA template (5 ng/ μ L)	2	2
Total Volume	25	25

At the beginning of method development, different primer concentrations (0.2 μ M and 0.4 μ M) were used to optimize PCR efficiency. A gradient setting was used for PCR in the iQ5 thermocycler (Bio-Rad) to subject samples to different annealing temperatures in one single run. The gradient ranged from 5 °C below the calculated primer concentration to 3 °C above. In order to analyse the effect of different primer concentrations and annealing temperatures, an agarose gel electrophoresis was performed (see below). After optimization 0.4 μ M primer concentration and 60 °C annealing temperatures were set as optimal conditions. The complete temperature program can be seen in Table 21. The PCR products were stored at -20 °C until further use.

Table 21: Temperature program of PCR for subsequent pyrosequencing, using the PyroMark PCR kit.

Step	Time	Temperature
Activation	15 min	95 °C
Denaturation	30 s	94 °C
Annealing	30 s	Variable/60 °C
Elongation	30 s	72 °C
Final Elongation	10 min	72 °C

6.8 Agarose gel electrophoresis

To determine the obtained amount of amplicon after PCR and check for possible by-products, agarose gel electrophoresis was performed.

A 50x TAE buffer stock solution was prepared by first dissolving 242 g Tris in dH₂O. 57.1 ml acetic acid and 100 ml of 0.5 M EDTA were added. After adjustment to pH 8, it was filled up to 1 l total volume. For the experiments 20 ml of this buffer was filled up to 1000 ml with dH₂O to prepare 1x buffer.

In order to prepare a 2 % gel, 2 g of agarose were dissolved in 100 ml 1x TAE buffer. The mixture was heated under mixing until the agarose was completely melted. 10 µl GelRed were then added. The liquid gel was casted into an appropriate frame with special regard on an even alignment. After gelation, it was transferred to the electrophoresis chamber, which was then filled with 1x TAE buffer.

When analysing PCR products that were obtained with the PyroMark PCR kit, 5 µL of the amplicon was directly put onto the gel. As reference a 25 bp ladder was used. A 2 µl aliquot was merged together with 8 µl RNase free water and 2 µl of 5x loading dye. A 10 µl aliquot was used for electrophoresis.

The separation was performed under a setting of 120 V for 1 h or until the run was finished. The results were analysed under UV-light and a picture was taken. For comparison of the obtained amplicon lengths, the separated ladder and the sizes of the fragments are displayed in Figure 37.

6.9 Pyrosequencing

By pyrosequencing, the methylation status of single CpG positions in the generated amplicons was determined. The assays were designed by loading the amplicon's sequence into the PyroMark Q24 Advanced software. In order to carry out the experiment, PyroMark Q24 Kit (Qiagen) in combination with the corresponding PyroMark Q24 instrument and working station was used according to its manual.

A binding buffer supermix (Table 22) was prepared and aliquoted to a 24-well plate. An additional sequencing primer solution was prepared (Table 23) and the cartridge filled with dNTP, enzyme- and substrate mix according to the pre-information sheet created by the software.

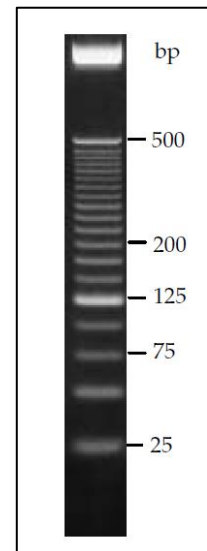


*Figure 35:
Separated DNA
fragments after
agarose gel
electrophoresis of
25 bp ladder.
Provided by the
manufacturer.*

Table 22: Composition of a single pyrosequencing sample.

Reagent	Volume for <i>IGF1R</i> and <i>DCX</i> Sequencing [μ L]	Volume for <i>FMR1</i> and <i>GRM5</i> Sequencing [μ L]
PyroMark Binding Buffer	40	40
Millipore H ₂ O	24	34
Streptavidin Sepharose High Performance	1	1
Per well	65	75
Biotinylated PCR product	15	5

Table 23: Primer annealing mix per sample for PSQ experiment.

Reagent	Volume [μ L]
Annealing Buffer	19.25
Sequencing Primer [10 μ M]	0.75
Primer-Mix per well	20

In a spatially separated place, the previously prepared amplicon was added, and the plate shaken (1400 rpm, 10 min). Using the PyroMark Q24 vacuum working station, the sepharose-bound amplicon was treated with 70 % ethanol and denaturation solution (Qiagen) for 5 s each. Afterwards it was incubated with washing buffer (Qiagen) for 10 s. The amplicon was added to 20 μ L sequencing primer with annealing buffer on a Q24-plate (Table 23) and immediately heated on 80 °C for 5 min. After submitting, the reactions and detection were then carried out by PyroMark Q24 instrument. Evaluation was performed by using the corresponding PyroMark Q24 software.

6.10 Data evaluation and statistics

The limit of detection (LOD) of each pyrosequencing method was determined for every single CpG, respectively. First, DNA standards with 0 % degree were analysed repeatedly. LOD was subsequently calculated by adding 3 times the standard deviation to the mean value of these samples.

The resulting methylation degrees were compared between animal groups (OMB, OMG and YM) and hippocampal subregions (CA1, CA3 and DG). This was performed for single CpGs and their mean value. Unreliable results were excluded from the analysis.

For gene expression analysis, the threshold cycle (Ct) was determined by setting the threshold for each gene individually. The results were standardised using the plate control, a sample that was co-determined in every run to make them comparable. Δ Ct was calculated by subtracting the standardised threshold cycle of the reference gene *GAPDH* from

standardized threshold cycle of the target gene (Figure 38, 1). The mean ΔCt value of all samples from the control group (YM) over all hippocampal subregions was determined per target gene and subtracted from the individual sample ΔCt in order to calculate $\Delta\Delta Ct$ (Figure 38, 2). The relative gene expression was finally calculated by using the formula in Figure 38, 3.

$$\begin{aligned}
 &1: \Delta Ct = Ct(\text{target gene}) - Ct(\text{reference gene}) \\
 &2: \Delta\Delta Ct = \Delta Ct(\text{target gene}) - \overline{\Delta Ct}(\text{target gene, control group}) \\
 &3: \text{Relative gene expression} = 2^{(-\Delta\Delta Ct)}
 \end{aligned}$$

Figure 36: Depiction of the used formulas in $\Delta\Delta Ct$ calculations for relative gene expression (Ct= threshold cycle).

Significant differences in the results of DNA methylation and gene expression analysis were evaluated by two-way analysis of variance (ANOVA) with post-hoc Bonferroni test. SPSS® Statistics software version 25 (IBM) was used for this purpose. P-values ≤ 0.05 were considered to be significant.

6.11 Materials and software

Table 24: List of chemicals used in this thesis.

Reagent	Supplier
Acetic Acid (conc.)	Roth
Buffer EB	Qiagen
Chloroform	Sigma-Aldrich
CpGenome™ Rat Methylated Genomic DNA	Merck
CpGenome™ Rat Unmethylated Genomic DNA Standard	Merck
Deionised H ₂ O	In-house distillation device
DNA Exitus Plus™ IF	AppliChem
Ethanol absolute (abs.)	VWR
Ethylenediaminetetraacetic acid (EDTA)	Merck
Glycogen for mol. biol.	Sigma-Aldrich
Invitrogen 25 bp DNA Ladder	Thermo Fisher Scientific
Isopropanol	VWR
Milli-Q H ₂ O	In-house Millipore filtered 18.2 MΩ·cm -resistance water
Oligonucleotides (Primer)	Sigma-Aldrich
RNase-free H ₂ O (ultra filtered and autoclaved)	Sigma-Aldrich
Sample Loading Buffer	Bio-Rad
Streptavidin Sepharose™ High Performance Affinity Resin	GE Healthcare
Tris(hydroxymethyl)aminomethane (TRIS)	Sigma-Aldrich
Trizol	Thermo Fisher Scientific

Table 25: List of kits used in this thesis.

Kit	Supply
EpiTect Fast DNA Bisulfite Kit	Qiagen
Rotor-Gene SYBR Green Kit	Qiagen
QuantiTect Reverse Transcription Kit	Qiagen
PyroMark Q24 Advanced CpG Reagents	Qiagen
PyroMark Wash Buffer	Qiagen
PyroMark Denaturation Solution	Qiagen

Table 26: List of consumable materials used in this thesis.

Material	Supply
Filter tips for micropipettes	Brand, Sarstedt
Microcentrifuge tubes (1.5 ml)	VWR
PCR tubes, sterile (0.2 ml)	Qiagen
PyroMark Q24 plate	Qiagen
Falcon® tubes (15/50 ml)	VWR
Strip tubes & caps (0.1 ml)	Qiagen
PyroMark Q24 Cartridge	Qiagen

Table 27: List of devices used in this thesis.

Equipment	Model	Manufacturer
Microcentrifuge	Centrifuge 5424 Rotor FA-45-24-11	Eppendorf
Real-time PCR Thermocycler	Rotor-Gene Q Cyclor 72-Well Rotor	Qiagen
Gradient Thermocycler	iQTM Multicolor Real-Time PCR Detection system + iCycler	Bio-Rad
Spectrophotometer	NanoDrop 2000c	Thermo Fisher Scientific
Analytical Balance	TE2114S	Sartorius
Refrigerated Centrifuge	Biofuge 28RS Rotor HFA28.1	Heraeus
Pyrosequencer	PyroMark Q24	Qiagen
Thermomixer	Thermomixer Comfort	Eppendorf

Equipment	Model	Manufacturer
Vortexmixer	VortexGenie2 Digital	Scientific Industries
Vortexmixer	VV2	VWR
Diverse Micropipettes	Eppendorf, Bio-Rad	Eppendorf, Bio-Rad
Gel Electrophoresis Device	Mini Sub Cell GT with Power Supply Power Pac HV	Bio-Rad

Table 28: List of software used in this thesis.

Software	Distributer
Excel 2016	Microsoft
PyroMark Assay Design 2.0.1.15	Qiagen
PyroMark Q24 Advanced 3.0.1	Qiagen
Nanodrop 2000/2000c	Thermo Fisher Scientific
Rotor-Gene Q Series Software 2.3.1	Qiagen
OriginPro 2018G b9.5.0.193	OriginLab Corporation
Bio-Rad iQ5-Standard-Edition 2.1.97.1001	Bio-Rad

7 Attachment

7.1 Abstract

It is memories and personal experiences that make us individual. In modern ages, new threats to these important resources arise, not at least, due to the significantly increased lifespan of human. Diseases like dementia and Alzheimer's disease are widely known to impair memory by decreasing the ability of acquiring new memory and accessing old ones. But the mechanisms responsible for these impairments of the brain are still unclear. In this thesis three hippocampal subregions of *Rattus norvegicus* (CA1, CA3 and DG) were studied.

Aims of the study were investigation of DNA methylation and relative gene expression on mRNA levels of the target genes *IGF1R*, *FMR1*, *DCX* and *GRM5*. New PCR and pyrosequencing methods were developed for this purpose. Depending on the gene, the methods were able to determine the methylation degree of 3 to 15 CpGs. The investigated tissue was taken from animals of different age that were trained in a radial arm maze to study the additional effect of learning and aging on the target genes.

No differences in DNA methylation were found and only the promoter region of *DCX* appeared slightly methylated. Despite that observation, *DCX* mRNA was significantly decreased in aged animals, especially in those with poor learning performance. *GRM5* expression was also found to be markedly reduced in subjects with poor training results. In addition, various expression differences were found regarding the hippocampal subregions. *FMR1* expression was significantly decreased in subregion CA3 compared to CA1 and DG, respectively. In addition, *GRM5* was found significantly increased in CA1 compared to CA3.

7.2 Zusammenfassung

Es sind Erinnerungen und persönliche Erfahrungen, die jede Person einzigartig machen. Doch in unseren modernen Zeiten häufen sich, nicht zuletzt wegen des rasanten Anstiegs der menschlichen Lebenserwartung, Gefahren für diesen wichtigen Teil eines Charakters. Krankheiten wie Demenz und die Alzheimer-Krankheit sind dafür bekannt das Gedächtnis zu beeinträchtigt, indem die Bildung neuer Erinnerungen verhindert und das Abrufen von alten verhindert wird. Doch die Mechanismen hinter diesen Schädigungen sind immer noch unklar.

In dieser Arbeit wurden drei Unterregionen des Hippocampus von *Rattus norvegicus* (CA1, CA3, DG) untersucht. Das Ziel der Studie war die Untersuchung von DNA Methylierung und Genexpression auf mRNA-Level der Gene *IGF1R*, *FMR1*, *DCX* und *GRM5*. Neue Methoden für PCR und Pyrosequenzierung wurden zu diesem Zweck entwickelt. Je nach Gen konnten diese Methoden den Methylierungsgrad von 3 bis 15 CpGs bestimmen. Das untersuchte Gewebe stammte von Tieren unterschiedlichen Alters, die in einem Radial Arm Maze trainiert wurden, um so den zusätzlichen Effekt des Lernens und Alters auf die Zielgene zu untersuchen.

Es wurden keine Unterschiede im Methylierungsgrad gefunden. Nur die Promoterregion von *DCX* war in allen Versuchsgruppen geringfügig methyliert. Unabhängig davon war die Expression von *DCX* mRNA in älteren Tieren geringer, besonders in jenen mit schlechten Lernresultaten. Auch *GRM5* wurde in Tieren mit schlechter Leistung schwächer exprimiert. Zusätzlich wurden diverse Unterschiede in der Genexpression zwischen den einzelnen Teilregionen des Hippocampus festgestellt. Beispielsweise konnte eine signifikant erhöhte Genexpression von *FMR1* in der Subregion CA3 festgestellt werden, wenn man sie mit CA1 und DG vergleicht. Außerdem wurde *GRM5* in CA1 signifikant höher exprimiert als in CA3.

7.3 List of abbreviations

Table 29: List of abbreviations used in this thesis.

Abbr.	Full Description	Abbr.	Full Description
A	Adenine	IGF1R	Insulin-like growth factor 1 receptor
AMP	Adenosine monophosphate	IR	Insulin receptor
APS	Adenosine phosphosulfate	LOD	Limit of detection
BDNF	Brain-derived neurotrophic factor	LTP	Long-term potentiation
C	Cytosine	MAP	Microtubule associated protein
CA1/2/3	Cornu Ammonis 1/2/3	MBD	Methyl CpG binding domain
cDNA	Complementary DNA	MeCP2	Methyl-CpG binding protein
CpG	Cytosine-guanine dinucleotide	mRNA	Messenger RNA
Ct	Threshold cycle	OMB	Aged rats with poor learning performance
dATP α S	Deoxyadenosine alphathio triphosphate	OMG	Aged rats with good learning performance
DCX	Doublecortin X	PCR	Polymerase chain reaction
DG	Dentate gyrus	PP1	Protein phosphatase 1
DNA	Deoxyribonucleic acid	PPI	Inorganic pyrophosphate
DNMT	DNA-methyl-transferase	PSQ	Pyrosequencing
dNTP	Deoxyribose nucleoside triphosphate	RAM	Radial arm maze
dsDNA	Double-stranded DNA	RMI	Reference memory index
FMR1	Fragile X mental retardation	RNA	Ribonucleic acid
FMRP	Fragile X mental retardation protein	SAM	S-adenosyl-L-methionine
FXTAS	Fragile X-associated tremor/ataxia syndrome	SNP	Single nucleotide polymorphism
G	Guanine	ssDNA	Single-stranded DNA
GAPDH	Glyceraldehyde 3-phosphate dehydrogenase	T	Thymine
gDNA	Genomic DNA	U	Uracil
GRM5	Glutamate metabotropic receptor 5	YM	Young rats without training
IGF	Insulin-like growth factor		

7.4 Raw data

7.4.1 Obtained RNA and DNA concentration of the extracts

Table 30: Concentration and yield of RNA and DNA obtained photometrically after extraction and of DNA after bisulfite conversion (BC, 2 aliquots per sample).

Sample		RNA Concentration [ng/μl]	RNA Yield [ng]	DNA Concentration [ng/μl]	DNA Yield [ng]	BC DNA Concentration [ng/μl]	BC DNA Yield [ng]
OMB26	CA1	281.1	5621.0	95.7	4782.5	9.3	139.5
						2.0	30.0
OMB26	CA3	377.7	7554.0	39.3	1965.0	10.8	162.0
						<LOD	<LOD
OMB26	DG	363.4	7268.0	119.9	5993.7	8.7	130.5
						2.1	31.5
OMB22	CA1	409.6	8191.0	94.4	4717.5	5.4	81.0
						2.0	30.0
OMB22	CA3	361.0	7219.0	33.3	1662.5	4.6	69.0
						1.4	21.0
OMB22	DG	450.3	9006.0	99.5	4972.5	28.7	429.8
						3.6	54.0
OMB86	CA1	450.4	8807.0	78.0	3120.0	5.5	82.5
						2.3	34.5
OMB86	CA3	11.1	222.0	103.9	4154.0	10.6	158.3
						3.8	57.0
OMB86	DG	472.1	9442.0	86.0	3438.0	17.8	267.0
						3.4	51.0
OMB14	CA1	330.3	9910.0	64.1	3205.0	4.7	70.5
						1.0	15.0
OMB14	CA3	406.8	12204.0	41.7	2082.5	3.0	45.0
						0.5	7.5
OMB14	DG	385.8	11572.5	111.1	5555.0	28.0	420.0
						4.9	73.5
OMB42	CA1	268.1	8043.0	74.3	3712.5	15.5	231.8
						2.8	42.0
OMB42	CA3	348.0	10438.5	56.0	2800.0	6.7	100.5
						1.8	27.0
OMB42	DG	251.0	2822.5	63.9	3192.5	15.8	236.3
						3.2	48.0
OMB38	CA1	337.1	10111.5	75.9	3793.5	20.9	312.8
						4.4	66.0
OMB38	CA3	503.4	15100.5	52.6	2628.3	7.6	114.0
						1.3	19.5
OMB38	DG	319.1	9573.0	75.0	3761.6	6.2	93.0
						1.5	22.5
OMG11	CA1	92.5	1850.0	218.3	10912.5	1.9	27.8
						0.6	8.3

Sample		RNA Concentration [ng/μl]	RNA Yield [ng]	DNA Concentration [ng/μl]	DNA Yield [ng]	BC DNA Concentration [ng/μl]	BC DNA Yield [ng]
OMG11	CA3	166.8	3336.0	181.9	9095.0	3.7	54.8
						0.9	13.5
OMG11	DG	197.9	3958.0	190.2	9510.0	4.4	66.0
						1.4	21.0
OMG18	CA1	81.4	1628.0	58.5	2925.0	11.5	172.5
						2.1	31.5
OMG18	CA3	355.1	7102.0	52.1	2602.5	5.9	88.5
						1.7	25.5
OMG18	DG	99.4	1987.0	55.6	2777.5	6.7	100.5
						1.7	25.5
OMG21	CA1	346.5	6929.0	32.3	1615.0	12.4	185.3
						3.1	46.5
OMG21	CA3	376.1	7522.5	78.8	3940.0	11.9	177.8
						2.3	34.5
OMG21	DG	555.6	11112.6	73.9	3692.5	17.2	258.0
						2.8	42.0
OMG2	CA1	368.9	11067.0	32.9	1645.0	14.3	214.5
						1.6	24.0
OMG2	CA3	332.0	9958.5	52.7	2632.5	1.4	21.0
						<LOD	<LOD
OMG2	DG	176.4	5292.0	50.9	2542.5	5.9	88.5
						0.5	7.5
OMG6	CA1	200.6	4011.0	56.5	2822.5	5.2	78.0
						0.3	4.5
OMG6	CA3	82.0	1639.0	59.8	2991.6	9.3	139.5
						1.2	18.0
OMG6	DG	160.6	3211.0	78.6	3931.6	12.9	192.8
						1.5	22.5
YM1	CA1	224.3	6727.5	60.3	3015.0	4.2	63.0
						1.6	24.0
YM1	CA3	277.4	8321.0	54.1	2702.5	6.3	94.5
						1.5	22.5
YM1	DG	388.5	11655.0	122.1	6103.3	25.8	386.3
						10.0	150.0
YM2	CA1	175.4	5262.0	113.6	5683.3	21.9	328.5
						4.7	70.5
YM2	CA3	301.1	9034.0	128.7	6435.0	21.9	328.5
						4.5	67.5
YM2	DG	411.5	12345.0	168.3	8416.6	29.4	441.0
						3.9	58.5
YM3	CA1	260.7	7821.0	59.0	2948.3	13.4	200.3
						1.8	27.0
YM3	CA3	205.6	6166.5	156.0	7801.6	6.5	97.5
						1.2	18.0

Sample		RNA Concentration [ng/μl]	RNA Yield [ng]	DNA Concentration [ng/μl]	DNA Yield [ng]	BC DNA Concentration [ng/μl]	BC DNA Yield [ng]
YM3	DG	283.3	8499.0	43.8	2190.0	3.4	51.0
						0.9	13.5
YM4	CA1	249.5	7485.0	104.8	5238.3	6.0	90.0
						2.0	30.0
YM4	CA3	338.6	10158.0	108.5	5426.6	9.8	147.0
						1.7	25.5
YM4	DG	516.3	15489.8	149.0	7450.0	7.3	109.5
						1.4	21.0
YM5	CA1	464.5	23223.3	103.1	5155.0	9.1	136.5
						1.9	28.5
YM5	CA3	480.3	24015.0	106.4	5317.5	6.6	99.0
						1.5	22.5
YM5	DG	721.4	21638.3	87.1	4352.5	4.9	73.5
						1.1	16.5
YM6	CA1	535.5	16064.0	105.6	5280.0	1.3	19.5
						0.5	7.5
YM6	CA3	631.0	18930.0	97.6	4880.0	9.4	141.0
						1.5	22.5
YM6	DG	637.1	19113.0	107.1	5356.6	16.3	244.5
						2.2	33.0

7.4.2 Data from gene expression analysis

Table 31: List of $\Delta\Delta Ct$ and relative expression values. Calculation is described in section 6.10

Sample		IGF1R		FMR1		DCX		GRM5	
		$\Delta\Delta Ct$	Rel. Exp.	$\Delta\Delta Ct$	Rel. Exp.	$\Delta\Delta Ct$	Rel. Exp.	$\Delta\Delta Ct$	Rel. Exp.
OMB14	CA1	-0.3444	1.2697	-0.3944	1.3144	-0.1656	1.1216	-0.3217	1.2498
OMB14	CA3	0.5456	0.6851	0.5256	0.6947	0.4744	0.7197	0.7783	0.5830
OMB14	DG	-0.9244	1.8980	-0.4444	1.3608	0.0644	0.9563	-0.2317	1.1742
OMB22	CA1	0.4356	0.7394	-0.1444	1.1053	1.2844	0.4105	0.0883	0.9406
OMB22	CA3	0.1156	0.9230	0.8256	0.5643	1.1644	0.4461	1.2183	0.4298
OMB22	DG	0.8256	0.5643	0.4056	0.7549	1.6344	0.3221	1.4383	0.3690
OMB26	CA1	1.6056	0.3286	-0.1044	1.0751	2.0344	0.2441	2.0583	0.2401
OMB26	CA3	2.5156	0.1749	0.9356	0.5228	2.9844	0.1264	3.3983	0.0948
OMB26	DG	0.3756	0.7708	0.4456	0.7343	2.1544	0.2246	1.2683	0.4151
OMB38	CA1	-0.6844	1.6071	-0.4344	1.3514	-0.3356	1.2619	-1.1517	2.2217
OMB38	CA3	0.3156	0.8035	0.2556	0.8377	0.0344	0.9764	0.9683	0.5111
OMB38	DG	-0.4144	1.3328	-0.0144	1.0101	0.3044	0.8098	0.2983	0.8132
OMB42	CA1	-0.4644	1.3798	-0.6944	1.6183	-0.1356	1.0985	-0.7217	1.6491
OMB42	CA3	-0.2244	1.1683	0.2456	0.8435	0.2344	0.8500	0.6883	0.6206
OMB42	DG	-0.0444	1.0313	0.3156	0.8035	1.9644	0.2562	0.7283	0.6036

Sample		<i>IGF1R</i>		<i>FMR1</i>		<i>DCX</i>		<i>GRM5</i>	
		$\Delta\Delta Ct$	Rel. Exp.	$\Delta\Delta Ct$	Rel. Exp.	$\Delta\Delta Ct$	Rel. Exp.	$\Delta\Delta Ct$	Rel. Exp.
OMB86	CA1	-0.1444	1.1053	0.5556	0.6804	1.5744	0.3358	0.8283	0.5632
OMB86	DG	-0.1044	1.0751	0.1156	0.9230	0.4744	0.7197	0.3083	0.8076
OMG11	CA1	-0.6344	1.5523	0.0356	0.9757	0.2044	0.8679	-0.6317	1.5494
OMG11	CA3	-0.2944	1.2264	0.3856	0.7655	0.0744	0.9497	0.0383	0.9738
OMG11	DG	-0.0144	1.0101	0.3856	0.7655	0.5844	0.6669	0.1183	0.9213
OMG18	CA1	0.4356	0.7394	-0.0544	1.0385	1.6644	0.3155	0.9683	0.5111
OMG18	CA3	-0.0044	1.0031	0.4056	0.7549	0.4344	0.7400	0.2483	0.8419
OMG18	DG	-0.8644	1.8206	-0.2244	1.1683	0.5344	0.6904	-0.0817	1.0582
OMG2	CA1	-0.9844	1.9786	-0.5944	1.5099	0.7644	0.5887	-0.9417	1.9207
OMG2	CA3	-0.4244	1.3421	-0.0444	1.0313	0.2444	0.8441	0.0883	0.9406
OMG2	DG	-0.8844	1.8461	-0.1944	1.1443	0.2944	0.8154	-0.4717	1.3867
OMG21	CA1	-0.0044	1.0031	-0.3844	1.3054	1.1844	0.4400	-0.4317	1.3488
OMG21	CA3	-0.0344	1.0242	0.7356	0.6006	1.1344	0.4555	0.7783	0.5830
OMG21	DG	-0.5544	1.4686	-0.2844	1.2179	1.0544	0.4815	0.2483	0.8419
OMG6	CA1	-0.5594	1.4737	0.1656	0.8916	0.1844	0.8800	-0.7217	1.6491
OMG6	CA3	-0.3744	1.2963	0.8356	0.5604	-0.0456	1.0321	0.0683	0.9537
OMG6	DG	-0.5444	1.4585	0.2056	0.8672	0.0644	0.9563	-0.0317	1.0222
YM1	CA1	-0.1244	1.0901	-0.5844	1.4995	-0.2656	1.2021	-0.9417	1.9207
YM1	CA3	0.0256	0.9824	0.6956	0.6175	-0.2556	1.1938	0.0683	0.9537
YM1	DG	-0.6944	1.6183	-0.5344	1.4484	-0.7956	1.7357	-0.6017	1.5175
YM2	CA1	-0.1344	1.0977	-0.3844	1.3054	-0.1956	1.1452	-1.2517	2.3812
YM2	CA3	-0.5044	1.4186	0.1556	0.8978	-0.6656	1.5862	0.0283	0.9806
YM2	DG	-0.4644	1.3798	-0.3644	1.2874	-0.5056	1.4197	-0.4617	1.3771
YM3	CA1	0.2956	0.8148	0.2156	0.8612	-0.1056	1.0759	0.7483	0.5953
YM3	CA3	0.6556	0.6348	0.5356	0.6899	0.6844	0.6222	0.9583	0.5147
YM3	DG	0.0356	0.9757	-0.2844	1.2179	-0.1456	1.1062	0.4283	0.7431
YM4	CA1	0.1356	0.9103	-0.1544	1.1130	0.1144	0.9237	-0.6517	1.5710
YM4	CA3	-0.0544	1.0385	0.3056	0.8091	-0.0056	1.0039	0.2083	0.8655
YM4	DG	-0.1644	1.1207	-0.0644	1.0457	-0.2756	1.2105	0.5583	0.6791
YM5	CA1	0.8256	0.5643	0.5256	0.6947	0.9844	0.5054	0.2683	0.8303
YM5	CA3	1.1756	0.4427	0.8856	0.5413	1.2244	0.4280	1.4483	0.3664
YM5	DG	0.8856	0.5413	0.3256	0.7980	0.6544	0.6353	0.8583	0.5516
YM6	CA1	-0.2444	1.1846	-0.5244	1.4384	-0.0256	1.0179	-1.2717	2.4144
YM6	CA3	-0.5544	1.4686	-0.0244	1.0171	-0.2556	1.1938	-0.1117	1.0805
YM6	DG	-1.0944	2.1353	-0.7244	1.6523	-0.1656	1.1216	-0.2817	1.2156

7.4.3 Determined methylation degree by pyrosequencing

Table 32: Determined methylation degrees of single CpG positions in IGF1R promoter region, obtained by the developed PSQ method. Calculations of LOD described in section 6.10

		Methylation Degree [%]								
	Label	CpG1	CpG2	CpG3	CpG4	CpG5	CpG6	CpG7	CpG8	CpG9
	LOD	3.4	3.1	4.8	5.8	5.0	4.1	4.4	3.4	2.0
	0% Std	2	2	2	3	2	2	3	2	2
	10% Std	14	14	14	15	16	15	14	14	14
	100% Std	92	96	96	95	96	96	94	87	91
OMB14	CA1	<3.4	<3.1	<4.8	<5.8	<5.0	<4.1	<4.4	<3.4	<2.0
OMB14	CA3	<3.4	<3.1	<4.8	<5.8	<5.0	<4.1	<4.4	<3.4	<2.0
OMB14	DG	<3.4	<3.1	<4.8	<5.8	<5.0	<4.1	<4.4	<3.4	<2.0
OMB22	CA1	<3.4	<3.1	<4.8	<5.8	<5.0	<4.1	<4.4	<3.4	<2.0
OMB22	CA3	<3.4	<3.1	<4.8	<5.8	<5.0	<4.1	<4.4	<3.4	<2.0
OMB22	DG	<3.4	<3.1	<4.8	<5.8	<5.0	<4.1	<4.4	<3.4	<2.0
OMB26	CA1	<3.4	<3.1	<4.8	<5.8	<5.0	<4.1	<4.4	<3.4	<2.0
OMB26	CA3	n.a.	n.a.	n.a.	n.a.	n.a.	n.a.	n.a.	n.a.	n.a.
OMB26	DG	<3.4	<3.1	<4.8	<5.8	<5.0	<4.1	<4.4	<3.4	<2.0
OMB38	CA1	<3.4	<3.1	<4.8	<5.8	<5.0	<4.1	<4.4	<3.4	<2.0
OMB38	CA3	<3.4	<3.1	<4.8	<5.8	<5.0	<4.1	<4.4	<3.4	<2.0
OMB38	DG	<3.4	<3.1	<4.8	<5.8	<5.0	<4.1	<4.4	<3.4	<2.0
OMB42	CA1	<3.4	<3.1	<4.8	<5.8	<5.0	<4.1	<4.4	<3.4	<2.0
OMB42	CA3	<3.4	<3.1	<4.8	<5.8	<5.0	<4.1	<4.4	<3.4	<2.0
OMB42	DG	<3.4	<3.1	<4.8	<5.8	<5.0	<4.1	<4.4	<3.4	<2.0
OMB86	CA1	<3.4	<3.1	<4.8	<5.8	<5.0	<4.1	<4.4	<3.4	<2.0
OMB86	CA3	<3.4	<3.1	<4.8	<5.8	<5.0	<4.1	<4.4	<3.4	2
OMB86	DG	<3.4	<3.1	<4.8	<5.8	<5.0	<4.1	<4.4	<3.4	<2.0
OMG11	CA1	<3.4	<3.1	<4.8	<5.8	<5.0	<4.1	<4.4	<3.4	<2.0
OMG11	CA3	<3.4	<3.1	<4.8	<5.8	<5.0	<4.1	<4.4	<3.4	<2.0
OMG11	DG	<3.4	<3.1	<4.8	<5.8	<5.0	<4.1	<4.4	<3.4	<2.0
OMG18	CA1	<3.4	<3.1	<4.8	<5.8	<5.0	<4.1	<4.4	<3.4	<2.0
OMG18	CA3	<3.4	<3.1	<4.8	<5.8	<5.0	<4.1	<4.4	<3.4	<2.0
OMG18	DG	<3.4	<3.1	<4.8	<5.8	<5.0	<4.1	<4.4	<3.4	<2.0
OMG2	CA1	<3.4	<3.1	<4.8	<5.8	<5.0	<4.1	<4.4	<3.4	<2.0
OMG2	CA3	<3.4	<3.1	<4.8	<5.8	<5.0	<4.1	<4.4	<3.4	2
OMG2	DG	<3.4	<3.1	<4.8	<5.8	<5.0	<4.1	<4.4	<3.4	<2.0
OMG21	CA1	<3.4	<3.1	<4.8	<5.8	<5.0	<4.1	<4.4	<3.4	<2.0
OMG21	CA3	<3.4	<3.1	<4.8	<5.8	<5.0	<4.1	<4.4	<3.4	<2.0
OMG21	DG	<3.4	<3.1	<4.8	<5.8	<5.0	<4.1	<4.4	<3.4	<2.0
OMG6	CA1	<3.4	<3.1	<4.8	<5.8	<5.0	<4.1	<4.4	<3.4	<2.0
OMG6	CA3	<3.4	<3.1	<4.8	<5.8	<5.0	<4.1	<4.4	<3.4	<2.0
OMG6	DG	<3.4	<3.1	<4.8	<5.8	<5.0	<4.1	<4.4	<3.4	<2.0
YM1	CA1	<3.4	<3.1	<4.8	<5.8	<5.0	<4.1	<4.4	<3.4	<2.0
YM1	CA3	<3.4	<3.1	<4.8	<5.8	<5.0	<4.1	<4.4	<3.4	<2.0
YM1	DG	<3.4	<3.1	<4.8	<5.8	<5.0	<4.1	<4.4	<3.4	<2.0

Methylation Degree [%]										
Label		CpG1	CpG2	CpG3	CpG4	CpG5	CpG6	CpG7	CpG8	CpG9
YM2	CA1	<3.4	<3.1	<4.8	<5.8	<5.0	<4.1	<4.4	<3.4	<2.0
YM2	CA3	<3.4	<3.1	<4.8	<5.8	<5.0	<4.1	<4.4	<3.4	<2.0
YM2	DG	<3.4	<3.1	<4.8	<5.8	<5.0	<4.1	<4.4	<3.4	<2.0
YM3	CA1	<3.4	<3.1	<4.8	<5.8	<5.0	<4.1	<4.4	<3.4	<2.0
YM3	CA3	<3.4	<3.1	<4.8	<5.8	<5.0	<4.1	<4.4	<3.4	<2.0
YM3	DG	<3.4	<3.1	<4.8	<5.8	<5.0	<4.1	<4.4	<3.4	<2.0
YM4	CA1	<3.4	<3.1	<4.8	<5.8	<5.0	<4.1	<4.4	<3.4	<2.0
YM4	CA3	<3.4	<3.1	<4.8	<5.8	<5.0	<4.1	<4.4	<3.4	<2.0
YM4	DG	<3.4	<3.1	<4.8	<5.8	<5.0	<4.1	<4.4	<3.4	<2.0
YM5	CA1	<3.4	<3.1	<4.8	<5.8	<5.0	<4.1	<4.4	<3.4	<2.0
YM5	CA3	<3.4	<3.1	<4.8	<5.8	<5.0	<4.1	<4.4	<3.4	<2.0
YM5	DG	<3.4	<3.1	<4.8	<5.8	<5.0	<4.1	<4.4	<3.4	<2.0
YM6	CA1	<3.4	<3.1	<4.8	<5.8	<5.0	<4.1	<4.4	<3.4	<2.0
YM6	CA3	<3.4	<3.1	<4.8	<5.8	<5.0	<4.1	<4.4	<3.4	<2.0
YM6	DG	<3.4	<3.1	<4.8	<5.8	<5.0	<4.1	<4.4	<3.4	<2.0

Table 33: Determined methylation degrees of single CpG positions in FMR1 promoter region, obtained by the developed PSQ method (Yellow= Required check by user, Red= Failed to analyse and therefore unreliable).

Methylation Degree [%]										
Label		CpG1	CpG2	CpG3	CpG4	CpG5	CpG6	CpG7	CpG8	CpG9
LOD		4.6	6.2	3.0	6.2	4.6	7.2	2.0	4.6	5.6
0% Std		4	3	4	3	2	3	4	3	5
10% Std		18	16	17	16	13	16	18	16	16
100% Std		96	97	95	98	97	96	97	95	95
OMB14	CA1	<4.6	<6.2	<3.0	<6.2	<4.6	<7.2	<2.0	<4.6	<5.6
OMB14	CA3	<4.6	<6.2	<3.0	<6.2	<4.6	<7.2	<2.0	<4.6	<5.6
OMB14	DG	<4.6	<6.2	<3.0	<6.2	<4.6	<7.2	<2.0	<4.6	<5.6
OMB22	CA1	<4.6	<6.2	<3.0	<6.2	<4.6	<7.2	<2.0	<4.6	<5.6
OMB22	CA3	<4.6	<6.2	<3.0	<6.2	<4.6	<7.2	<2.0	<4.6	<5.6
OMB22	DG	<4.6	<6.2	<3.0	<6.2	<4.6	<7.2	<2.0	<4.6	<5.6
OMB26	CA1	<4.6	<6.2	<3.0	<6.2	<4.6	<7.2	<2.0	<4.6	<5.6
OMB26	CA3	<4.6	<6.2	<3.0	<6.2	<4.6	<7.2	<2.0	<4.6	<5.6
OMB26	DG	<4.6	<6.2	<3.0	<6.2	<4.6	<7.2	<2.0	<4.6	<5.6
OMB38	CA1	<4.6	<6.2	<3.0	<6.2	<4.6	<7.2	<2.0	<4.6	<5.6
OMB38	CA3	<4.6	<6.2	<3.0	<6.2	<4.6	<7.2	<2.0	<4.6	<5.6
OMB38	DG	<4.6	<6.2	<3.0	<6.2	<4.6	<7.2	<2.0	<4.6	<5.6
OMB42	CA1	<4.6	<6.2	<3.0	<6.2	<4.6	<7.2	<2.0	<4.6	<5.6
OMB42	CA3	<4.6	<6.2	<3.0	<6.2	<4.6	<7.2	<2.0	<4.6	<5.6
OMB42	DG	<4.6	<6.2	<3.0	<6.2	<4.6	<7.2	<2.0	<4.6	<5.6
OMB86	CA1	<4.6	<6.2	<3.0	<6.2	<4.6	<7.2	<2.0	<4.6	<5.6
OMB86	CA3	<4.6	<6.2	<3.0	<6.2	<4.6	<7.2	<2.0	<4.6	<5.6
OMB86	DG	<4.6	<6.2	<3.0	<6.2	<4.6	<7.2	<2.0	<4.6	<5.6
OMG11	CA1	<4.6	<6.2	<3.0	<6.2	<4.6	<7.2	<2.0	<4.6	<5.6
OMG11	CA3	<4.6	<6.2	<3.0	<6.2	<4.6	<7.2	<2.0	<4.6	<5.6

Methylation Degree [%]										
Label		CpG1	CpG2	CpG3	CpG4	CpG5	CpG6	CpG7	CpG8	CpG9
OMG11	DG	<4.6	<6.2	<3.0	<6.2	<4.6	<7.2	<2.0	<4.6	<5.6
OMG18	CA1	<4.6	<6.2	<3.0	<6.2	<4.6	<7.2	<2.0	<4.6	<5.6
OMG18	CA3	<4.6	<6.2	<3.0	<6.2	<4.6	<7.2	<2.0	<4.6	<5.6
OMG18	DG	<4.6	<6.2	<3.0	<6.2	<4.6	<7.2	<2.0	<4.6	<5.6
OMG2	CA1	<4.6	<6.2	<3.0	<6.2	<4.6	<7.2	<2.0	<4.6	<5.6
OMG2	CA3	<4.6	<6.2	<3.0	<6.2	<4.6	<7.2	<2.0	<4.6	<5.6
OMG2	DG	<4.6	<6.2	<3.0	<6.2	<4.6	<7.2	<2.0	<4.6	<5.6
OMG21	CA1	<4.6	<6.2	<3.0	<6.2	<4.6	<7.2	<2.0	<4.6	<5.6
OMG21	CA3	<4.6	<6.2	<3.0	<6.2	<4.6	<7.2	<2.0	<4.6	<5.6
OMG21	DG	<4.6	<6.2	<3.0	<6.2	<4.6	<7.2	<2.0	<4.6	<5.6
OMG6	CA1	<4.6	<6.2	3	<6.2	<4.6	<7.2	<2.0	<4.6	<5.6
OMG6	CA3	<4.6	<6.2	<3.0	<6.2	<4.6	<7.2	<2.0	<4.6	<5.6
OMG6	DG	<4.6	<6.2	<3.0	<6.2	<4.6	<7.2	<2.0	<4.6	<5.6
YM1	CA1	<4.6	<6.2	<3.0	<6.2	<4.6	<7.2	<2.0	<4.6	<5.6
YM1	CA3	<4.6	<6.2	<3.0	<6.2	<4.6	<7.2	<2.0	<4.6	<5.6
YM1	DG	<4.6	<6.2	<3.0	<6.2	<4.6	<7.2	<2.0	<4.6	<5.6
YM2	CA1	<4.6	<6.2	<3.0	<6.2	<4.6	<7.2	<2.0	<4.6	<5.6
YM2	CA3	<4.6	<6.2	<3.0	<6.2	<4.6	<7.2	<2.0	<4.6	<5.6
YM2	DG	<4.6	<6.2	<3.0	<6.2	<4.6	<7.2	<2.0	<4.6	<5.6
YM3	CA1	<4.6	<6.2	<3.0	<6.2	<4.6	<7.2	<2.0	<4.6	<5.6
YM3	CA3	<4.6	<6.2	<3.0	<6.2	<4.6	<7.2	<2.0	<4.6	<5.6
YM3	DG	<4.6	<6.2	<3.0	<6.2	<4.6	<7.2	<2.0	<4.6	<5.6
YM4	CA1	<4.6	<6.2	<3.0	<6.2	<4.6	<7.2	<2.0	<4.6	<5.6
YM4	CA3	<4.6	<6.2	<3.0	<6.2	<4.6	<7.2	<2.0	<4.6	<5.6
YM4	DG	<4.6	<6.2	<3.0	<6.2	<4.6	<7.2	<2.0	<4.6	<5.6
YM5	CA1	<4.6	<6.2	<3.0	<6.2	<4.6	<7.2	<2.0	<4.6	<5.6
YM5	CA3	<4.6	<6.2	<3.0	<6.2	<4.6	<7.2	<2.0	<4.6	<5.6
YM5	DG	<4.6	<6.2	<3.0	<6.2	<4.6	<7.2	<2.0	<4.6	<5.6
YM6	CA1	<4.6	<6.2	<3.0	<6.2	<4.6	<7.2	<2.0	<4.6	<5.6
YM6	CA3	<4.6	<6.2	<3.0	<6.2	<4.6	<7.2	<2.0	<4.6	<5.6
YM6	DG	<4.6	<6.2	<3.0	<6.2	<4.6	<7.2	<2.0	<4.6	<5.6

Table 34: Determined methylation degrees of single CpG positions in DCX promoter region, obtained by the developed PSQ method (Yellow= Required check by user, Red= Failed to analyse and therefore unreliable).

DCX-Methylation Degree [%]						
Sample		CpG1	CpG2	CpG3	Mean Value	MW (CpG2+3)
0% Std		3	1	1	1.7	1.0
10% Std		25	19	19	21.0	19.0
100% Std		100	92	94	95.3	93.0
LOD		10.1	5.6	4.6	/	/
OMB14	CA1	39	28	21	29.3	24.5
OMB14	CA3	33	19	17	23.0	18.0
OMB14	DG	20	13	11	14.7	12.0
OMB22	CA1	40	26	21	29.0	23.5
OMB22	CA3	35	20	16	23.7	18.0
OMB22	DG	18	15	13	15.3	14.0
OMB26	CA1	39	23	23	28.3	23.0
OMB26	CA3	34	22	17	24.3	19.5
OMB26	DG	24	15	14	17.7	14.5
OMB38	CA1	40	22	17	26.3	19.5
OMB38	CA3	36	23	18	25.7	20.5
OMB38	DG	31	19	16	22.0	17.5
OMB42	CA1	39	27	20	28.7	23.5
OMB42	CA3	33	24	19	25.3	21.5
OMB42	DG	23	16	13	17.3	14.5
OMB86	CA1	42	30	22	31.3	26.0
OMB86	CA3	33	23	19	25.0	21.0
OMB86	DG	26	20	13	19.7	16.5
OMG11	CA1	32	26	23	27.0	24.5
OMG11	CA3	39	24	23	28.7	23.5
OMG11	DG	20	14	11	15.0	12.5
OMG18	CA1	44	23	21	29.3	22.0
OMG18	CA3	33	20	17	23.3	18.5
OMG18	DG	33	23	21	25.7	22.0
OMG2	CA1	41	24	20	28.3	22.0
OMG2	CA3	39	37	26	34.0	31.5
OMG2	DG	26	16	14	18.7	15.0
OMG21	CA1	48	29	20	32.3	24.5
OMG21	CA3	38	20	17	25.0	18.5
OMG21	DG	23	15	11	16.3	13.0
OMG6	CA1	39	17	14	23.3	15.5
OMG6	CA3	24	13	12	16.3	12.5
OMG6	DG	20	10	10	13.3	10.0
YM1	CA1	38	20	16	24.7	18.0
YM1	CA3	37	27	22	28.7	24.5
YM1	DG	24	15	13	17.3	14.0
YM2	CA1	44	23	17	28.0	20.0

DCX-Methylation Degree [%]						
Sample		CpG1	CpG2	CpG3	Mean Value	MW (CpG2+3)
YM2	CA3	36	20	16	24.0	18.0
YM2	DG	22	13	12	15.7	12.5
YM3	CA1	33	20	18	23.7	19.0
YM3	CA3	40	25	20	28.3	22.5
YM3	DG	26	18	15	19.7	16.5
YM4	CA1	47	30	22	33.0	26.0
YM4	CA3	40	23	19	27.3	21.0
YM4	DG	34	19	16	23.0	17.5
YM5	CA1	39	26	23	29.3	24.5
YM5	CA3	26	17	15	19.3	16.0
YM5	DG	28	19	16	21.0	17.5
YM6	CA1	38	24	17	26.3	20.5
YM6	CA3	37	23	19	26.3	21.0
YM6	DG	30	20	15	21.7	17.5

Table 35: Determined methylation degrees of single CpG positions in GRM5 promoter region, obtained by the developed PSQ method (Yellow= Required check by user, Red= Failed to analyse and therefore unreliable).

GRM5-Methylation Degree [%]																
Sample		CpG1	CpG2	CpG3	CpG4	CpG5	CpG6	CpG7	CpG8	CpG9	CpG10	CpG11	CpG12	CpG13	CpG14	CpG15
0% Std		5	3	4	2	3	3	2	3	2	2	2	2	0	0	0
10% Std		14	12	16	13	13	16	14	16	11	12	11	11	14	14	12
100% Std		97	94	95	92	96	96	100	99	88	85	85	87	87	97	87
LOD		1.0	1.0	3.0	1.0	2.0	2.0	4.0	5.0	1.0	1.0	1.0	1.0	3.0	3.0	2.0
OMB14	CA1	<1.0	<1.0	<3.0	<1.0	<2.0	<2.0	<4.0	<5.0	<1.0	<1.0	<1.0	<1.0	<3.0	<3.0	<2.0
OMB14	CA3	<1.0	<1.0	<3.0	<1.0	<2.0	3	<4.0	<5.0	<1.0	<1.0	<1.0	<1.0	<3.0	<3.0	<2.0
OMB14	DG	<1.0	<1.0	<3.0	<1.0	<2.0	<2.0	<4.0	<5.0	<1.0	<1.0	<1.0	<1.0	<3.0	<3.0	<2.0
OMB22	CA1	<1.0	<1.0	<3.0	<1.0	<2.0	<2.0	<4.0	<5.0	<1.0	<1.0	<1.0	<1.0	<3.0	<3.0	<2.0
OMB22	CA3	<1.0	<1.0	<3.0	<1.0	3	<2.0	<4.0	<5.0	<1.0	<1.0	<1.0	<1.0	<3.0	<3.0	<2.0
OMB22	DG	<1.0	<1.0	3	<1.0	<2.0	2.5	<4.0	<5.0	<1.0	<1.0	<1.0	<1.0	<3.0	<3.0	<2.0
OMB26	CA1	<1.0	<1.0	<3.0	<1.0	<2.0	<2.0	<4.0	<5.0	<1.0	<1.0	<1.0	<1.0	<3.0	<3.0	<2.0
OMB26	CA3	<1.0	<1.0	<3.0	<1.0	<2.0	<2.0	<4.0	<5.0	<1.0	<1.0	<1.0	<1.0	<3.0	<3.0	<2.0
OMB26	DG	<1.0	<1.0	<3.0	<1.0	<2.0	<2.0	<4.0	<5.0	<1.0	<1.0	<1.0	<1.0	<3.0	<3.0	<2.0
OMB38	CA1	<1.0	<1.0	<3.0	<1.0	<2.0	<2.0	<4.0	<5.0	<1.0	<1.0	<1.0	<1.0	<3.0	<3.0	<2.0
OMB38	CA3	<1.0	<1.0	<3.0	<1.0	<2.0	2.5	<4.0	<5.0	<1.0	<1.0	<1.0	<1.0	<3.0	<3.0	<2.0
OMB38	DG	<1.0	<1.0	<3.0	<1.0	<2.0	<2.0	<4.0	<5.0	<1.0	<1.0	<1.0	<1.0	<3.0	<3.0	<2.0
OMB42	CA1	<1.0	<1.0	<3.0	<1.0	3	3	<4.0	<5.0	<1.0	<1.0	<1.0	<1.0	<3.0	<3.0	<2.0
OMB42	CA3	<1.0	<1.0	3	<1.0	<2.0	<2.0	<4.0	<5.0	<1.0	<1.0	<1.0	<1.0	<3.0	<3.0	<2.0
OMB42	DG	<1.0	<1.0	<3.0	<1.0	<2.0	<2.0	<4.0	<5.0	<1.0	<1.0	<1.0	<1.0	<3.0	<3.0	<2.0
OMB86	CA1	<1.0	<1.0	3	<1.0	3	4	<4.0	<5.0	<1.0	<1.0	<1.0	3	<3.0	<3.0	<2.0

GRM5-Methylation Degree [%]

[illegible]

7.5 Index of Figures

Figure 1: Molecular structure of DNA/RNA and the hydrogen bonds between them.	12
Figure 2: Simplified depiction of transcription and splicing.	13
Figure 3: Depiction of the single steps during PCR.	15
Figure 4: Depiction of the four phases in real-time PCR: baseline, exponential, linear, plateau.	17
Figure 5: Comparison between melting curve and derivative.	18
Figure 6: Reaction mechanism of bisulfite conversion (Source: Shapiro et al. [134]).	19
Figure 7: Depiction of the processes during pyrosequencing and the generation of signals (modified from Kreutz et al. [138]).	21
Figure 8: Position of <i>IGF1R</i> primers and the generated amplicon within the NCBI database entry M37807.1.	23
Figure 9: Results of agarose gel electrophoresis for investigating the optimal annealing temperature of <i>IGF1R</i> PCR using different methylation standards and 0.4 μ M primer concentration. See Table 2 for sample IDs.	24
Figure 10: 1= PSQ results for a 50 % methylation standard obtained by the developed method for <i>IGF1R</i> . 2= Histogram showing the expected peak pattern.	25
Figure 11: Amplification curves of <i>IGF1R</i> gene expression analysis. Different dilutions of cDNA were applied as template to investigate the optimal starting amount.	26
Figure 12: Melt plot obtained after gene expression analysis of <i>IGF1R</i> during method testing.	26
Figure 13: Dot plots of relative <i>IGF1R</i> expression sorted by animal group.	27
Figure 14: Position of <i>FMR1</i> primers and the generated amplicon within the NCBI database entry AY630337.1.	29
Figure 15: Results of agarose gel electrophoresis for investigating the optimal annealing temperature of <i>FMR1</i> PCR using different methylation standards and 0.4 μ M primer concentration. See Table 5 for sample IDs.	30
Figure 16: 1= PSQ results for a 50 % methylation standard obtained by the developed method for <i>FMR1</i> using 1:3 diluted amount of amplicon. 2= Histogram showing the expected peak pattern.	31
Figure 17: Amplification curves of <i>FMR1</i> gene expression analysis. Different dilutions of cDNA were applied as template to investigate the optimal starting amount.	32
Figure 18: Melt plot obtained after gene expression analysis of <i>FMR1</i> during method testing.	33
Figure 19: Depiction of <i>FMR1</i> amplicon from gene expression analysis to show different melting domains.	33
Figure 20: Dot plots of relative <i>FMR1</i> expression sorted by animal group.	34
Figure 21: Position of <i>DCX</i> primers and the generated amplicon within a section of the reference sequence Rnor_6.0:X:115089017:115183701:1.	35
Figure 22: Results of agarose gel electrophoresis for investigating the optimal annealing temperature and primer concentration of <i>DCX</i> PCR using different methylation standards. See Table 8 for sample IDs.	36
Figure 23: 1= PSQ results for a 50 % methylation standard obtained by the developed method for <i>DCX</i> . 2= Histogram showing the expected peak pattern.	37
Figure 24: Amplification curves of <i>DCX</i> gene expression analysis. Different dilutions of cDNA were applied as template to investigate the optimal starting amount.	39
Figure 25: Melt plot obtained after gene expression analysis of <i>DCX</i> during method testing.	39
Figure 26: Methylation degree of single CpGs in the <i>DCX</i> promoter in rats. Unreliable results were excluded.	40
Figure 27: Dot plot of methylation degrees of analysed CpG positions in the <i>DCX</i> promoter region over all groups. Unreliable results were excluded.	41
Figure 28: Dot plots of relative <i>DCX</i> expression sorted by animal group.	42

Figure 29: Position of <i>GRM5</i> primers and the generated amplicon within the NCBI database entry AH007692.2.	43
Figure 30: Results of agarose gel electrophoresis for investigating the optimal primer concentration and annealing temperature of <i>GRM5</i> PCR using different methylation standards. See Table 11 for sample IDs.	45
Figure 31: 1= PSQ results for a 10 % methylation standard obtained by the developed method for <i>GRM5</i> using a 1:3 diluted amount of amplicon. 2= Histogram showing the expected peak pattern... ..	46
Figure 32: Amplification curves of <i>GRM5</i> gene expression analysis. Different dilutions of cDNA were applied as template to investigate the optimal starting amount.	47
Figure 33: Melt plot obtained after gene expression analysis of <i>GRM5</i> during method testing.....	48
Figure 34: Dot plots of relative <i>GRM5</i> expression sorted by hippocampal subregion and animal group.	49
Figure 35: Amplification curves of <i>GAPDH</i> gene expression analysis. Different dilutions of cDNA were applied as template to investigate the optimal starting amount.	51
Figure 36: Melt plot obtained after gene expression analysis of <i>GAPDH</i> during method testing.	51
Figure 37: Separated DNA fragments after agarose gel electrophoresis of 25 bp ladder. Provided by the manufacturer	60
Figure 38: Depiction of the used formulas in $\Delta\Delta C_t$ calculations for relative gene expression.	62

7.6 Index of Tables

Table 1: Properties of the designed primers for <i>IGF1R</i> PCR and PSQ analysis.....	23
Table 2: Loading scheme for the agarose gel in Figure 9 for <i>IGF1R</i> PCR method optimization using a primer concentration of 0.4 μ M.....	24
Table 3: Primer and amplicon sequences for gene expression analysis of <i>IGF1R</i>	25
Table 4: Properties of the designed primers for <i>FMR1</i> PCR and PSQ analysis.....	28
Table 5: Loading scheme for the agarose gel in Figure 15 for <i>FMR1</i> PCR method optimization using a primer concentration of 0.4 μ M.....	30
Table 6: Primer and amplicon sequences for gene expression analysis of <i>FMR1</i> cDNA.....	32
Table 7: Properties of the designed primers for <i>DCX</i> PCR and PSQ analysis.	35
Table 8: Loading scheme for the agarose gel in Figure 22 for <i>DCX</i> PCR method optimization.....	37
Table 9: Primer and amplicon sequences for gene expression analysis of <i>DCX</i>	38
Table 10: Properties of the designed primers for <i>GRM5</i> PCR and PSQ analysis.	44
Table 11: Loading scheme for the agarose gel for <i>GRM5</i> PCR method optimization.	45
Table 12: Primer and amplicon sequences for gene expression analysis of <i>GRM5</i>	47
Table 13: Primer and amplicon sequences for gene expression analysis of <i>GAPDH</i>	50
Table 14: Composition of one sample for previous gDNA wipe-out during reverse transcription, using the Quantitect Reverse Transcription Kit (Qiagen).	56
Table 15: Composition of one sample during reverse transcription using the Quantitect Reverse Transcription Kit (Qiagen).	56
Table 16: Reaction mix for one real-time PCR sample, using Rotor-Gene SYBR Green Kit (Qiagen). ...	56
Table 17: Cycling program and signal acquisition plan for real-time PCR of cDNA, using the Rotor-Gene SYBR Green Kit (Qiagen).	57
Table 18: Reaction mix of one sample for bisulfite conversion, using EpiTect Fast Bisulfite Conversion kit.....	57
Table 19: Temperature program for bisulfite conversion.....	58
Table 20: Composition of a single reaction mix for amplification of DNA for subsequent pyrosequencing, using PyroMark PCR kit (Qiagen).....	59

Table 21: Temperature program of PCR for subsequent pyrosequencing, using the PyroMark PCR kit.....	59
Table 22: Composition of a single pyrosequencing sample.	61
Table 23: Primer annealing mix per sample for PSQ experiment.	61
Table 24: List of chemicals used in this thesis.	63
Table 25: List of kits used in this thesis.	64
Table 26: List of consumable materials used in this thesis.	64
Table 27: List of devices used in this thesis.	64
Table 28: List of software used in this thesis.	65
Table 29: List of abbreviations used in this thesis.....	67
Table 30: Concentration and yield of RNA and DNA obtained photometrically after extraction and of DNA after bisulfite conversion.	68
Table 31: List of $\Delta\Delta C_t$ and relative expression values.	70
Table 32: Determined methylation degrees of single CpG positions in <i>IGF1R</i> promoter region, obtained by the developed PSQ method.	72
Table 33: Determined methylation degrees of single CpG positions in <i>FMR1</i> promoter region, obtained by the developed PSQ method.	73
Table 34: Determined methylation degrees of single CpG positions in <i>DCX</i> promoter region, obtained by the developed PSQ method.....	75
Table 35: Determined methylation degrees of single CpG positions in <i>GRM5</i> promoter region, obtained by the developed PSQ method.	76

7.7 References

- [1] R.D. Kornberg, Chromatin structure: a repeating unit of histones and DNA, *Science*. 184 (1974) 868–871.
- [2] A.J. Bannister, T. Kouzarides, Regulation of chromatin by histone modifications, *Cell Res.* 21 (2011) 381–395.
- [3] M. Ehrlich, M.A. Gama-Sosa, L.H. Carreira, L.G. Ljungdahl, K.C. Kuo, C.W. Gehrke, DNA methylation in thermophilic bacteria: N4-methylcytosine, 5-methylcytosine, and N6-methyladenine, *Nucleic Acids Res.* 13 (1985) 1399–1412.
- [4] R.D. Hotchkiss, The quantitative separation of purines, pyrimidines, and nucleosides by paper chromatography, *J. Biol. Chem.* 175 (1948) 315–332.
- [5] Y. Liu, E.J. Oakeley, L. Sun, J.P. Jost, Multiple domains are involved in the targeting of the mouse DNA methyltransferase to the DNA replication foci, *Nucleic Acids Res.* 26 (1998) 1038–1045.
- [6] M. Okano, D.W. Bell, D.A. Haber, E. Li, DNA methyltransferases Dnmt3a and Dnmt3b are essential for de novo methylation and mammalian development, *Cell*. 99 (1999) 247–257.
- [7] F. Santos, B. Hendrich, W. Reik, W. Dean, Dynamic reprogramming of DNA methylation in the early mouse embryo, *Dev. Biol.* 241 (2002) 172–182.
- [8] S. Seisenberger, J.R. Peat, W. Reik, Conceptual links between DNA methylation reprogramming in the early embryo and primordial germ cells, *Curr. Opin. Cell Biol.* 25 (2013) 281–288.
- [9] S. Pradhan, A. Bacolla, R.D. Wells, R.J. Roberts, Recombinant human DNA (cytosine-5) methyltransferase. I. Expression, purification, and comparison of de novo and maintenance methylation, *J. Biol. Chem.* 274 (1999) 33002–33010.
- [10] S.H. Cross, J.A. Charlton, X. Nan, A.P. Bird, Purification of CpG islands using a methylated DNA binding column, *Nat. Genet.* 6 (1994) 236–244.

- [11] R.S. Illingworth, U. Gruenewald-Schneider, S. Webb, A.R.W. Kerr, K.D. James, D.J. Turner *et al.*, Orphan CpG islands identify numerous conserved promoters in the mammalian genome, *PLoS Genet.* 6 (2010) e1001134.
- [12] A.P. Bird, CpG-rich islands and the function of DNA methylation, *Nature.* 321 (1986) 209–213.
- [13] F. Mohn, M. Weber, M. Rebhan, T.C. Roloff, J. Richter, M.B. Stadler *et al.*, Lineage-specific polycomb targets and de novo DNA methylation define restriction and potential of neuronal progenitors, *Mol. Cell.* 30 (2008) 755–766.
- [14] R. Stein, A. Razin, H. Cedar, In vitro methylation of the hamster adenine phosphoribosyltransferase gene inhibits its expression in mouse L cells, *Proc. Natl. Acad. Sci. U.S.A.* 79 (1982) 3418–3422.
- [15] A. Lazarovici, T. Zhou, A. Shafer, A.C. Dantas Machado, T.R. Riley, R. Sandstrom *et al.*, Probing DNA shape and methylation state on a genomic scale with DNase I, *Proc. Natl. Acad. Sci. U.S.A.* 110 (2013) 6376–6381.
- [16] P.L. Jones, G.C. Jan Veenstra, P.A. Wade, D. Vermaak, S.U. Kass, N. Landsberger *et al.*, Methylated DNA and MeCP2 recruit histone deacetylase to repress transcription, *Nat. Genet.* 19 (1998) 187–191.
- [17] M.P. Ball, J.B. Li, Y. Gao, J.-H. Lee, E.M. LeProust, I.-H. Park *et al.*, Targeted and genome-scale strategies reveal gene-body methylation signatures in human cells, *Nat. Biotechnol.* 27 (2009) 361–368.
- [18] D. Aran, G. Toperoff, M. Rosenberg, A. Hellman, Replication timing-related and gene body-specific methylation of active human genes, *Hum. Mol. Genet.* 20 (2011) 670–680.
- [19] A.K. Maunakea, I. Chepelev, K. Cui, K. Zhao, Intragenic DNA methylation modulates alternative splicing by recruiting MeCP2 to promote exon recognition, *Cell Res.* 23 (2013) 1256–1269.
- [20] S. Li, J. Zhang, S. Huang, X. He, Genome-wide analysis reveals that exon methylation facilitates its selective usage in the human transcriptome, *Brief. Bioinformatics.* 19 (2018) 754–764.
- [21] M.F. Fraga, E. Ballestar, M.F. Paz, S. Ropero, F. Setien, M.L. Ballestar *et al.*, Epigenetic differences arise during the lifetime of monozygotic twins, *Proc. Natl. Acad. Sci. U.S.A.* 102 (2005) 10604–10609.
- [22] S. Maegawa, G. Hinkal, H.S. Kim, L. Shen, L. Zhang, J. Zhang *et al.*, Widespread and tissue specific age-related DNA methylation changes in mice, *Genome Res.* 20 (2010) 332–340.
- [23] F. Noreen, M. Rössli, P. Gaj, J. Pietrzak, S. Weis, P. Urfer *et al.*, Modulation of age- and cancer-associated DNA methylation change in the healthy colon by aspirin and lifestyle, *J. Natl. Cancer Inst.* 106 (2014).
- [24] I. Peters, B. Vaske, K. Albrecht, M.A. Kuczyk, U. Jonas, J. Serth, Adiposity and age are statistically related to enhanced RASSF1A tumor suppressor gene promoter methylation in normal autopsy kidney tissue, *Cancer Epidemiol. Biomarkers Prev.* 16 (2007) 2526–2532.
- [25] M.F. Fraga, R. Agrelo, M. Esteller, Cross-talk between aging and cancer: the epigenetic language, *Ann. N. Y. Acad. Sci.* 1100 (2007) 60–74.
- [26] S. Chanda, U.B. Dasgupta, D. Guhamazumder, M. Gupta, U. Chaudhuri, S. Lahiri *et al.*, DNA hypermethylation of promoter of gene p53 and p16 in arsenic-exposed people with and without malignancy, *Toxicol. Sci.* 89 (2006) 431–437.
- [27] S. De Prins, G. Koppen, G. Jacobs, E. Dons, E. Van de Mieroop, V. Nelen *et al.*, Influence of ambient air pollution on global DNA methylation in healthy adults: a seasonal follow-up, *Environ. Int.* 59 (2013) 418–424.
- [28] W.B. Scoville, B. Milner, Loss of recent memory after bilateral hippocampal lesions, *J. Neuropsychiatry Clin. Neurosci.* 12 (2000) 103–113.
- [29] D.O. Hebb, in: *The Organization of Behavior*, Wiley, New York, 1949: pp. 62–66.
- [30] B.E. Alger, T.J. Teyler, Long-term and short-term plasticity in the CA1, CA3, and dentate regions of the rat hippocampal slice, *Brain Res.* 110 (1976) 463–480.
- [31] C. Lüscher, R.C. Malenka, NMDA receptor-dependent long-term potentiation and long-term depression (LTP/LTD), *Cold Spring Harb. Perspect. Biol.* 4 (2012).

- [32] S. Maren, M.S. Fanselow, Synaptic plasticity in the basolateral amygdala induced by hippocampal formation stimulation in vivo, *J. Neurosci.* 15 (1995) 7548–7564.
- [33] A. Kemp, D. Manahan-Vaughan, Hippocampal long-term depression and long-term potentiation encode different aspects of novelty acquisition, *Proc. Natl. Acad. Sci. U.S.A.* 101 (2004) 8192–8197.
- [34] J. Altman, G.D. Das, Autoradiographic and histological evidence of postnatal hippocampal neurogenesis in rats, *J. Comp. Neurol.* 124 (1965) 319–335.
- [35] E.A. Markakis, F.H. Gage, Adult-generated neurons in the dentate gyrus send axonal projections to field CA3 and are surrounded by synaptic vesicles, *J. Comp. Neurol.* 406 (1999) 449–460.
- [36] A. Sahay, K.N. Scobie, A.S. Hill, C.M. O’Carroll, M.A. Kheirbek, N.S. Burghardt *et al.*, Increasing adult hippocampal neurogenesis is sufficient to improve pattern separation, *Nature*. 472 (2011) 466–470.
- [37] S.S. Deshmukh, J.J. Knierim, *Hippocampus*, Wiley Interdiscip. Rev. Cogn. Sci. 3 (2012) 231–251.
- [38] S.I. Wiener, C.A. Paul, H. Eichenbaum, Spatial and behavioral correlates of hippocampal neuronal activity, *J. Neurosci.* 9 (1989) 2737–2763.
- [39] J. O’Keefe, L. Nadel, in: *The Hippocampus as a Cognitive Map*, Clarendon Press ; Oxford University Press, Oxford : New York, 1978: pp. 62–79.
- [40] N. Burgess, The 2014 Nobel prize in physiology or medicine: a spatial model for cognitive neuroscience, *Neuron*. 84 (2014) 1120–1125.
- [41] J. Feng, Y. Zhou, S.L. Campbell, T. Le, E. Li, J.D. Sweatt *et al.*, Dnmt1 and Dnmt3a maintain DNA methylation and regulate synaptic function in adult forebrain neurons, *Nat. Neurosci.* 13 (2010) 423–430.
- [42] F.D. Lubin, T.L. Roth, D. Sweatt, Epigenetic regulation of BDNF gene transcription in the consolidation of fear memory, *J. Neurosci.* 28 (2008) 10576–10586.
- [43] K. Martinowich, D. Hattori, H. Wu, S. Fouse, F. He, Y. Hu *et al.*, DNA methylation-related chromatin remodeling in activity-dependent BDNF gene regulation, *Science*. 302 (2003) 890–893.
- [44] C. Mitchelmore, L. Gede, Brain derived neurotrophic factor: epigenetic regulation in psychiatric disorders, *Brain Res.* 1586 (2014) 162–172.
- [45] S. Balaratnasingam, A. Janca, Brain derived neurotrophic factor: a novel neurotrophin involved in psychiatric and neurological disorders, *Pharmacol. Ther.* 134 (2012) 116–124.
- [46] C.A. Miller, J.D. Sweatt, Covalent modification of DNA regulates memory formation, *Neuron*. 53 (2007) 857–869.
- [47] F. Serpeloni, K. Radtke, S.G. de Assis, F. Henning, D. Nätt, T. Elbert, Grandmaternal stress during pregnancy and DNA methylation of the third generation: an epigenome-wide association study, *Transl. Psychiatry*. 7 (2017) e1202.
- [48] C. Murgatroyd, A.V. Patchev, Y. Wu, V. Micale, Y. Bockmühl, D. Fischer *et al.*, Dynamic DNA methylation programs persistent adverse effects of early-life stress, *Nat. Neurosci.* 12 (2009) 1559–1566.
- [49] T.L. Roth, F.D. Lubin, A.J. Funk, J.D. Sweatt, Lasting epigenetic influence of early-life adversity on the BDNF gene, *Biol. Psychiatry*. 65 (2009) 760–769.
- [50] I.C.G. Weaver, N. Cervoni, F.A. Champagne, A.C. D’Alessio, S. Sharma, J.R. Seckl *et al.*, Epigenetic programming by maternal behavior, *Nat. Neurosci.* 7 (2004) 847–854.
- [51] S. Ridder, S. Chourbaji, R. Hellweg, A. Urani, C. Zacher, W. Schmid *et al.*, Mice with genetically altered glucocorticoid receptor expression show altered sensitivity for stress-induced depressive reactions, *J. Neurosci.* 25 (2005) 6243–6250.
- [52] P.O. McGowan, A. Sasaki, A.C. D’Alessio, S. Dymov, B. Labonté, M. Szyf *et al.*, Epigenetic regulation of the glucocorticoid receptor in human brain associates with childhood abuse, *Nat. Neurosci.* 12 (2009) 342–348.
- [53] M. Roser, OurWorldinData.org, (2017). <https://ourworldindata.org/life-expectancy> (accessed February 13, 2018).

- [54] Alzheimer's Association, 2016 Alzheimer's disease facts and figures, *Alzheimers Dement.* 12 (2016) 459–509.
- [55] L. Ianov, A. Riva, A. Kumar, T.C. Foster, DNA methylation of synaptic genes in the prefrontal cortex is associated with aging and age-related cognitive impairment, *Front. Aging. Neurosci.* 9 (2017) 249.
- [56] M.R. Penner, R.R. Parrish, L.T. Hoang, T.L. Roth, F.D. Lubin, C.A. Barnes, Age-related changes in *Egr1* transcription and DNA methylation within the hippocampus, *Hippocampus.* 26 (2016) 1008–1020.
- [57] M.R. Penner, T.L. Roth, M.K. Chawla, L.T. Hoang, E.D. Roth, F.D. Lubin *et al.*, Age-related changes in *Arc* transcription and DNA methylation within the hippocampus, *Neurobiol. Aging.* 32 (2011) 2198–2210.
- [58] A.M.M. Oliveira, T.J. Hemstedt, H. Bading, Rescue of aging-associated decline in *Dnmt3a2* expression restores cognitive abilities, *Nat. Neurosci.* 15 (2012) 1111–1113.
- [59] V.L. Wilson, R.A. Smith, S. Ma, R.G. Cutler, Genomic 5-methyldeoxycytidine decreases with age, *J. Biol. Chem.* 262 (1987) 9948–9951.
- [60] N.C. Berchtold, P.D. Coleman, D.H. Cribbs, J. Rogers, D.L. Gillen, C.W. Cotman, Synaptic genes are extensively downregulated across multiple brain regions in normal human aging and Alzheimer's disease, *Neurobiol. Aging.* 34 (2013) 1653–1661.
- [61] A.A. Johnson, K. Akman, S.R.G. Calimport, D. Wuttke, A. Stolzing, J.P. de Magalhães, The role of DNA methylation in aging, rejuvenation, and age-related disease, *Rejuvenation Res.* 15 (2012) 483–494.
- [62] R.P. Haberman, C.K. Quigley, M. Gallagher, Characterization of CpG island DNA methylation of impairment-related genes in a rat model of cognitive aging, *Epigenetics.* 7 (2012) 1008–1019.
- [63] L. Laviola, A. Natalicchio, F. Giorgino, The IGF-I signaling pathway, *Curr. Pharm. Des.* 13 (2007) 663–669.
- [64] A. Ullrich, A. Gray, A.W. Tam, T. Yang-Feng, M. Tsubokawa, C. Collins *et al.*, Insulin-like growth factor I receptor primary structure: comparison with insulin receptor suggests structural determinants that define functional specificity, *EMBO J.* 5 (1986) 2503–2512.
- [65] G. Pandini, R. Vigneri, A. Costantino, F. Frasca, A. Ippolito, Y. Fujita-Yamaguchi *et al.*, Insulin and insulin-like growth factor-I (IGF-I) receptor overexpression in breast cancers leads to insulin/IGF-I hybrid receptor overexpression: evidence for a second mechanism of IGF-I signaling, *Clin. Cancer Res.* 5 (1999) 1935–1944.
- [66] M.A. Aberg, N.D. Aberg, H. Hedbäcker, J. Oscarsson, P.S. Eriksson, Peripheral infusion of IGF-I selectively induces neurogenesis in the adult rat hippocampus, *J. Neurosci.* 20 (2000) 2896–2903.
- [67] F. Su, H. Shu, Q. Ye, Z. Wang, C. Xie, B. Yuan *et al.*, Brain insulin resistance deteriorates cognition by altering the topological features of brain networks, *Neuroimage Clin.* 13 (2017) 280–287.
- [68] K. Talbot, H.-Y. Wang, H. Kazi, L.-Y. Han, K.P. Bakshi, A. Stucky *et al.*, Demonstrated brain insulin resistance in Alzheimer's disease patients is associated with IGF-1 resistance, IRS-1 dysregulation, and cognitive decline, *J. Clin. Invest.* 122 (2012) 1316–1338.
- [69] S. Logan, G.A. Pharaoh, M.C. Marlin, D.R. Masser, S. Matsuzaki, B. Wronowski *et al.*, Insulin-like growth factor receptor signaling regulates working memory, mitochondrial metabolism, and amyloid- β uptake in astrocytes, *Mol. Metab.* 9 (2018) 141–155.
- [70] J.L. Trejo, J. Piriz, M.V. Llorens-Martin, A.M. Fernandez, M. Bolós, D. LeRoith *et al.*, Central actions of liver-derived insulin-like growth factor I underlying its pro-cognitive effects, *Mol. Psychiatry.* 12 (2007) 1118–1128.
- [71] J.L. Mason, S. Xuan, I. Dragatsis, A. Efstratiadis, J.E. Goldman, Insulin-like growth factor (IGF) signaling through type 1 IGF receptor plays an important role in remyelination, *J. Neurosci.* 23 (2003) 7710–7718.
- [72] A.F. Bokov, N. Garg, Y. Ikeno, S. Thakur, N. Musi, R.A. DeFronzo *et al.*, Does reduced IGF-1R signaling in *Igf1r*^{+/-} mice alter aging?, *PLoS One.* 6 (2011) e26891.

- [73] J.C. Darnell, S.J. Van Driesche, C. Zhang, K.Y.S. Hung, A. Mele, C.E. Fraser *et al.*, FMRP stalls ribosomal translocation on mRNAs linked to synaptic function and autism, *Cell*. 146 (2011) 247–261.
- [74] V. Brown, P. Jin, S. Ceman, J.C. Darnell, W.T. O'Donnell, S.A. Tenenbaum *et al.*, Microarray identification of FMRP-associated brain mRNAs and altered mRNA translational profiles in fragile X syndrome, *Cell*. 107 (2001) 477–487.
- [75] A. Maddalena, C.S. Richards, M.J. McGinniss, A. Brothman, R.J. Desnick, R.E. Grier *et al.*, Technical standards and guidelines for fragile X: the first of a series of disease-specific supplements to the Standards and Guidelines for Clinical Genetics Laboratories of the American College of Medical Genetics. Quality Assurance Subcommittee of the Laboratory Practice Committee, *Genet. Med.* 3 (2001) 200–205.
- [76] S.-Y. Yim, B.H. Jeon, J.A. Yang, H.J. Kim, Fragile X syndrome in Korea: a case series and a review of the literature, *J. Korean Med. Sci.* 23 (2008) 470–476.
- [77] M.A. Leehey, R.P. Munhoz, A.E. Lang, J.A. Brunberg, J. Grigsby, C. Greco *et al.*, The fragile X premutation presenting as essential tremor, *Arch. Neurol.* 60 (2003) 117–121.
- [78] J. Grigsby, A.G. Brega, S. Jacquemont, D.Z. Loesch, M.A. Leehey, G.K. Goodrich *et al.*, Impairment in the cognitive functioning of men with fragile X-associated tremor/ataxia syndrome (FXTAS), *J. Neurol. Sci.* 248 (2006) 227–233.
- [79] A.J. Verkerk, M. Pieretti, J.S. Sutcliffe, Y.H. Fu, D.P. Kuhl, A. Pizzuti *et al.*, Identification of a gene (FMR-1) containing a CGG repeat coincident with a breakpoint cluster region exhibiting length variation in fragile X syndrome, *Cell*. 65 (1991) 905–914.
- [80] F. Tassone, R.J. Hagerman, D.N. Iklé, P.N. Dyer, M. Lampe *et al.*, FMRP expression as a potential prognostic indicator in fragile X syndrome, *Am. J. Med. Genet.* 84 (1999) 250–261.
- [81] D. Gothelf, J.A. Furfaro, F. Hoeft, M.A. Eckert, S.S. Hall, R. O'Hara *et al.*, Neuroanatomy of fragile X syndrome is associated with aberrant behavior and the fragile X mental retardation protein (FMRP), *Ann. Neurol.* 63 (2008) 40–51.
- [82] M. Pieretti, F.P. Zhang, Y.H. Fu, S.T. Warren, B.A. Oostra, C.T. Caskey *et al.*, Absence of expression of the FMR-1 gene in fragile X syndrome, *Cell*. 66 (1991) 817–822.
- [83] F. Niere, J.R. Wilkerson, K.M. Huber, Evidence for a fragile X mental retardation protein-mediated translational switch in metabotropic glutamate receptor-triggered Arc translation and long-term depression, *J. Neurosci.* 32 (2012) 5924–5936.
- [84] H.G.S. Martin, O. Lassalle, J.T. Brown, O.J. Manzoni, Age-dependent long-term potentiation deficits in the prefrontal cortex of the FMR1 knockout mouse model of fragile X syndrome, *Cereb. Cortex*. 26 (2016) 2084–2092.
- [85] F. Francis, A. Koulakoff, D. Boucher, P. Chafey, B. Schaar, M.C. Vinet *et al.*, Doublecortin is a developmentally regulated, microtubule-associated protein expressed in migrating and differentiating neurons, *Neuron*. 23 (1999) 247–256.
- [86] S. Couillard-Despres, B. Winner, S. Schaubeck, R. Aigner, M. Vroemen, N. Weidner *et al.*, Doublecortin expression levels in adult brain reflect neurogenesis, *Eur. J. Neurosci.* 21 (2005) 1–14.
- [87] O. von Bohlen und Halbach, Immunohistological markers for proliferative events, gliogenesis, and neurogenesis within the adult hippocampus, *Cell Tissue Res.* 345 (2011) 1–19.
- [88] J.G. Gleeson, P.T. Lin, L.A. Flanagan, C.A. Walsh, Doublecortin is a microtubule-associated protein and is expressed widely by migrating neurons, *Neuron*. 23 (1999) 257–271.
- [89] C.A. Moores, M. Perderiset, F. Francis, J. Chelly, A. Houdusse, R.A. Milligan, Mechanism of microtubule stabilization by doublecortin, *Mol. Cell*. 14 (2004) 833–839.
- [90] J. Spampinato, R.K. Sullivan, F.R. Turpin, P.F. Bartlett, P. Sah, Properties of doublecortin expressing neurons in the adult mouse dentate gyrus, *PLoS One*. 7 (2012) e41029.
- [91] V. des Portes, J.M. Pinard, P. Billuart, M.C. Vinet, A. Koulakoff, A. Carrié *et al.*, A novel CNS gene required for neuronal migration and involved in X-linked subcortical laminar heterotopia and lissencephaly syndrome, *Cell*. 92 (1998) 51–61.

- [92] R.J. Leventer, D.T. Pilz, N. Matsumoto, D.H. Ledbetter, W.B. Dobyns, Lissencephaly and subcortical band heterotopia: molecular basis and diagnosis, *Mol. Med. Today*. 6 (2000) 277–284.
- [93] A.E. Fry, T.D. Cushion, D.T. Pilz, The genetics of lissencephaly, *Am. J. Med. Genet. C. Semin. Med. Genet.* 166C (2014) 198–210.
- [94] M.-A. Jang, H.I. Woo, J.-W. Kim, J. Lee, C.-S. Ki, Identification of DCX gene mutation in lissencephaly spectrum with subcortical band heterotopia using whole exome sequencing, *Pediatr. Neurol.* 48 (2013) 411–414.
- [95] W.B. Dobyns, The clinical patterns and molecular genetics of lissencephaly and subcortical band heterotopia, *Epilepsia*. 51 Suppl 1 (2010) 5–9.
- [96] T. Abe, H. Sugihara, H. Nawa, R. Shigemoto, N. Mizuno, S. Nakanishi, Molecular characterization of a novel metabotropic glutamate receptor mGluR5 coupled to inositol phosphate/Ca²⁺ signal transduction, *J. Biol. Chem.* 267 (1992) 13361–13368.
- [97] J.M. Servitja, R. Masgrau, E. Sarri, F. Picatoste, Group I metabotropic glutamate receptors mediate phospholipase D stimulation in rat cultured astrocytes, *J. Neurochem.* 72 (1999) 1441–1447.
- [98] V. Kumar, Y.-J.I. Jong, K.L. O'Malley, Activated nuclear metabotropic glutamate receptor mGlu5 couples to nuclear Gq/11 proteins to generate inositol 1,4,5-trisphosphate-mediated nuclear Ca²⁺ release, *J. Biol. Chem.* 283 (2008) 14072–14083.
- [99] D. Balschun, W. Zuschratter, W. Wetzel, Allosteric enhancement of metabotropic glutamate receptor 5 function promotes spatial memory, *Neuroscience*. 142 (2006) 691–702.
- [100] D. Manahan-Vaughan, K.-H. Braunewell, The metabotropic glutamate receptor, mGluR5, is a key determinant of good and bad spatial learning performance and hippocampal synaptic plasticity, *Cereb. Cortex*. 15 (2005) 1703–1713.
- [101] D. Manahan-Vaughan, R.T. Ngomba, M. Storto, A. Kulla, M.V. Catania, S. Chiechio *et al.*, An increased expression of the mGlu5 receptor protein following LTP induction at the perforant path-dentate gyrus synapse in freely moving rats, *Neuropharmacology*. 44 (2003) 17–25.
- [102] G. Riedel, G. Casabona, B. Platt, E.M. Macphail, F. Nicoletti, Fear conditioning-induced time- and subregion-specific increase in expression of mGlu5 receptor protein in rat hippocampus, *Neuropharmacology*. 39 (2000) 1943–1951.
- [103] J.M. Berg, J.L. Tymoczko, L. Stryer, G.J. Gatto, in: *Biochemie*, 7. Auflage, korrigierter Nachdruck, Springer Spektrum, Berlin Heidelberg, 2014: pp. 111–116.
- [104] J.M. Berg, J.L. Tymoczko, L. Stryer, G.J. Gatto, in: *Biochemie*, 7. Auflage, korrigierter Nachdruck, Springer Spektrum, Berlin Heidelberg, 2014: pp. 111–112.
- [105] B. Alberts, in: *Molecular Biology of the Cell*, Sixth edition, Garland Science, Taylor and Francis Group, New York, NY, 2015: pp. 415–417.
- [106] N.L. Barbosa-Morais, M. Irimia, Q. Pan, H.Y. Xiong, S. Gueroussov, L.J. Lee *et al.*, The evolutionary landscape of alternative splicing in vertebrate species, *Science*. 338 (2012) 1587–1593.
- [107] Q. Xu, B. Modrek, C. Lee, Genome-wide detection of tissue-specific alternative splicing in the human transcriptome, *Nucleic Acids Res.* 30 (2002) 3754–3766.
- [108] TRIzol Reagent (DNA isolation) user guide - Pub. no. MAN0016385 - Rev. A.0 - MAN0016385_TRIzol_Reagent_DNA_Isol_UG.pdf, https://assets.thermofisher.com/TFS-Assets/LSG/manuals/MAN0016385_TRIzol_Reagent_DNA_Isol_UG.pdf (accessed March 14, 2018).
- [109] P.A. Kirkland, J. Busby, S. Stevens, J.A. Maupin-Furlow, Trizol-based method for sample preparation and isoelectric focusing of halophilic proteins, *Anal. Biochem.* 351 (2006) 254–259.
- [110] P. Reddy, A. Rao, D. Malhotra, S. Sharma, R. Kumar, R. Jain *et al.*, A simple protein extraction method for proteomic analysis of diverse biological specimens, *Curr. Proteomics*. 10 (2014) 298–311.

- [111] W. Sun, Chapter 4 - Nucleic extraction and amplification, in: *Molecular Diagnostics*, Academic Press, 2010: pp. 35–47.
- [112] D.H. Farkas, C.A. Holland, Chapter 3 - Overview of molecular diagnostic techniques and instrumentation, in: *Cell and Tissue Based Molecular Pathology*, Churchill Livingstone, 2009: pp. 19–32.
- [113] P. Chomczynski, N. Sacchi, The single-step method of RNA isolation by acid guanidinium thiocyanate-phenol-chloroform extraction: twenty-something years on, *Nat. Protoc.* 1 (2006) 581–585.
- [114] P.N. Hengen, Methods and reagents: carriers for precipitating nucleic acids, *Trends Biochem. Sci.* 21 (1996) 224–225.
- [115] C.F. Barbas, D.R. Burton, J.K. Scott, G.J. Silverman, Quantitation of DNA and RNA, *CSH Protoc.* 2007 (2007) pdb.ip47.
- [116] 260/280 and 260/230 Ratios, <http://www.nhm.ac.uk/content/dam/nhmwww/our-science/dpts-facilities-staff/Coreresearchlabs/nanodrop.pdf> (accessed February 28, 2018).
- [117] The nobel prize in chemistry 1993, http://www.nobelprize.org/nobel_prizes/chemistry/laureates/1993/ (accessed March 12, 2018).
- [118] M. Mcpherson, S. Moller, in: *PCR: The Basics.*, 2nd ed., Taylor & Francis Ltd., Hoboken, 2006: pp. 14–19.
- [119] T.C. Lorenz, Polymerase chain reaction: basic protocol plus troubleshooting and optimization strategies, *J. Vis. Exp.* (2012) e3998.
- [120] R.K. Saiki, D.H. Gelfand, S. Stoffel, S.J. Scharf, R. Higuchi, G.T. Horn *et al.*, Primer-directed enzymatic amplification of DNA with a thermostable DNA polymerase, *Science.* 239 (1988) 487–491.
- [121] S. Ishino, Y. Ishino, DNA polymerases as useful reagents for biotechnology - the history of developmental research in the field, *Front. Microbiol.* 5 (2014) 465.
- [122] M. Mcpherson, S. Moller, in: *PCR: The Basics.*, 2nd ed., Taylor & Francis Ltd., Hoboken, 2006: pp. 185–188.
- [123] A. Raso, R. Biassoni, Twenty years of qPCR: a mature technology?, *Methods Mol. Biol.* 1160 (2014) 1–3.
- [124] R.D. Barber, D.W. Harmer, R.A. Coleman, B.J. Clark, GAPDH as a housekeeping gene: analysis of GAPDH mRNA expression in a panel of 72 human tissues, *Physiol. Genomics.* 21 (2005) 389–395.
- [125] R. Gilsbach, M. Kouta, H. Bönisch, M. Brüss, Comparison of in vitro and in vivo reference genes for internal standardization of real-time PCR data, *BioTechniques.* 40 (2006) 173–177.
- [126] M. Sirakov, I. Zarrella, M. Borra, F. Rizzo, E. Biffali, M. Arnone *et al.*, Selection and validation of a set of reliable reference genes for quantitative RT-PCR studies in the brain of the Cephalopod Mollusc *Octopus vulgaris*, *BMC Mol. Biol.* 10 (2009) 70.
- [127] T.K. Wojdacz, A. Dobrovic, Methylation-sensitive high resolution melting (MS-HRM): a new approach for sensitive and high-throughput assessment of methylation, *Nucleic Acids Res.* 35 (2007) e41.
- [128] J. Worm, A. Aggerholm, P. Guldberg, In-tube DNA methylation profiling by fluorescence melting curve analysis, *Clin. Chem.* 47 (2001) 1183–1189.
- [129] A. Panjkovich, F. Melo, Comparison of different melting temperature calculation methods for short DNA sequences, *Bioinformatics.* 21 (2005) 711–722.
- [130] K.M. Ririe, R.P. Rasmussen, C.T. Wittwer, Product differentiation by analysis of DNA melting curves during the polymerase chain reaction, *Anal. Biochem.* 245 (1997) 154–160.
- [131] P.Y. Lee, J. Costumbrado, C.-Y. Hsu, Y.H. Kim, Agarose gel electrophoresis for the separation of DNA fragments, *J. Vis. Exp.* (2012).
- [132] M.W. McDonell, M.N. Simon, F.W. Studier, Analysis of restriction fragments of T7 DNA and determination of molecular weights by electrophoresis in neutral and alkaline gels, *J. Mol. Biol.* 110 (1977) 119–146.

- [133] M. Frommer, L.E. McDonald, D.S. Millar, C.M. Collis, F. Watt, G.W. Grigg *et al.*, A genomic sequencing protocol that yields a positive display of 5-methylcytosine residues in individual DNA strands, *Proc. Natl. Acad. Sci. U. S. A.* 89 (1992) 1827–1831.
- [134] R. Shapiro, R.E. Servis, M. Welcher, Reactions of uracil and cytosine derivatives with sodium bisulfite, *J. Am. Chem. Soc.* 92 (1970) 422–424.
- [135] K. Patterson, L. Molloy, W. Qu, S. Clark, DNA methylation: bisulphite modification and analysis, *J. Vis. Exp.* (2011).
- [136] A.M. Raizis, F. Schmitt, J.P. Jost, A bisulfite method of 5-methylcytosine mapping that minimizes template degradation, *Anal. Biochem.* 226 (1995) 161–166.
- [137] P. Nyrén, The history of pyrosequencing, *Methods Mol. Biol.* 373 (2007) 1–14.
- [138] M. Kreutz, G. Schock, J. Kaiser, N. Hochstein, R. Peist, PyroMark® instruments, chemistry, and software for Pyrosequencing® analysis, *Methods Mol. Biol.* 1315 (2015) 17–27.
- [139] J. Tost, I.G. Gut, DNA methylation analysis by pyrosequencing, *Nat. Protoc.* 2 (2007) 2265–2275.
- [140] J. Hami, A. Sadr-Nabavi, M. Sankian, H. Haghir, Sex differences and left-right asymmetries in expression of insulin and insulin-like growth factor-1 receptors in developing rat hippocampus, *Brain Struct. Funct.* 217 (2012) 293–302.
- [141] J. Zhang, H. Li, Z. Wu, X. Tan, F. Liu, X. Huang *et al.*, Differentiation of rat iPS cells and ES cells into granulosa cell-like cells in vitro, *Acta Biochim. Biophys. Sin.* 45 (2013) 289–295.
- [142] Z. Dwight, R. Palais, C.T. Wittwer, uMELT: prediction of high-resolution melting curves and dynamic melting profiles of PCR products in a rich web application, *Bioinformatics.* 27 (2011) 1019–1020.
- [143] D.R. Zerbino, P. Achuthan, W. Akanni, M.R. Amode, D. Barrell, J. Bhai *et al.*, Ensembl 2018, *Nucleic Acids Res.* 46 (2018) D754–D761.
- [144] S. Fu, S. O’Neal, L. Hong, W. Jiang, W. Zheng, Elevated adult neurogenesis in brain subventricular zone following in vivo manganese exposure: roles of copper and DMT1, *Toxicol. Sci.* 143 (2015) 482–498.
- [145] Z. Cai, G.P. Schools, H.K. Kimelberg, Metabotropic glutamate receptors in acutely isolated hippocampal astrocytes: developmental changes of mGluR5 mRNA and functional expression, *Glia.* 29 (2000) 70–80.
- [146] A.M.S. Kindlundh-Höglberg, A. Blomqvist, R. Malki, H.B. Schiöth, Extensive neuroadaptive changes in cortical gene-transcript expressions of the glutamate system in response to repeated intermittent MDMA administration in adolescent rats, *BMC Neurosci.* 9 (2008).
- [147] W.A. Kibbe, OligoCalc: an online oligonucleotide properties calculator, *Nucleic Acids Res.* 35 (2007) W43–46.
- [148] A.R. Gruber, R. Lorenz, S.H. Bernhart, R. Neuböck, I.L. Hofacker, The Vienna RNA websuite, *Nucleic Acids Res.* 36 (2008) W70–74.
- [149] OligoAnalyzer 3.1, <https://eu.idtdna.com/calc/analyzer> (accessed June 9, 2017).
- [150] E.D. Levin, O.A. Timofeeva, L. Yang, A. Petro, I.T. Ryde, *et al.*, Early postnatal parathion exposure in rats causes sex-selective cognitive impairment and neurotransmitter defects which emerge in aging, *Behav. Brain Res.* 208 (2010) 319–327.
- [151] TRI Reagent® DNA/Protein isolation protocol | Thermo Fisher Scientific, (2018). <https://www.thermofisher.com/at/en/home/references/protocols/nucleic-acid-purification-and-analysis/dna-extraction-protocols/tri-reagent-dna-protein-isolation-protocol.html>.